Research Square

Preprints are preliminary reports that have not undergone peer review.
They should not be considered conclusive, used to inform clinical practice,
or referenced by the media as validated information.

Pathogenesis and Immune Dynamics of African Swine Fever Virus Across Diverse Suid Species

Martin Beer

Martin.Beer@fli.de

Friedrich-Loeffler-Institute https://orcid.org/0000-0002-0598-5254

Virginia Friedrichs

Friedrich-Loeffler-Institut

Alexander Schäfer

Friedrich-Loeffler-Institut

Quentin Wright

Commonwealth Scientific and Industrial Research Organisation

Tobias Britzke

Department of Experimental Animal Facilities and Biorisk Management, Friedrich-Loeffler-Institut, Federal Research Institute of animal health https://orcid.org/0009-0001-8177-4766

Richard Küchler

Friedrich-Loeffler-Institut

Mirette Eshak

Friedrich-Loeffler-Institut

Ferran Jori

Agricultural Research for Development

Sascha Knauf

Friedrich-Loeffler-Institut https://orcid.org/0000-0001-5744-4946

Nadège Balmelle

Sciensano

Angele Breithaupt

Friedrich-Loeffler-Institut https://orcid.org/0000-0002-6373-5923

Julia Sehl-Ewert

Friedrich Loeffler institute

Marylene Tignon

Sciensano

Axel Karger

Friedrich-Loeffler-Institut

Florian Pfaff

Friedrich-Loeffler-Institut

Jörg Beckmann
Bremerhaven Zoo
Sandra Blome
Friedrich-Loeffler-Institut

Article

Keywords:

Posted Date: September 18th, 2026

DOI: https://doi.org/10.21203/rs.3.rs-10677148/v1

License: This work is licensed under a Creative Commons Attribution 4.0 International License.
Read Full License

Additional Declarations: There is **NO** Competing Interest.

Pathogenesis and Immune Dynamics of African Swine Fever Virus Across Diverse Suid Species

Virginia Friedrichs[1,2], Alexander Schäfer[1], Quentin Wright[3], Tobias Britzke[4], Richard Küchler[5], Mirette Eshak[1], Ferran Jori[6], Sascha Knauf[7,8], Study Group wild pigs, Nadège Balmelle[9], Angele Breithaupt[4], Julia Sehl-Ewert[4], Marylene Tignon[9], Axel Karger[5], Florian Pfaff[1], Jörg Beckmann[2,10,11], Martin Beer[1], Sandra Blome[1,2]

[1], Institute of Diagnostic Virology, Friedrich-Loeffler-Institut, Greifswald-Insel Riems, Germany

[2], IUCN SSC Wild Pig Specialist Group

[3], Infectious Immunology Group, Health and Biosecurity (H&B) at the Australian Centre for Disease Preparedness (ACDP), CSIRO, Geelong, Australia

[4], Department of Experimental Animal Facilities and Biorisk Management, Friedrich-Loeffler-Institut, Greifswald-Insel Riems, Germany

[5], Institute of Molecular Virology and Cell Biology, Friedrich-Loeffler-Institut, Greifswald-Insel Riems, Germany

[6], Agricultural Research for Development (CIRAD), Montpellier, France

[7], Institute of International Animal Health and One Health, Friedrich-Loeffler-Institut, Greifswald-Insel Riems, Germany

[8], Faculty of Veterinary Medicine, Justus Liebig Universität, Gießen, Germany

[9], Unit Viral Re-Emerging, Enzootic and Bee Diseases, Department Infectious Diseases in Animals, Sciensano, Ukkel, Belgium

[10], Bremerhaven Zoo, Bremerhaven, Germany

[11], Nuremberg Zoo, Nuremberg, Germany

#For correspondence: Martin Beer (Martin.Beer@fli.de), Sandra Blome (Sandra.Blome@fli.de)

Classification: Biological Sciences, Virology, Immunology and Inflammation

Keywords: African swine fever virus, host response, domestic pig, red river hog, warthog, wild boar, immunity, inflammation, antiviral immunity, antigen presentation

Abstract

African swine fever virus (ASFV) causes a severe hemorrhagic disease in Eurasian suids, whereas African suids are considered susceptible, but resistant to disease. To investigate the basis of this differential clinical fate, domestic pigs, Eurasian wild boar, red river hogs and common warthogs were inoculated with the virulent ASFV strain *Armenia08*. Host responses to ASFV infection were characterized using classical virological and immunological methods, supplemented by pathology and multi-omics analyses integrating single-cell RNA sequencing, transcriptomics and proteomics. Domestic pigs and wild boar developed acute-lethal disease with high viraemia, while red river hogs and warthogs remained clinically unaffected despite detectable viral replication. Disease severity correlated with the abundance of ASFV-positive monocytes and pronounced inflammatory signatures in Eurasian suids. By contrast, African suids exhibited limited monocyte infection, preserved MHC class II-mediated antigen presentation, and myeloid cell composition. These findings identify coordinated immune regulation and restricted monocyte vulnerability to viral immune evasion mechanisms as key features underlying ASFV tolerance in African suids.

Introduction

African swine fever (ASF) is a high-impact viral disease affecting global pork production, rural livelihoods, and wildlife biodiversity[1]. Its causative agent, ASF virus (ASFV), a large double-stranded DNA virus of the family *Asfarviridae*, infects a broad range of suid species with host-dependent disease outcomes[2]. Infection of Eurasian suids, including domestic pigs (DP, *Sus scrofa domesticus*) and Eurasian wild boar (WB, *Sus scrofa scrofa*), results in an acute, frequently fatal hemorrhagic disease[3]. ASFV additionally threatens Asian suids, e.g. the Sulawesi babirusa (*Babyrousa celebensis*) and the bearded pig (*Sus barbatus*)[4,5].

In its historic endemic range in eastern and southern Africa, ASFV is thought to persist in a sylvatic cycle involving soft ticks (*Ornithodoros moubata* complex) and the common warthog (WH, *Phacochoerus africanus*)[6]. However, the evidence supporting this cycle is often indirect or circumstantial[7], and ASFV persistence outside Africa demonstrates that viral maintenance is not dependent on WH or ticks. African wild suids, including WH and red river hogs (RRH, *Potamochoerus porcus*; often discussed together with bushpigs, *P. larvatus*), are generally considered clinically tolerant hosts, potentially reflecting a long history of host–virus co-evolution accompanied by species-specific adaptation of immune pathways. Early experimental studies by Montgomery and others demonstrated ASFV susceptibility in WH and *Potamochoerus* spp. despite only mild clinical signs and transient viraemia[8-12]. However, experimental studies addressing host responses in African suids using modern immunological and multi-omics approaches are lacking.

ASFV primarily infects cells of the myeloid lineage, particularly monocytes and macrophages. Host immune responses during infection are party strain-dependent and incompletely understood[13].

ASFV manipulates host defenses through multiple immune evasion mechanisms[14], including interference with pattern-recognition receptor signaling, NF-κB activation and type-I-interferon responses via viral proteins such as A238L and members of the multigene families (MGF) 360 and 505[15-17]. Protective immunity further requires cellular immune responses, particularly CD8α+ T cells[13,18], whereas ASFV impairs adaptive immunity by disrupting antigen presentation and co-stimulation in antigen-presenting cells[19]. However, comparative analyses of these responses across susceptible and tolerant suid species remain limited.

Here, we experimentally inoculated DP and Eurasian WB, as well as African WH and RRH, with a highly virulent genotype II ASFV strain to investigate the relationship between viral replication dynamics, clinical outcome and host responses using an integrated multi-omics approach. Although all suid taxa were susceptible to infection, only Eurasian suids developed severe disease with widespread viral dissemination and fatal immune dysregulation. In contrast, African suids restricted systemic inflammation and maintained key myeloid immune functions despite detectable viral replication. These findings provide mechanistic insights into ASFV immunopathology and disease tolerance, advancing our understanding of species-specific host responses and informing future vaccine strategies.

Results

Highly virulent ASFV infection causes fulminant disease in Eurasian but not African wild pigs

To compare ASFV infection outcomes across suid taxa, DP, WB, RRH, and WH were inoculated intramuscularly with the highly virulent ASFV strain *Armenia08*. Animals were sampled longitudinally for virological, immunological, and multi-omics analyses, including flow cytometry, scRNA-seq, transcriptomics, and proteomics of peripheral blood leukocytes (Fig. 1a). Additional *in vitro* infections of purified naïve monocytes were performed to assess species-specific cellular responses to ASFV. Serum, plasma, and tissues were further analyzed for inflammatory markers, antibody responses, viral dissemination, and pathology.

DP and WB rapidly developed severe disease characterized by pyrexia, lethargy, anorexia, and cutaneous hemorrhages beginning at 2–3 dpi (Fig. 1b,c). In contrast, RRH and WH remained clinically inapparent and afebrile throughout the 100-day observation period. Although viraemia was detectable in all species by 2 dpi, viral genome loads diverged markedly thereafter (Fig. 1d). DP and WB developed high-level viraemia reaching $>10^7$ genome copies/ml blood 7 dpi, whereas RRH and WH maintained low viral loads and cleared detectable ASFV genomes by 100 dpi at the latest.

This divergence in viral replication was accompanied by profound differences in systemic inflammation. Acute phase proteins, including CRP and MAP, as well as complement activation products C3a and C5a, increased strongly in DP and WB but remained largely unchanged in RRH and WH (Fig. 1e,f; Fig. S1a,b). Despite the absence of overt disease, both African wild suid species seroconverted, developing ASFV-specific antibody responses over time (Fig. 1g; Fig. S1c,d).

Patterns of tissue dissemination mirrored systemic viral loads. DP and WB showed widespread ASFV dissemination with high viral genome loads and infectious virus detected across all organs analyzed at

necropsy (Fig. S1e). In contrast, ASFV distribution in RRH and WH remained limited, with infectious virus recovered only from selected tissues early after infection. Additionally, no ASFV genome was found in RRH or WH oral and nasal swabs, only in DP and WB (Fig. S2f,g).

Leukocyte dynamics further distinguished susceptible and tolerant hosts. Monocyte counts increased during infection in DP, WB and WH, whereas RRH showed little modulation (Fig. 1h). DP and WB additionally developed lymphopenia and increased polymorphonuclear neutrophil frequencies (Fig. S2a-c). Most strikingly, ASFV-p72^{+} monocytes expanded dramatically in DP and WB, reaching mean frequencies of 24.7% and 52.4%, respectively, while remaining rare in RRH and WH (~0.85%; Fig. 1i,j).

Histopathology further demonstrated severe splenic lesions in DP and WB, including lymphoid depletion, hemorrhage and extensive ASFV antigen staining, whereas RRH and WH displayed only mild alterations with comparatively few ASFV-positive cells (Fig. 1k). Quantitative histopathological scoring corroborated these qualitative observations, with semiquantitative splenic lesion and ASFV-IHC scores markedly elevated in DP and WB relative to RRH and WH across all necropsy timepoints (Fig. S3).

ASFV transcriptional and proteomic kinetics reveal constrained viral immune-evasion programs in African wild suids

To resolve ASFV replication dynamics and immune-evasion programs across suid taxa, we quantified viral transcripts in whole-blood leukocytes and profiled viral protein expression in both whole blood leukocytes and purified monocytes (Fig. 2, Fig. S4-S7). Bulk RNAseq revealed strong ASFV transcriptional activity in DP and WB 4 and 7 dpi, whereas viral transcript abundance remained low in RRH and WH throughout infection (Fig. 2a,b; Fig. S4, S5). In DP and WB, most of the ASFV transcriptome was already detectable by 4 dpi and further increased 7 dpi, consistent with rapid systemic replication and severe disease. By contrast, viral transcription in RRH and WH remained delayed, reduced, and frequently restricted to individual animals.

Across all taxa, the most abundant viral transcripts encoded major structural proteins, including *B646L* (p72), *CP204L* (p30), and *CP312R* (Fig. S5). However, DP and WB additionally displayed strong expression of ASFV genes associated with innate immune antagonism and interference with antigen presentation. These included members of the *MGF360* and *MGF505* families, as well as viral regulators targeting IFN-I signaling, IRF3, STAT1, and the cGAS–STING axis. In contrast, expression of these immunomodulatory genes remained markedly lower in RRH and WH, although selected *MGF100/110* family members were detectable in RRH 4 dpi, indicating that African wild suids support canonical ASFV immune-evasion programs under constrained viral burdens.

Proteomic analyses corroborated these findings (Fig. 2, Fig. S4, S6, S7). Whole blood leukocytes from African suids contained comparatively low levels of ASFV proteins, whereas purified monocytes provided a higher-resolution view of productive infection in the principal target cell population (Fig. 2a,c; Fig. S4, S6). Monocytes from DP and WB rapidly accumulated early, intermediate, and late viral proteins, including structural and virion-associated components such as CP204L, CP312R, B646L, K78R, and D117L,

consistent with efficient virion production (Fig. 2d; Fig. S7). Multiple viral immunomodulatory proteins, including DP96R, I215L and members of the *MGF360* and *MGF505* families, were similarly abundant.

RRH monocytes displayed comparatively limited and heterogeneous viral protein accumulation, particularly for late viral proteins. In contrast, WH monocytes supported substantial ASFV protein production at 24–48 hpi, in some individuals approaching levels observed in DP and WB (Fig. S7). Thus, WH monocytes are not intrinsically non-permissive to ASFV replication at the cellular level. Instead, the clinically tolerant phenotype in African wild suids appears to reflect restriction of systemic viral amplification and immune dysregulation *in vivo* rather than complete cellular resistance to infection.

ASFV induces divergent antiviral and inflammatory programs that track clinical susceptibility

To define how ASFV shapes host immunity *in vivo*, we integrated scRNAseq, bulk RNAseq, and proteomics of whole blood leukocytes with targeted analyses of inflammatory and antiviral mediators. This multi-omics framework enabled cross-species resolution of ASFV-induced immune states and their association with divergent disease outcomes.

Bulk transcriptomic profiling revealed rapid and extensive immune remodeling in Eurasian suids, whereas African wild suids displayed more moderate and delayed responses (Fig. 3, Fig. 4). In DP and WB, genes associated with innate immune activation, cytokine signaling, and leukocyte recruitment were broadly induced throughout acute infection (Fig. 3a; Fig. 4h; Fig. S12, S13, table S1). This included strong activation of the interferon axis, with increased expression of *IFNB1*, multiple *IFNA* subtypes, *STAT1/2*, *IRF1/3/7,* and numerous interferon-stimulated genes (ISGs), including *MX1/2*, *ISG15*, *OAS* family members, *IFIT1-3*, *RSAD2* and *DDX58*. Pattern-recognition receptors and signaling adaptors linked to antiviral sensing, including *TLR3/7/8/9*, *cGAS-STING*, *MAVS,* and *TBK1*, were similarly enriched in DP and WB. In contrast, RRH and WH exhibited lower and more heterogeneous induction of these pathways (Fig. 4h; Fig. S12, table S1).

Proteomic analyses largely mirrored the transcriptomic signatures (Fig. 4l; Fig. S14, S15). Hallmark ISGs and inflammatory mediators, including CXCL10, MX1, RIG-I, ISG15, and IFIT proteins, accumulated strongly in DP and WB and increased with disease progression, fever, and tissue pathology. In RRH and WH, antiviral responses were detectable but remained substantially lower in magnitude, particularly in RRH.

Unsupervised UMAP embedding further highlighted the divergent immune trajectories across species. DP and WB separated progressively by dpi, reflecting rapid systemic immune remodeling during acute disease (Fig. 3b; Fig. S8, S9). Comparison of monocyte DEG sets identified a shared 'core' transcriptional response to ASFV infection across all four species, alongside a substantially larger species-specific component in DP and WB, consistent with the more extensive transcriptional remodeling observed in these hosts (Fig. S10). Quantification of PBMC subset composition confirmed a progressive expansion of the monocyte compartment in DP and WB over the course of infection, a shift that was not observed in RRH and WH (Fig. S9). This transition was characterized by expansion of inflammatory monocyte populations together with loss or transcriptional silencing of antigen-presenting cell (APC) subsets, concordant with the high abundance of ASFV-positive monocytes in these species (Fig. 3a, Fig. S8). In contrast, RRH and WH

maintained comparatively stable leukocyte landscapes with preserved monocyte populations and more restricted antiviral transcriptional programs.

Single-cell analyses identified monocytes as the principal source of ASFV-induced transcriptional remodeling (Fig. 3c). Monocytes from DP and WB displayed extensive reprogramming already at 2 dpi, progressing further at 7 dpi with strong induction of antiviral ISGs, inflammatory chemokines and cytokines, including *TNF* and *IL1B* (Fig. S12, S13). By contrast, monocytes from RRH and WH mounted more selective antiviral responses while largely lacking inflammatory amplification programs. Across species, scRNAseq revealed that DP and WB develop a strong, time-dependent increase in inflammatory and antiviral gene activity, whereas RRH and WH largely maintain baseline levels. In susceptible animals, top DEGs at 7 dpi included classical ISGs (*IFIT3, DDX58/RIG-I, IFIH1, DHX58, PLSCR1, USP18, DDX60, HERC5, OAS1, RSAD2*) and inflammatory mediators (*CD82, CXCL8, IRF7, G0S2, BST2, C3AR1, CCL2, ABCA1, CXCL10, PADI4*), with high mean $\log_2$ fold-changes from baseline, demonstrating broad and sustained upregulation of antiviral and inflammatory programs that is largely absent in the resistant suids (Fig. 4 a-c). Consistent with these findings, ELISA confirmed strong systemic induction of TNF-α, IFN-α, IL-1β and IL-1Ra in DP and WB, whereas these mediators remained largely undetectable in RRH and WH (Fig. 4d-g).

Proteomic profiling corroborated the species-specific patterns observed in bulk RNAseq and scRNAseq data. In DP and WB, proteins associated with antiviral and inflammatory pathways were broadly and progressively induced at 2, 4, and 7 dpi, with high numbers of upregulated proteins in both categories (Fig. 4l; Fig. S14, S15). In contrast, RRH and WH showed markedly fewer differentially abundant proteins in these pathways, with many time points remaining close to baseline.

MHC class II-dependent antigen presentation collapses in Eurasian pigs but is preserved in African suids

We next assessed how ASFV infection reshapes MHC class II-dependent antigen presentation across species by integrating scRNA-seq, bulk RNA-seq and proteomic profiling of circulating leukocytes. Across all modalities, DP and WB exhibited a near-complete collapse of MHC class II expression and MHC class II^+ cell signatures, whereas RRH and WH retained intact antigen-presentation programs throughout infection.

At the transcriptomic level in scRNAseq/RNAseq, DP and WB showed strong downregulation of canonical MHC class II genes, including *SLA-DRA/DRB*, *SLA-DQA/DQB* and *SLA-DPA/DPB*, together with multiple components required for antigen processing and peptide loading, such as *CD74*, *CTSS/L*, *PSMB8/10*, *TAP1/2* and *LAMP1/2* (Fig. 5a-c; Fig. S16, S17). Molecules involved in co-stimulation and immunological synapse formation, including *CD86*, and *ICAM1*, were similarly reduced (Fig. S18). This loss became most pronounced at peak disease (7 dpi), when expression of several genes dropped below detection thresholds relative to baseline. Non-classical MHC class II-associated genes, including *SLA-DMA/DMB* and *SLA-DOA/DOB*, followed the same pattern, indicating broad disruption of antigen processing and MHC class II-mediated presentation in Eurasian suids. In contrast, the MHC class I-processing/loading module score increased over the course of infection in all four species, indicating that ASFV infection selectively disrupts MHC class II-, rather than globally suppressing, antigen-presentation machinery (Fig. S16). RRH and WH

maintained stable expression of these pathways across all time points (Fig. 5b,c). Bulk RNAseq confirmed these findings (Fig. 5d,e; Fig. S18).

Proteomic analyses substantiated a functional shutdown of MHC class II-mediated antigen presentation in DP and WB (Fig. 5d; Fig. S19). Protein levels of MHC class II complexes (SLA-DR, SLA-DP, SLA-DQ), associated factors (CD74, LAMP1/2) and immunoproteasome components were reduced or failed to increase despite pronounced antiviral and inflammatory activation. In RRH and WH, MHC class II proteins and antigen-processing components remained comparatively stable. These findings aligned with flow cytometry and scRNAseq data demonstrating a near-complete loss of MHC class II$^+$ monocytes and other APC subsets in DP and WB, whereas stable frequencies of MHC class II$^+$ cells persisted in RRH and WH throughout infection. Multi-modal data (scRNAseq, bulk RNAseq, proteomics, and flow cytometry) consistently demonstrate a collapse of MHC class II$^+$ APCs in DP/WB versus preserved antigen-presenting capacity in RRH/WH.

Discussion

Our results reveal fundamental differences in host responses to ASFV infection between Eurasian (DP and WB) and African wild suids. African suids (RRH and WH). By experimentally infecting these four taxa under a harmonized study design, we show that disease outcome is determined less by susceptibility to infection itself than by the immune and cellular context in which viral replication occurs. Eurasian suids developed fulminant disease with high viraemia, widespread tissue dissemination, and severe pathology, whereas African suids remained clinically inapparent despite confirmed viral replication and seroconversion. Both RRH and WH were susceptible to infection with a highly virulent genotype II ASFV, yet avoided the monocyte-associated viral amplification, inflammatory dysregulation and collapse of antigen presentation that characterized fatal disease in Eurasian suids. Together, these findings support a model in which African wild suids tolerate ASFV through preservation of innate and adaptive immune function rather than sterilizing resistance[21], which is consistent with earlier observations that WH and *Potamochoerus* spp. can sustain ASFV infection with limited clinical disease despite detectable viraemia and viral distribution in tissues[7,8,10-12,20].

Although disease outcome is likely shaped by multiple immune compartments, our analyses identified divergent monocyte responses as a central correlate of susceptibility versus tolerance. This is consistent with the established tropism of ASFV for monocytes and macrophages[22,23] and with recent scRNA-seq studies demonstrating progressive infection of immature monocytes during acute ASFV infection[22]. Single-cell transcriptomic studies of ASFV-infected porcine alveolar macrophages have further shown that host-virus dynamics are strain-dependent, with an IRF7-mediated feedback loop distinguishing virulent from attenuated infection outcomes[24,25]. Moreover, virulent-strain *in vitro* infection of monocytes can selectively disrupt endoplasmic reticulum structure and function, driving SLA class I (MHC class I) surface downregulation, aggresome formation, and impaired antigen presentation, which is the mechanism demonstrated using the same *Armenia08* strain employed in the present study[26]. Our data extend these findings across distinct suid taxa *in vivo*. In DP and WB, expansion of ASFV-p72$^+$ monocytes closely tracked viraemia, inflammatory activation and fatal disease. In RRH and WH, monocytes remained abundant but

were only rarely ASFV-positive in circulation, indicating that susceptibility is not directly linked to the presence of target cells only. Instead, fatal ASF appears to require conversion of the myeloid compartment into a virus- and inflammation-amplifying environment. African suids, by contrast, mounted more restricted antiviral responses while avoiding systemic inflammatory escalation.

Transcriptomic and proteomic analyses further indicated that ASFV replication and immune-evasion programs remained quantitatively constrained in RRH and WH. In DP and WB, high expression of structural and immunomodulatory ASFV genes, including members of the *MGF360* and *MGF505* families, coincided with rapid systemic viral dissemination. Multiple ASFV MGF proteins interfere with IFN-I induction and signaling through effects on cGAS–STING, IRF3, JAK–STAT, and related pathways[14-16,19,27,28], and deletion of selected *MGF360/MGF505* genes attenuates virulence in experimentally infected pigs[17,29]. More specifically, MGF505-6R has been shown to target STING for autophagy-lysosomal degradation, blocking downstream IRF3 activation[30], and a systems-level mapping of individual ASFV MGF and non-MGF proteins onto sequential nodes of the cGAS-STING-TBK1-IRF3-NF-κB cascade illustrates how this gene family achieves redundant, multi-point interferon antagonism[31]. In contrast, African suids displayed substantially lower *in vivo* expression of these viral programs despite confirmed susceptibility to infection. Interestingly, purified WH monocytes supported robust viral protein accumulation *in vitro*, indicating that WH cells are not intrinsically non-permissive to ASFV replication. These findings suggest that tolerance in African suids depends less on cell-autonomous resistance mechanisms than on host-level restriction of viral amplification and immune feedback loops.

Another key observation was the dissociation between antiviral activation and protection. DP and WB mounted broad antiviral and inflammatory responses characterized by induction of interferon pathways, chemokines, and pro-inflammatory mediators. However, these responses failed to control viral dissemination and instead coincided with fever, complement activation, leukocyte dysregulation, and severe tissue pathology. This pattern is consistent with previous studies linking virulent ASFV infection to excessive cytokine responses, lymphoid depletion, and hemorrhagic disease[14,32]. Acute-phase protein responses, including Pig-MAP, have similarly been shown to track disease severity and clinical course in experimental ASF[33], and elevated CRP alongside leukopenia and thrombocytopenia has been documented specifically for genotype II isolates[34], consistent with the acute-phase signature observed here. In a related cohort infected with the same *Armenia08* strain used in this study, we previously showed that survivors mounted a restricted complement response (elevated C3a alone), whereas animals that succumbed to infection showed combined C3a and C5a activation linked to the lectin pathway[35], which is a distinction that parallels the dissociation between restrained and escalating inflammatory trajectories described here across suid taxa. In contrast, RRH and WH never entered a high systemic inflammatory state. WH displayed detectable antiviral activation, including IFN-α and ISG induction, but without progression towards the TNF-α-, IL-1Ra-, and acute-phase-associated signatures observed in fatal disease. Thus, protection in African suids does not reflect immunological silence, but is rather grounded in adequate antiviral responses with restricted inflammatory amplification.

Preservation of MHC class II-dependent antigen presentation emerged as a major mechanistic distinction between tolerant and susceptible hosts. In DP and WB, ASFV infection induced near-complete loss of MHC class II-positive cells together with broad downregulation of MHC class II genes, peptide-loading

machinery, and co-stimulatory molecules during peak viraemia. These findings are consistent with previous reports linking virulent ASFV infection to impaired antigen presentation and T-cell dysfunction[14,36]. This pattern extends beyond monocytes to dendritic cells: SLA-DR/DQ downregulation on both cell types has been documented alongside impaired T-cell cytokine production despite transient early activation[36], and dose- and severity-correlated repression of MHC class II pathway genes (including SLA-DQB1, SLA-DOB, SLA-DMB, SLA-DRA, and SLA-DQA1) has been reported across genetically diverse domestic pig populations[37], suggesting that the magnitude of MHC class II collapse scales with disease severity rather than representing an all-or-none phenomenon. By contrast, RRH and WH maintained stable MHC class II-associated programs throughout infection, despite detectable viral replication. Preservation of antigen-presenting function may therefore contribute to the ability of African suids to mount adaptive immune responses while avoiding progression towards systemic immune collapse.

These findings also refine current interpretations of the reservoir status of African wild suids. ASFV ecology in Africa is typically framed around asymptomatic WH and *Ornithodoros* ticks within a sylvatic cycle[6,7]. Our data demonstrate that clinically inapparent infection is compatible with transient viral replication, tissue dissemination, and adaptive immune activation, while remaining below the threshold for systemic inflammatory disease. Importantly, RRH and WH were both tolerant, but differed in the magnitude and distribution of viral replication and immune activation, arguing against a uniform “African suid phenotype”. RRH showed the most restricted systemic viral burden, whereas WH exhibited broader early tissue dissemination and greater monocyte permissiveness *in vitro*. These differences suggest that disease tolerance, reservoir competence and transmission potential may represent partially independent host traits shaped by species-specific immune regulation. However, studies with other pathogens in African suids are missing, which complicates generalized conclusions. Comparative genomic studies have implicated pathways involving *LDHB*, TRIM-family genes, and NF-κB-associated signaling in WH tolerance[38], although these remain starting points rather than comprehensive explanations of the tolerant phenotype. A gut-microbiome contribution has also been proposed: fecal microbiota transplantation from WH to DP confers partial protection against attenuated ASFV challenge, indicating that microbiome composition may act alongside host genetics in shaping tolerance[39]. Notably, previous single-cell work is confined to domestic-pig-derived macrophages[25,39] and transcriptomic or multi-omic studies of ASFV infection have investigated WH or *Potamochoerus* spp. tissue, positioning the comparative, multi-omic design used here as a first step toward closing this gap.

Our findings further hold implications for vaccine development. Protective immunity against ASFV remains incompletely defined, but successful control likely requires coordinated innate and adaptive immune responses, including preserved antigen presentation and effective T-cell activation[13]. Live attenuated candidates such as *ASFV-G-ΔI177L* can induce sterile immunity against circulating genotype II strains[40], and a systems-immunology analysis of a related gene-deletion vaccine identified early sustained IFN-α responses, induction of antigen-presentation-associated blood transcription modules, and controlled IL-8 alongside T cell memory induction as correlates of protection[41]. This is a profile that closely mirrors the preserved antigen-presentation and restrained inflammatory signature we observed in tolerant African suids. Live attenuated vaccine candidates based on targeted gene deletions have shown promise experimentally, yet concerns regarding safety, genetic stability, and reversion to virulence remain[42]. The tolerant phenotype

observed in African suids provides a complementary host-derived reference state. Effective vaccine-induced immunity may require preservation of antigen-presenting myeloid cells while limiting viral and inflammatory amplification loops that characterize fatal ASF. In this context, vaccine candidates should be evaluated not only for reduction of viraemia or antibody induction, but also for their capacity to preserve functional myeloid immune programs during early infection.

Several limitations should be considered when interpreting our findings. First, experimental group sizes were necessarily limited because African suids are only rarely available for controlled infection studies in Europe. Second, all animals studied were subadults or adults, whereas the natural sylvatic cycle is thought to involve WH piglets in association with *Ornithodoros* ticks[7]. Age-dependent differences in immune maturation may therefore influence susceptibility and disease outcome[43]. Third, infections were performed using a genotype II ASFV strain, which dominates outbreaks in Europe and Asia, but does not reflect ASFV ecology in the native origin of WH and RRH[44,45]. Finally, cross-species transcriptomic and proteomic comparisons remain constrained by differences in genome annotation, antibody compatibility, and orthology assignment. Nevertheless, the same species-associated separation was consistently observed across independent clinical, virological, cytometric, transcriptomic, proteomic, and pathological datasets, supporting the robustness of the central conclusions while highlighting the need for future functional studies in primary cells and tissues.

Methods

Animal origin, husbandry, experimental design and ethics

Due to housing capacities and availability of African wild pigs and Eurasian wild boar, the animal study was divided into two equivalent experimental cohorts. The initial cohort included six red river hogs (*Potamochoerus porcus*) and six domestic pigs (*Sus scrofa domesticus*), while the subsequent cohort comprised six common warthogs (*Phacochoerus africanus*) and six Eurasian wild boars (*Sus scrofa scrofa*). All animals were transferred to the Friedrich-Loeffler-Institut (FLI) Riems high containment facility at least 14 days prior to inoculation to facilitate acclimatization to the facility and personnel. The animals' origins included red river hogs and warthogs obtained from several German zoological institutions, domestic pigs from a commercial German pig farm, and wild boars from the FLI wild boar breeding group. The details regarding each individuals origin, age at inoculation, sex, and individual identifiers are provided in Table 1. All animals were fed species-appropriate diets to meet their nutritional requirements. All procedures performed within this study adhered to current German animal welfare regulations and received ethical approval from the competent authority (Landesamt für Landwirtschaft, Lebensmittelsicherheit und Fischerei Mecklenburg-Vorpommern [LALLF M-V]), file reference 7221.3-1-034/23. To ensure unequivocal individual identification, each animal was fitted with a unique ear tag upon arrival. Although the study was conducted in two sequential parts, experimental protocols were harmonized to enable direct comparison of results. While all domestic pigs were housed in a single pen, other species were separated into sub-groups to minimize stress and prevent hierarchical aggression. Wild boar were kept in two pens (comprising five and two animals, respectively, with the adult female in the second group). Red river hogs were housed separately according to their origin and sex. Warthogs were divided into three groups: two animals from

Magdeburg in the first, two animals from Münster in the second, and one animal each from Münster and Osnabrück in the third group. Each stable measured 24 m^2 and was enriched with periodically varying environmental stimuli. Animals were monitored 24/7 via remote camera systems and were daily checked for their general health status.

Table 1: Background information of all animals included in this study.

animal ID [#]	species	sex	origin	age at infection [months]
1	Eurasian wild boar	male	FLI	11
2	Eurasian wild boar	male	FLI	11
3	Eurasian wild boar	male	FLI	11
4	Eurasian wild boar	male	FLI	11
5	Eurasian wild boar	male	FLI	11
6	Domestic pig	male	German pig farm (BHZP)	5
7	Domestic pig	female	German pig farm (BHZP)	5
8	Domestic pig	male	German pig farm (BHZP)	5
9	Domestic pig	female	German pig farm (BHZP)	5
10	Domestic pig	female	German pig farm (BHZP)	5
11	Domestic pig	male	German pig farm (BHZP)	5
12	Red river hog	female	Opel-Zoo (Kronberg)	18
13	Red river hog	female	Opel-Zoo (Kronberg)	18
14	Red river hog	female	Opel-Zoo (Kronberg)	18
15	Red river hog	male	Cologne Zoo	19
16	Red river hog	male	Cologne Zoo	19
17	Red river hog	male	Cologne Zoo	19
18	Eurasian wild boar	female	FLI	36
19	Common warthog	male	Osnabrück Zoo	10
20	Common warthog	male	Allwetterzoo Münster	24
21	Common warthog	male	Allwetterzoo Münster	13
22	Common warthog	male	Allwetterzoo Münster	13
23	Common warthog	female	Magdeburg Zoo	23
24	Common warthog	male	Magdeburg Zoo	23

All animals received an intramuscular inoculation of 1 ml of the highly virulent ASFV strain *Armenia08* at a dose of 1×10^3 hemadsorbing units 50% (HAU_{50}). Intramuscular application was administered via short-range darting (3 ml dart syringe with a 1.2 x 38 mm needle, Telinject) with a blow pipe (B31.C, Telinject, length 1 m, caliber 11 mm) or via syringe (DP). To establish baseline (steady state) values for comparative analysis, each individual was sampled prior to inoculation (at 0 dpi). One warthog (#20) was euthanized at 0 dpi due to an unmanageable clinical condition resulting from *Trueperella pyogenes* infection. Subsequently, all animals were sampled at 2, 4, and 7 dpi. RRH and WH were further sampled at 14, 28, 42, 56, 70, 84, and 100 dpi, with 100 dpi designated as the end of the trial, at which point necropsies were performed on all remaining individuals. Throughout the experimental period, animals were monitored daily using a cumulative clinical scoring system adapted from Mittelholzer et al.[46], assessing behavioural alterations, including lethargy and anorexia, together with clinical manifestations such as skin lesions, haemorrhages, oedema, gastrointestinal and respiratory signs, and neurological impairment associated with African swine fever. Individual clinical parameters for the cumulative score were recorded from 0 to 3 according to severity. Predefined humane endpoints requiring immediate euthanasia irrespective of the cumulative score were defined for several parameters (table S2). Rectal temperatures were recorded daily

in domestic pigs, while in wild boar, red river hogs and warthogs measurements were restricted to sampling days to minimize handling-associated stress and ensure personnel safety. To enable comparative analyses of ASFV pathogenesis across species, a late humane endpoint was applied and animals were euthanized upon reaching a cumulative clinical score of 15 or upon manifestation of severe clinical signs considered incompatible with animal welfare, including paralysis or refractory neurological disease.

Sample collection and necropsy

Sampling involved collection of EDTA-blood for e.g. leukocyte isolation and qPCR, native (clotted) blood for serology, as well as oral and nasal swabs for evaluation of viral shedding. Blood was drawn from the *Vena jugularis externalis* using aspiration collection tubes (KABE Labortechnik). Domestic pigs were immobilized and sampled using a restraining sling applied to the upper jaw. All other animals were anesthetized via darting (3 ml dart syringe with a 1.2 x 38 mm needle, Telinject) with a blow pipe (B31.C, Telinject, length 1 m, caliber 11 mm) and a mixture of 0.06 mg/kg medetomidine (Dormitor®, Vetquinol), 0.3 mg/kg midazolam (Ethypharm), and 0.3 mg/kg butorphanol (Torbugesic® vet, Zoetis). After sample acquisition, anesthesia was reversed by intramuscular injection of 3.33 mg/kg atipamezole (Antisedan®, Vetquinol). Immediately following blood collection, 200 µl of whole blood were subjected to complete blood count (CBC) analysis on a ProCyte Dx hematology analyzer (IDEXX). Euthanasia prior to necropsy was performed by administering anesthetic agents as described above. In deep anesthesia, EDTA-blood was obtained via cardiac puncture, and animals were euthanized via intraventricular injection of pentobarbital sodium (Release, WDT). Necropsies were conducted either after reaching humane endpoints or at the scheduled terminal time point at 100 dpi. Additionally, to allow comparative pathological and dissemination studies, two red river hogs and one warthog were subjected to necropsy at 7 dpi (expected maximum for clinical score and viraemia in DP and WB), irrespective of their clinical status on that day. During necropsy, tissue samples from the following sites were collected for qPCR and virus isolation: central nervous system (cerebrum, cerebellum), lymphatic tissues (tonsils, spleen, bone marrow, mandibular, gastrohepatic, renal, draining, and mesenteric lymph nodes), thoracic tissue (lungs), and abdominal organs (liver, kidneys, small intestine, large intestine). Approximately 200 mg of each tissue were homogenized in a 2 ml centrifugation tube containing 1 ml of PBS (Thermo Fisher Scientific) and a 5 mm stainless steel bead using a tissue homogenizer (TissueLyzer II, Qiagen) at 30 Hz for 3 min. Additionally, ~ 8 g of each tissue were stored at -80°C for subsequent analyses.

Histopathological analyses

Formalin-fixed tissue samples were routinely processed, paraffin embedded and sectioned at 2-3µm thickness. Sections were stained with hematoxylin and eosin (H&E) for histomorphological evaluation.

During necropsy, a comprehensive panel of tissues was collected from all animals. However, for the present study, analyses were focused on the spleen, as this organ consistently exhibited detectable viral antigen across all investigated suid taxa and thus allowed for a robust comparative assessment and correlation with histopathological changes. Histopathological evaluation was performed based on

previously described ASF-associated splenic lesions, encompassing alterations of the white pulp (lymphoid depletion, fibrinonecrotizing vasculitis, hemorrhages) and red pulp (congestion and necrosis)[47-50].

On consecutive sections, immunohistochemistry was performed to detect viral antigen as described previously[51]. Briefly, sections were incubated for 1h at room temperature with an in-house generated rabbit polyclonal antibody directed against the major capsid protein p72 of ASFV (1:1600 dilution in TBS). This was followed by incubation with a goat-anti-rabbit secondary antibody (1:200 dilution in TBS) for 30 min at room temperature. Antigen detection was visualized using the avidin-biotin complex (ABC) method with horseradish peroxidase converting the chromogen 3-amino-9-ethylcarbazole (AEC) into insoluble red-reaction products at sites of antigen localization.

Consecutive sections incubated with an irrelevant antibody directed against the matrix (M) protein of Influenza A virus (ATCC clone Hb64) served as negative controls. ASF-positive tissue was included as a positive control. Slides were digitized using a Hamamatsu S60 scanner and evaluated using NDPview.2 plus software (Version 2.8.24, Hamamatsu Photonics, K.K. Japan). Histopathological changes were scored using an ordinal scale ranging from 0 to 4: 0 = no lesion, 1 = minimal, 1-3 foci (5%); 2 = mild, multifocal (6-40%); 3 = moderate; coalescing (41-80%), 4 = severe, diffuse (>80%). The distribution of viral antigen was assessed in the most severely affected area (800 × 450 µm) of each tissue section and scored on a scale from 0 to 4: 0 = no antigen, 1 = 1-3 cells, 2 = 4-15 cells, 3 = 16-30 cells, 4 = > 30 cells).

Virus titration, virus isolation, and in vitro inoculation of purified monocytes

To prepare darts or syringes for inoculation, a cell culture supernatant containing ASFV *Armenia08* was used. The virus was propagated on primary porcine monocytes derived from freshly isolated peripheral blood mononuclear cells (PBMCs). For PBMC isolation, EDTA-blood obtained from healthy donor domestic pigs housed at the FLI quarantine facility. Whole EDTA-blood was mixed with a 10% Hanks' dextran solution (0.0001 M DEAE-dextran in ddH_2O) at a 1:10 ratio, and separation was performed at room temperature (RT) for 90 min. The cell-rich supernatant was then collected and washed with PBS containing 2.5 mM EDTA (PBS-EDTA). Cells were seeded at a density of 3×10^6 cells/ml into 175 cm^3 flasks using Dulbecco's Modified Eagle's Medium (DMEM), supplemented with 10% fetal calf serum and 0.01% penicillin/streptomycin. The cells were maintained for 48 h prior to inoculation with ASFV *Armenia08*; added at a volume of 500 µl of ASFV-containing supernatant (titer: 1×10^5 HAD_{50}/ml) per 10 ml of PBMC suspension. After incubation for 48 h at 37°C and 5% CO_2 in a humidified atmosphere, flasks were frozen at -80°C to facilitate virion release.

For virus titration, PBMCs were isolated and seeded as described above into 96-well plates. Post-Hanks' dextran separation, the fraction containing red blood cells (RBCs) was collected and diluted 1:10 in 1x PBS for hemadsorption tests (HATs). After an incubation of 48 h, ASFV-containing inocula was added to the cells (100 µl/well) in a 10-fold serial dilution. All titrations were performed in triplicate, with four replicate wells per dilution. After 24 h, donor-specific RBCs were added to each well at a ratio of 1:40. Results were evaluated at 24 h and 48 h post-infection. These HATs served both to titrate the inoculum prior to experimental use, ensuring adequate ASFV titers for infection of the animals, and as a subsequent back-titration to validate

viral quantity. Furthermore, to assess the early innate response of monocytes, the ASFV target cells, monocytes from each individual were isolated via magnetic enrichment and infected with ASFV *Armenia08 in vitro*. In brief, PBMCs obtained at 0 dpi, prior to ASFV exposure, were subjected to magnetic enrichment using an anti-pig CD172a antibody. Initially, PBMCs were washed with 1 × IMag buffer (BD Biosciences with 0.09% sodium azide), centrifuged at 350 × g at 4°C for 5 min, and incubated with a primary mouse IgG1 anti-pig-CD172a monoclonal antibody (mouse IgG1, clone 74-22-15, in-house) at a 1:10 dilution for 15 min at 4°C. After washing, cells were incubated with BD IMag magnetic particles (10 µl per 10^7 cells, BD Biosciences) for 30 min at 4°C. Magnetically labelled cells were then separated by incubation on a magnet for 6 min at RT. Supernatant, containing non-labelled cells, was removed in between incubation steps. The magnetically retained cells were resuspended in sorting buffer and incubated on the magnet for an additional 3 minutes at RT, repeated twice to enrich for CD172a-positive monocytes. For each individual, 1×10^4 monocytes were seeded into eight wells of a 96-well Primaria plate (Thermo Fisher Scientific) in DMEM. ASFV *Armenia08* was added to four wells at an estimated MOI of 2. To investigate early cellular responses to ASFV infection, cells were harvested 6 h, 12 h, 24 h, and 48 h after inoculation, resulting in paired samples of infected (ASFV+) and uninfected (ASFV-) cells per individual.

DNA extraction and qPCR

For nucleic acid extraction, tissue homogenates and whole blood were processed using the Nucleo-Mag VET Kit (Macherey-Nagel) on a KingFisher 96 Flex platform (Thermo Fisher Scientific), according to manufacturer's instructions. For EDTA-blood, 80 µl were used for extraction, whereas 100 µl of tissue homogenate were used. An ASFV genome-negative serum sample served as extraction control. For qPCR, the virotype ASFV 2.0 PCR kit (Indical) was used in accordance with manufacturer's instructions for multiplexed detection of the ASFV genome (FAM), porcine ACTB gene as internal reference control (HEX), and a heterologous internal control to ensure inhibition-free performance (Cy5). All qPCR reactions were conducted on a Bio-Rad C1000 thermal cycler equipped with the CFX96™ Real-Time System (Bio-Rad). ASFV genome copy numbers were quantified relative to a standard curve derived from a PCR standard containing a known quantity of ASFV DNA (8×10^7 genome copies/ml) in RSB_{50} buffer (RNA-safe-buffer: 50 ng/µL carrier RNA, 0.05% Tween-20, and 0.05% sodium azide in UltraPure DNase/RNase-free water (Invitrogen)).

Leukocyte isolation for multiomics

Immediately after sample collection, whole blood was subjected to leukocyte isolation to preserve optimal cell viability. Initially, 2 ml of whole blood was mixed with 5 ml of 1 x RBC lysis buffer (BioLegend) and incubated at RT until translucent (~ 5 min). Cells were washed with cold 1 x PBS-EDTA to avoid cell aggregate formation and centrifuged at 350 × g for 10 min at 4°C. The pellet was examined and RBC lysis was repeated if a significant residual RBC presence was observed. After washing, the cell pellet was resuspended in cold TRIzol LS reagent (Thermo Fisher Scientific). The aqueous phase was collected for RNA isolation and subsequent bulk-RNA-seq, while the organic phase was utilized for protein isolation prior to mass spectrometry analysis (MS).

For scRNAseq and corresponding proteomic analyses of PBMCs, the remaining whole blood (~ 16 ml) was subjected to density gradient centrifugation. In brief, 8 ml of whole blood was layered onto 4 ml of Pancoll animal with a density of 1.077 g/ml (PAN Biotech) and centrifuged at 760 × g for 30 min without brakes or acceleration. Mononuclear cells were collected, washed twice with 13 ml PBS-EDTA-BSA (1x PBS, supplemented with 2.5 mM EDTA and 20 µg/ml UltraPure BSA (Thermo Fisher Scientific)). Remaining plasma was collected and subjected to plasmacytological analysis. Cells were counted and set to 3×10^5 cells/ml in PBS-EDTA-BSA. A total of 200,000 cells were lysed in 1 ml of TRIzol LS reagent and stored at -80°C for proteomic analysis. For scRNAseq, 500 µl of the cell suspension was filtered through 70 µm Flowmi cell strainers (Sigma Aldrich) into Protein LoBind tubes (Eppendorf) until loading of the scRNAseq chip, to minimize leukocyte loss.

Serology and plasmacytology

To assess the kinetics of ASFV-specific antibody responses, all serum samples were analyzed using multiple serological methodologies. Initially, antibodies targeting ASFV were detected employing two commercially available ELISA kits: the ID Screen® ASF Competition (ID.vet), which identifies antibodies directed against ASFV-p32, and the INgezim PPA COMPAC (Gold Standard Diagnostics), which detects ASFV-p72 targeting antibodies. All assays were performed in accordance with manufacturer's instructions. Given that these kits are specifically detecting antibodies targeting distinct ASFV proteins, an indirect ELISA protocol was employed to assess total ASFV-specific IgG in all sera. Purified ASFV-antigen was sourced from the European Union Reference Laboratory for ASF (EURL-ASF), CISA-INIA (Spain). Microtiter plates (medium-binding capacity, Greiner) were coated with ASFV antigen in sodium carbonate buffer, as described in the SOP provided by the EURL-ASF (SOP/CISA/ASF/ELISA/1, REV.5, 2021). In brief, all plates were washed after incubation overnight, then washed, dried, and stored at -20°C until further use. To minimize nonspecific binding, all plates were blocked with 1 x PBS supplemented with 5% horse serum for 3 h at RT. Serum samples were diluted 1:30 with wash buffer (1 x PBS containing 0.05% Tween-20) immediately prior to assay execution. Following incubation and washing, a polyclonal anti-pig IgG HRP-conjugated secondary antibody (Biomol) was added at a 1:10,000 dilution. Signal was acquired using an ELISA reader (TECAN). Additionally, the semiquantitative ASFV-specific IgG titers were determined for each serum sample via immunoperoxidase test (IPT), which is regarded as the most sensitive serological assay for accurate detection of ASFV-targeting antibodies. The IPT was performed following the SOP provided by the EURL-ASF (SOP/CISA/ASF/IPT/1). Serial dilutions of each serum sample included: 1:40, 1:200, 1:1,000, 1:5,000, 1:25,000, 1:50,000, 1:100,000, 1:125,000, and 1:625,000.

Furthermore, plasma samples from all animals were subjected to quantitative assessment of various humoral inflammation and immune system activation markers. Acute phase proteins (APPs) specifically C-reactive protein (CRP, MyBioSource) and pig major acute-phase protein (MAP, MyBioSource), along with activated complement factors (C3a and C5a, MyBioSource) were quantified by ELISA Additionally a panel of pro- and anti-inflammatory cytokines was included in the analysis: IL-1Ra (R&D), IL-1β (R&D), TNF-α (R&D), IL-10 R&D), and IFN-α (Invitrogen). Evaluation of all humoral markers was performed on plasma samples, as evidence indicates that plasma provides superior sensitivity and specificity for detecting soluble biomarkers compared to serum samples[52]. Since all commercially available ELISA kits used in this study

are licensed exclusively for domestic pig (and wild boar as both are considered the same species), a protein homology analysis was conducted to confirm potential cross-reactivity with orthologous proteins in red river hog and warthog (Table S3).

Bulk-RNA-sequencing (bulk-RNA-seq)

Total RNA was isolated from the aqueous phase of all whole blood leukocyte trizol samples using the RNAdvance Tissue kit (Beckman Coulter) according to manufacturer's instructions on an automated KingFisher platform. From the extracted total RNA, mRNA was further purified utilizing the Dynabeads® mRNA DIRECT™ Micro kit (Invitrogen) in conjunction with the ERCC RNA Spike-In Mix kit (Invitrogen). The ERCC Spike-In kit incorporates a standardized set of external RNA controls, facilitating the evaluation of technical variability attributable to factors such as initial input material, RNA yield, or extraction efficiency. The purified mRNA was quantified and assessed for integrity using High Sensitivity RNA ScreenTapes (Agilent) with the corresponding RNA ladder (Agilent) and sample buffer (Agilent). The ScreenTape assays were conducted on an Agilent TapeStation system. After all mRNA samples passed quality testing, they were subjected to library preparation for Illumina sequencing. Library construction was performed using the Collibri™ Stranded RNA Library Prep Kit (Invitrogen), adhering to manufacturer's instructions. During the library amplification step, all libraries were indexed with unique dual indices (UDIs) to enable accurate sample demultiplexing after sequencing as multiplexed pools. Quantification and quality control of prepared libraries were conducted using DNA D1000 ScreenTapes (Agilent) with the associated DNA ladder (Agilent) and sample buffer (Agilent) on the TapeStation system. After libraries were found to be of satisfactory quality, sequencing was performed at Novogene on an Illumina NovaSeq 6000 instrument.

Bulk-RNAseq - Data analysis

Raw reads were subsequently trimmed using TrimGalore (v0.6.10; (70)) and then analyzed using the nf-core "RNAseq" pipeline (version 3.14.0). In detail, the domestic pig reference genome GCF_000003025.6 was used for splice-aware mapping with STAR (v2.7.9a) and subsequent quantification with salmon (v1.10.1). The quantification data was then further analyzed in R (version 4.3.1) and differentially expressed genes (DEGs) were deduced using the DESeq2 package (v1.40). Log2-fold changes were shrinked using the function "lfcShrink" with the "apeglm" shrinkage estimator. The cut-off values for DEGs were set to absolute shrinked log2-fold change > 1 and adjusted p-value < 0.05. Raw count data were transformed using the regularized log (RLD) transformation implemented in DESeq2. The RLD transformation was applied to stabilize the variance across the expression range and to reduce the dependence of variance on the mean, which is typical for count-based RNA-seq data. The resulting RLD values were used for exploratory data visualization. To explore global gene expression patterns, principal component analysis (PCA) was performed using R (version 4.3.1) on the RLD-transformed expression values. In addition, RLD values of selected genes were extracted and combined with the corresponding sample metadata to visualize gene expression kinetics over time. Individual animals and/or group-level mean trends were displayed to describe temporal expression patterns across species and infection conditions. Bulk-RNAseq data have been deposited in ArrayExpress under accession E-MTAB-XXXX.

Single-cell-RNA-sequencing (scRNAseq)

To generate libraries for scRNAseq, the GEXSCOPE Single Cell RNA Library Kit V2 (Singleron Biotechnologies) was employed according to manufacturer's instructions. Initially, a suspension of 3×10^4 cells in 100 µl of each individual within a species was pooled immediately prior to loading onto the SCOPE-chip SD included in the kit. An overview of pooled individuals for each library is provided in Table S4. All cDNA synthesis and library preparation steps were performed in DNA LoBind tubes (Eppendorf) to avoid transcript loss. Generated cDNAs and libraries were assessed for quality using a BioAnalyzer with HD-chip technology. During the library amplification process, all libraries were indexed with an UDI. Sequencing was conducted on an Illumina NovaSeq 6000 in paired-end mode (28 cycles for Read 1 and 91 cycles for Read 2) at Singleron Biotechnologies.

Raw Data Processing and Read Alignment

Single-cell RNA sequencing libraries were processed using the Singleron CeleScope RNA workflow (https://github.com/singleron-RD/CeleScope/tree/master/celescope/rna). Raw sequencing reads from domestic pig, wild boar, red river hog, and warthog samples were aligned to the *Sus scrofa* (Sscrofa11.1) NCBI reference genome (GCF_000003025.6). The CeleScope pipeline performed cell barcode correction, UMI counting, and gene expression quantification, (https://www.ncbi.nlm.nih.gov/datasets/genome/GCF_000003025.6/).

scRNAseq - Quality Control and Preprocessing

A unified features file was constructed combining manual annotations[53], UniProt database entries, and biomaRt conversions (v2.64.0[54]) to ensure consistent gene nomenclature across samples. Since all four species were aligned to the same Sus scrofa reference genome (Sscrofa11.1: GCA_000003025.6 GCF_000003025.6) , no ortholog mapping was required. Features files from each species were merged, deduplicated by ENSEMBL gene ID, and duplicate gene symbols were resolved using numbered suffixes. Ambient RNA contamination was removed using SoupX (v1.6.2[55]) on a per-sample basis. Potential doublets were identified using scDblFinder[56] applied individually to each sample.

Cells were filtered based on the following criteria: minimum 200 detected features per cell, minimum 500 total UMI counts per cell, and maximum 15% mitochondrial gene expression. Mitochondrial percentages were calculated using curated mitochondrial genes (*ND1, ND2, COX1, COX2, ATP8, ATP6, ND3, ND4L, ND4, ND5, ND6*).

scRNAseq - Data Integration and Analysis

Gene expression data were normalized using Seurat's (v5.3.0[57]) NormalizeData() function with default parameters. Variable features were identified using variance stabilizing transformation, and data were scaled using Seurat's standard workflow. To correct for technical variation between species and timepoints, Harmony integration (v1.2.4[58]) was applied to the first 20 principal components. Unsupervised clustering was performed using the Louvain algorithm at resolution 1.0 applied to Harmony-corrected principal

components. UMAP was used for two-dimensional visualization. Low-quality clusters were identified and removed based on poor gene expression profiles.

scRNAseq - Cell Type Annotation

Cell type identification was performed using multiple complementary approaches: SingleR annotation (v2.10.0[59]) with the Monaco Immune Cell Database[60], Azimuth mapping[61], scType analysis[62], and manual annotation using established immune cell markers from Herrera-Uribe et al.[53]. Final cell type assignments integrated results from all annotation methods with manual curation based on canonical marker gene expression patterns.

Flow cytometry

For flow cytometry, 100 µl of whole blood were subjected to washing with FACS buffer (1x PBS supplemented with 2 mM EDTA, and 1% FCS). All centrifugation steps were performed at 350 × g for 5 min at 4°C, and all incubation steps were conducted at 4°C in the dark for 15 min unless stated otherwise. Antibodies for surface and intracellular marker staining are detailed in Table S5. A fixable viability dye, Zombie Aqua (BioLegend), was included in all stainings to discriminate and exclude dead cells. Prior to fixation and permeabilisation, RBC lysis was performed using 1x RBC lysis buffer as described above. Following RBC lysis, cells were fixed using fixation buffer (BioLegend). Intracellular staining was performed by incubating the cells with respective antibodies for 30 min at RT in the dark. Intracellular antibodies were diluted in 1x Intracellular Staining Permeabilisation Wash Buffer (BioLegend), with all subsequent washing steps performed using the same buffer. A minimum of 10^5 live, singlet cells were analyzed per sample. Data acquisition was executed on a BD Symphony A3 flow cytometer equipped with five lasers (UV 355 nm, Violet 405 nm, Blue 488 nm, Yellow-Green 560 nm, Red 633 nm) and 28 fluorescence detection channels (UV 7, Violet 8, Blue 6, Yellow-Green 4, Red 3), using BD FACS DIVA Software (BD Biosciences). Data analysis was conducted with FlowJo v10.10 software (BD Biosciences). A comprehensive gating strategy to delineate leukocyte subsets is illustrated in Fig. S20, representative plots for each species are presented in Fig. S21.

Mass spectrometry

For MS analysis the proteins were isolated from TRIzol samples of whole blood leukocytes (corresponding to bulk-RNA-seq) or from purified and *in vitro* inoculated monocytes as suggested by the manufacturer (Thermo Fisher). After the protein precipitation step, protein pellets were resuspended in 100 µL sodiumdeoxycholate (SDC) lysis buffer (1% SDC, 0.1 M TRIS-HCl, pH 8.5) and lysed for 10 min at 95°C. After centrifugation for 10 min at 14,000 x g and 4°C, the clear protein lysate was recovered and the protein concentration measured by BCA[63] assay. Aliquots containing 10 µg protein were digested using an in-solution protocol based on earlier publications[64,65]. In short, proteins were reduced and alkylated by addition of Tris(2-carboxyethyl)phosphin-hydrochlorid/2-Chloracetamid to final concentrations of 10 mM and 40 mM, respectively, and shaking for 10 min at 45°C and 800 rpm. After cooling to 20°C, trypsin (Promega) was added at an enzyme to protein ratio of 1:100 and digestion was carried out over night by shaking at 600 rpm

at 37°C. Then, SDC was precipitated by addition of 10% TFA to a final concentration of 1% and removed by centrifugation for 5 min 14,000 g and 4°C. The supernatant was transferred to a new LoBind Eppendorf microcentrifugation tube and the centrifugation was repeated for a complete removal of SDC. This final supernatant was desalted with in-house prepared STAGE[66] tips, and 800 ng samples were measured on a MS platform consisting of a nanoElute II nano HPLC and a timsTOF HT mass spectrometer (Bruker). Peptides were separated on a reversed-phase analytical column (25 cm × 75 µm i.d., Ionopticks Aurora3) with a binary gradient from 2 to 34% acetonitrile (ACN) using 0.1% formic acid in water (solvent A) and in ACN (solvent B), respectively. For the *in vitro* infected macrophages, a 60 min gradient was applied (B concentrations raised to 2%, 15%, 24%, 34% at 0, 38, 52, and 60 min, respectively), for the leukocytes, a 30 min gradient (B concentrations raised to 2%, 24%, 34% at 0, 24, 30 min, respectively) was used. The flow rate was 300 nl/min and the column temperature was maintained at 40°C. MS analysis of eluting peptides was performed in dia-PASEF mode as recommended by the manufacturer of the mass spectrometer for proteomic samples. For the database query as well as the calculation of the spectral library, DIANN software[67] (version 1.9) was used. A spectral library was precalculated representing the Uniprot[68] porcine proteome and the ASFV proteome of the *Georgia 2007/1* isolate (GenBank[69] accession FR682468.2), downloaded on February 20th 2024. For the query of the spectra, carbamidomethylation was set as fixed modification, methionine oxidation and N-terminal acetylation were allowed as optional modifications. A maximum of two missed cleavages per peptide was allowed. DIANN results were processed with R scripts[70,71] and manually evaluated with Perseus software[72] (version 2.0.11). Heatmaps were generate with the heatmap R-package[73]. MS data was uploaded to the PRIDE repository[74].

Statistical analyses

Flow cytometry, qPCR, CBC, plasmacytology

Analysis was performed using GraphPad Prism 10 (GraphPad Software Inc.). Shapiro-Wilk normality testing was employed for data distribution assessment. Mixed-effects models were employed to evaluate statistical significance between species. For multiple comparisons, the Tukey post-hoc testing was applied for correction. Statistically significant differences were defined as $P < 0.05$. To facilitate readability, statistical significances, independent of exact *p* values, are depicted as compact letter display in each figure legend. Single letters ('a', 'b', 'c') indicates a result with no statistical significance, while use of multiple letters indicate statistical significance. Exact descriptions are provided in each figure legend. ChatGPT was used to improve the readability and language of the manuscript; it did not contribute to the scientific content, study design, data analysis, interpretation, or conclusions.

Acknowledgements

We would like to thank Ulrike Kleinert, Barbara Bettin, and Anja Schulz for excellence during sample preparation and conduction of experiments. Further, we would like to thank Matthias Jahn, Domenique Lux, Patrice Mary, and Steffen Brenz for excellent animal husbandry. Additionally, we thank Andreas Bath, Marco Beerbohm, and Ralf Henkel for assistance during necropsies. We thank Aparna Sekar, Rulla

Gabarine and Charlotte Münch (Singleron Biotechnologies) for continuous support in establishing the scRNAseq pipeline in the high containment facility of FLI. Furthermore, we thank Tomasz Rusek, Danny de Man, Bengt Holst, Volker Homes, and Julia Kögler for continued support, especially in the preparatory phase of the study.

Author Contributions

Conceptualization: S.B., J.B., V.F., F.J., S.K., M.B.; Methodology: S.B., V.F., A.S., Q.W., A.K., F.P., J.B. ; Investigation – Animal sampling: S.B., V.F., A.S., J.B.; Investigation – qPCR, serology, flow cytometry: V.F., A.S., N.B., M.T.; Investigation – RNAseq library generation, sequencing, analysis: VF., M.E., F.P.; Investigation – scRNAseq library generation, sequencing, analysis: V.F., A.S., Q.W.; Investigation – proteome library generation, mass spectrometry, analysis: R.K., A.K.; Investigation – pathology, histopathological analysis: A.B., T.B., V.F., A.S., S.B., J.S.-E.; Resources: S.B., M.B., J.B., Study Group wild pigs, Q.W.; Data curation: V.F., A.S., A.K., Q.W., F.P., J.S.-E.; Formal analysis: V.F., A.S., Q.W., A.K., F.P., J.S.-E.; Visualization: V.F., A.S., Q.W., A.K., F.P., J.S.-E.; Writing – original draft: V.F.; Writing – review & editing: all co-authors; Supervision: S.B., V.F., A.S., M.B.; Project administration: S.B.; Funding acquisition: S.B., J.B.

Data Availability

The single-cell RNA sequencing (scRNA-seq) and bulk RNA sequencing (RNA-seq) data are available in Data Repository Array Express. The mass spectrometry proteomics data have been deposited to the ProteomeXchange Consortium via the PRIDE[74] partner repository. All data in available upon request from the corresponding authors.

Competing interests

The authors declare no competing interests.

References

1 WOAH, W. O. f. A. H. African swine fever (ASF) Situation Report 74. (2026).

2 Gaudreault, N. N., Madden, D. W., Wilson, W. C., Trujillo, J. D. & Richt, J. A. African Swine Fever Virus: An Emerging DNA Arbovirus. *Front Vet Sci* **7**, 215 (2020). https://doi.org/10.3389/fvets.2020.00215

3 Sanchez-Vizcaino, J. M., Mur, L., Gomez-Villamandos, J. C. & Carrasco, L. An update on the epidemiology and pathology of African swine fever. *J Comp Pathol* **152**, 9-21 (2015). https://doi.org/10.1016/j.jcpa.2014.09.003

4 Luskin, M. S. *et al.* African swine fever threatens Southeast Asia's 11 endemic wild pig species. *Conservation Letters* **14**, e12784 (2021).

5 Luskin, M. S. *et al.* The mass mortality of Asia's native pigs induced by African swine fever. *Wildlife Letters* **1**, 8-14 (2023). https://doi.org/10.1002/wll2.12009

6 Jori, F. *et al.* Review of the sylvatic cycle of African swine fever in sub-Saharan Africa and the Indian ocean. *Virus Res* **173**, 212-227 (2013). https://doi.org/10.1016/j.virusres.2012.10.005

7 Penrith, M. L., Bastos, A. D., Etter, E. M. C. & Beltran-Alcrudo, D. Epidemiology of African swine fever in Africa today: Sylvatic cycle versus socio-economic imperatives. *Transbound Emerg Dis* **66**, 672-686 (2019). https://doi.org/10.1111/tbed.13117

8 Anderson, E. C., Hutchings, G. H., Mukarati, N. & Wilkinson, P. J. African swine fever virus infection of the bushpig (Potamochoerus porcus) and its significance in the epidemiology of the disease. *Vet Microbiol* **62**, 1-15 (1998). https://doi.org/10.1016/s0378-1135(98)00187-4

9 Detray, D. E. African Swine Fever. *Adv Vet Sci* **8**, 299-333 (1963).

10 Luther, N. J. *et al.* Detection of African swine fever virus genomic DNA in a Nigerian red river hog (Potamochoerus porcus). *Vet Rec* **160**, 58-59 (2007). https://doi.org/10.1136/vr.160.2.58

11 Oura, C. A., Powell, P. P., Anderson, E. & Parkhouse, R. M. The pathogenesis of African swine fever in the resistant bushpig. *J Gen Virol* **79 (Pt 6)**, 1439-1443 (1998). https://doi.org/10.1099/0022-1317-79-6-1439

12 Ståhl, K. *et al.* Understanding the dynamics and spread of African swine fever virus at the wildlife-livestock interface: insights into the potential role of the bushpig, Potamochoerus larvatus. (2014).

13 Schäfer, A. *et al.* Adaptive Cellular Immunity against African Swine Fever Virus Infections. *Pathogens* **11** (2022). https://doi.org/10.3390/pathogens11020274

14 Zhu, J. J. *et al.* Mechanisms of African swine fever virus pathogenesis and immune evasion inferred from gene expression changes in infected swine macrophages. *PLoS One* **14**, e0223955 (2019). https://doi.org/10.1371/journal.pone.0223955

15 de Oliveira, V. L. *et al.* A novel TLR3 inhibitor encoded by African swine fever virus (ASFV). *Arch Virol* **156**, 597-609 (2011). https://doi.org/10.1007/s00705-010-0894-7

16 Granja, A. G., Sanchez, E. G., Sabina, P., Fresno, M. & Revilla, Y. African swine fever virus blocks the host cell antiviral inflammatory response through a direct inhibition of PKC-theta-mediated p300 transactivation. *J Virol* **83**, 969-980 (2009). https://doi.org/10.1128/JVI.01663-08

17 Ding, M. *et al.* Combinational Deletions of MGF360-9L and MGF505-7R Attenuated Highly Virulent African Swine Fever Virus and Conferred Protection against Homologous Challenge. *J Virol* **96**, e0032922 (2022). https://doi.org/10.1128/jvi.00329-22

18 Oura, C. A. L., Denyer, M. S., Takamatsu, H. & Parkhouse, R. M. E. In vivo depletion of CD8+ T lymphocytes abrogates protective immunity to African swine fever virus. *J Gen Virol* **86**, 2445-2450 (2005). https://doi.org/10.1099/vir.0.81038-0

19 Lv, P. *et al.* Immunoevasion strategies for African swine fever virus: Modulation of antigen presentation pathways. *Virulence* **16**, 2541711 (2025). https://doi.org/10.1080/21505594.2025.2541711

20 Montgomery, R. E. On a form of swine fever occurring in British East Africa (Kenya Colony). *Journal of comparative pathology and therapeutics* **34**, 159-191 (1921).

21 Medzhitov, R., Schneider, D. S. & Soares, M. P. Disease tolerance as a defense strategy. *Science* **335**, 936-941 (2012). https://doi.org/10.1126/science.1214935

22 Zhu, Z. *et al.* Single-cell profiling of African swine fever virus disease in the pig spleen reveals viral and host dynamics. *Proc Natl Acad Sci U S A* **121**, e2312150121 (2024). https://doi.org/10.1073/pnas.2312150121

23 Zsak, L. *et al.* African swine fever virus multigene family 360 and 530 genes are novel macrophage host range determinants. *J Virol* **75**, 3066-3076 (2001). https://doi.org/10.1128/JVI.75.7.3066-3076.2001

24 Zheng, Y. *et al.* Transcriptome profiling in swine macrophages infected with African swine fever virus at single-cell resolution. *Proc Natl Acad Sci U S A* **119**, e2201288119 (2022). https://doi.org/10.1073/pnas.2201288119

25 Zhao, X. *et al.* Diversities of African swine fever virus host-virus dynamics revealed by single-cell profiling. *J Virol* **99**, e0203524 (2025). https://doi.org/10.1128/jvi.02035-24

26 Brose, L. *et al.* Virulent African swine fever virus infection of porcine monocytes causes SLA I subversion due to loss of proper ER structure/function. *J Immunol* **214**, 532-550 (2025). https://doi.org/10.1093/jimmun/vkae063

27 Wang, S. *et al.* Cytokine Storm in Domestic Pigs Induced by Infection of Virulent African Swine Fever Virus. *Front Vet Sci* **7**, 601641 (2020). https://doi.org/10.3389/fvets.2020.601641
28 Wu, L. *et al.* Regulation and Evasion of Host Immune Response by African Swine Fever Virus. *Front Microbiol* **12**, 698001 (2021). https://doi.org/10.3389/fmicb.2021.698001
29 Rathakrishnan, A. *et al.* Differential Effect of Deleting Members of African Swine Fever Virus Multigene Families 360 and 505 from the Genotype II Georgia 2007/1 Isolate on Virus Replication, Virulence, and Induction of Protection. *J Virol* **96**, e0189921 (2022). https://doi.org/10.1128/jvi.01899-21
30 Yao, M. *et al.* African swine fever virus MGF505-6R attenuates type I interferon production by targeting STING for degradation. *Front Immunol* **15**, 1380220 (2024). https://doi.org/10.3389/fimmu.2024.1380220
31 Lin, C. *et al.* How Does African Swine Fever Virus Evade the cGAS-STING Pathway? *Pathogens* **13** (2024). https://doi.org/10.3390/pathogens13110957
32 Franzoni, G., Pedrera, M. & Sanchez-Cordon, P. J. African Swine Fever Virus Infection and Cytokine Response In Vivo: An Update. *Viruses* **15** (2023). https://doi.org/10.3390/v15010233
33 Carpintero, R. *et al.* Pig major acute-phase protein and apolipoprotein A-I responses correlate with the clinical course of experimentally induced African Swine Fever and Aujeszky's disease. *Vet Res* **38**, 741-753 (2007). https://doi.org/10.1051/vetres:2007030
34 Walczak, M. *et al.* Blood Counts, Biochemical Parameters, Inflammatory, and Immune Responses in Pigs Infected Experimentally with the African Swine Fever Virus Isolate Pol18_28298_O111. *Viruses* **13** (2021). https://doi.org/10.3390/v13030521
35 Friedrichs, V. *et al.* Duration of immunity following infection with moderately virulent ASFV. *PLoS Pathog* **22**, e1014018 (2026). https://doi.org/10.1371/journal.ppat.1014018
36 Tian, Y. *et al.* Immune cell early activation, apoptotic kinetic, and T-cell functional impairment in domestic pigs after ASFV CADC_HN09 strain infection. *Front Microbiol* **15**, 1328177 (2024). https://doi.org/10.3389/fmicb.2024.1328177
37 Machuka, E. M. *et al.* Transcriptome profile of spleen tissues from locally-adapted Kenyan pigs (Sus scrofa) experimentally infected with three varying doses of a highly virulent African swine fever virus genotype IX isolate: Ken12/busia.1 (ken-1033). *BMC Genomics* **23**, 522 (2022). https://doi.org/10.1186/s12864-022-08754-8
38 Feng, W. *et al.* Comparative Genomic Analysis of Warthog and Sus Scrofa Identifies Adaptive Genes Associated with African Swine Fever. *Biology (Basel)* **12** (2023). https://doi.org/10.3390/biology12071001
39 Zhang, J. *et al.* Fecal microbiota transplantation from warthog to pig confirms the influence of the gut microbiota on African swine fever susceptibility. *Sci Rep* **10**, 17605 (2020). https://doi.org/10.1038/s41598-020-74651-3
40 Borca, M. V. *et al.* Development of a Highly Effective African Swine Fever Virus Vaccine by Deletion of the I177L Gene Results in Sterile Immunity against the Current Epidemic Eurasia Strain. *J Virol* **94** (2020). https://doi.org/10.1128/JVI.02017-19
41 Lotonin, K. *et al.* Correlates of protection against African swine fever virus identified by a systems immunology approach. *Elife* **14** (2026). https://doi.org/10.7554/eLife.107579
42 Deutschmann, P. *et al.* Assessment of African swine fever vaccine candidate ASFV-G-ΔMGF in a reversion to virulence study. *NPJ Vaccines* **8**, 78 (2023). https://doi.org/10.1038/s41541-023-00669-z
43 Simon, A. K., Hollander, G. A. & McMichael, A. Evolution of the immune system in humans from infancy to old age. *Proc Biol Sci* **282**, 20143085 (2015). https://doi.org/10.1098/rspb.2014.3085
44 Malogolovkin, A. *et al.* Comparative analysis of African swine fever virus genotypes and serogroups. *Emerg Infect Dis* **21**, 312-315 (2015). https://doi.org/10.3201/eid2102.140649
45 Njau, E. P. *et al.* African Swine Fever Virus (ASFV): Biology, Genomics and Genotypes Circulating in Sub-Saharan Africa. *Viruses* **13** (2021). https://doi.org/10.3390/v13112285
46 Mittelholzer, C., Moser, C., Tratschin, J.-D. & Hofmann, M. A. Analysis of classical swine fever virus replication kinetics allows differentiation of highly virulent from avirulent strains. *Veterinary microbiology* **74**, 293-308 (2000).

47 Gomez-Villamandos, J. C., Bautista, M. J., Sanchez-Cordon, P. J. & Carrasco, L. Pathology of African swine fever: the role of monocyte-macrophage. *Virus Res* **173**, 140-149 (2013). https://doi.org/10.1016/j.virusres.2013.01.017

48 Wikstrom-Lassa, E. *et al.* Comparative evaluation of histopathological lesions and viral antigen distribution in domestic pigs and wild boar inoculated intranasally with the highly virulent ASFV genotype II strain "Armenia 2007". *Vet Res* **57**, 19 (2026). https://doi.org/10.1186/s13567-025-01701-x

49 Salguero, F. J. Comparative Pathology and Pathogenesis of African Swine Fever Infection in Swine. *Front Vet Sci* **7**, 282 (2020). https://doi.org/10.3389/fvets.2020.00282

50 Porras, N. *et al.* Histopathologic evaluation system of African swine fever in wild boar infected with high (Arm07) and low virulence (Lv17/WB/Riel) isolates. *Vet Pathol* **61**, 928-942 (2024). https://doi.org/10.1177/03009858241266944

51 Sehl, J. *et al.* Comparative Pathology of Domestic Pigs and Wild Boar Infected with the Moderately Virulent African Swine Fever Virus Strain "Estonia 2014". *Pathogens* **9** (2020). https://doi.org/10.3390/pathogens9080662

52 Rosenberg-Hasson, Y., Hansmann, L., Liedtke, M., Herschmann, I. & Maecker, H. T. Effects of serum and plasma matrices on multiplex immunoassays. *Immunol Res* **58**, 224-233 (2014). https://doi.org/10.1007/s12026-014-8491-6

53 Herrera-Uribe, J. *et al.* Reference Transcriptomes of Porcine Peripheral Immune Cells Created Through Bulk and Single-Cell RNA Sequencing. *Front Genet* **12**, 689406 (2021). https://doi.org/10.3389/fgene.2021.689406

54 Durinck, S., Spellman, P. T., Birney, E. & Huber, W. Mapping identifiers for the integration of genomic datasets with the R/Bioconductor package biomaRt. *Nat Protoc* **4**, 1184-1191 (2009). https://doi.org/10.1038/nprot.2009.97

55 Young, M. D. & Behjati, S. SoupX removes ambient RNA contamination from droplet-based single-cell RNA sequencing data. *Gigascience* **9** (2020). https://doi.org/10.1093/gigascience/giaa151

56 Germain, P. L., Lun, A., Garcia Meixide, C., Macnair, W. & Robinson, M. D. Doublet identification in single-cell sequencing data using scDblFinder. *F1000Res* **10**, 979 (2021). https://doi.org/10.12688/f1000research.73600.2

57 Stuart, T. *et al.* Comprehensive Integration of Single-Cell Data. *Cell* **177**, 1888-1902 e1821 (2019). https://doi.org/10.1016/j.cell.2019.05.031

58 Korsunsky, I. *et al.* Fast, sensitive and accurate integration of single-cell data with Harmony. *Nat Methods* **16**, 1289-1296 (2019). https://doi.org/10.1038/s41592-019-0619-0

59 Aran, D. *et al.* Reference-based analysis of lung single-cell sequencing reveals a transitional profibrotic macrophage. *Nat Immunol* **20**, 163-172 (2019). https://doi.org/10.1038/s41590-018-0276-y

60 Monaco, G. *et al.* RNA-Seq Signatures Normalized by mRNA Abundance Allow Absolute Deconvolution of Human Immune Cell Types. *Cell Rep* **26**, 1627-1640 e1627 (2019). https://doi.org/10.1016/j.celrep.2019.01.041

61 Hao, Y. *et al.* Integrated analysis of multimodal single-cell data. *Cell* **184**, 3573-3587 e3529 (2021). https://doi.org/10.1016/j.cell.2021.04.048

62 Ianevski, A., Giri, A. K. & Aittokallio, T. Fully-automated and ultra-fast cell-type identification using specific marker combinations from single-cell transcriptomic data. *Nat Commun* **13**, 1246 (2022). https://doi.org/10.1038/s41467-022-28803-w

63 Stoscheck, C. M. Quantitation of protein. *Methods Enzymol* **182**, 50-68 (1990).

64 Humphrey, S. J., Karayel, O., James, D. E. & Mann, M. High-throughput and high-sensitivity phosphoproteomics with the EasyPhos platform. *Nature protocols* **13**, 1897-1916 (2018). https://doi.org/10.1038/s41596-018-0014-9

65 Zhou, J. *et al.* Evaluation of the application of sodium deoxycholate to proteomic analysis of rat hippocampal plasma membrane. *Journal of proteome research* **5**, 2547-2553 (2006). https://doi.org/10.1021/pr060112a

66 Rappsilber, J., Mann, M. & Ishihama, Y. Protocol for micro-purification, enrichment, pre-fractionation and storage of peptides for proteomics using StageTips. *Nat.Protoc.* **2**, 1896-1906 (2007).
67 Demichev, V., Messner, C. B., Vernardis, S. I., Lilley, K. S. & Ralser, M. DIA-NN: neural networks and interference correction enable deep proteome coverage in high throughput. *Nat Methods* **17**, 41-44 (2020). https://doi.org/10.1038/s41592-019-0638-x
68 UniProt, C. UniProt: the Universal Protein Knowledgebase in 2025. *Nucleic Acids Res* **53**, D609-D617 (2025). https://doi.org/10.1093/nar/gkae1010
69 Sayers, E. W. *et al.* Database resources of the National Center for Biotechnology Information in 2025. *Nucleic Acids Res* **53**, D20-D29 (2025). https://doi.org/10.1093/nar/gkae979
70 Rudolph, J. PerseusR: Perseus R Interop. (2025).
71 R_Core_Team. R: A language and environment for statistical computing. R Foundation for Statistical Computing. (2020).
72 Tyanova, S., Temu, T. & Cox, J. The MaxQuant computational platform for mass spectrometry-based shotgun proteomics. *Nat Protoc* **11**, 2301-2319 (2016). https://doi.org/10.1038/nprot.2016.136
73 pheatmap : Pretty Heatmaps.
74 Perez-Riverol, Y. *et al.* The PRIDE database at 20 years: 2025 update. *Nucleic Acids Res* **53**, D543-D553 (2025). https://doi.org/10.1093/nar/gkae1011

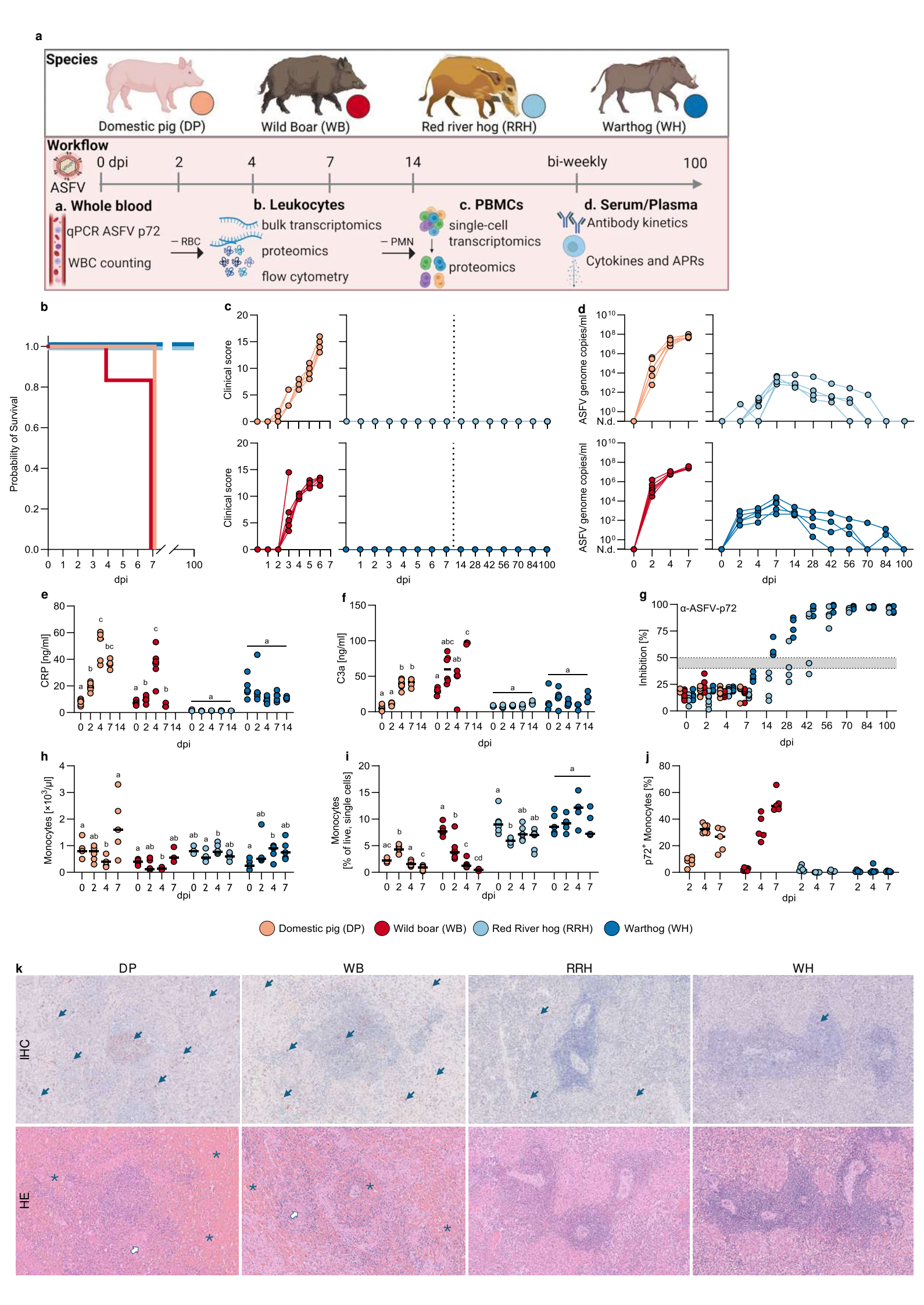
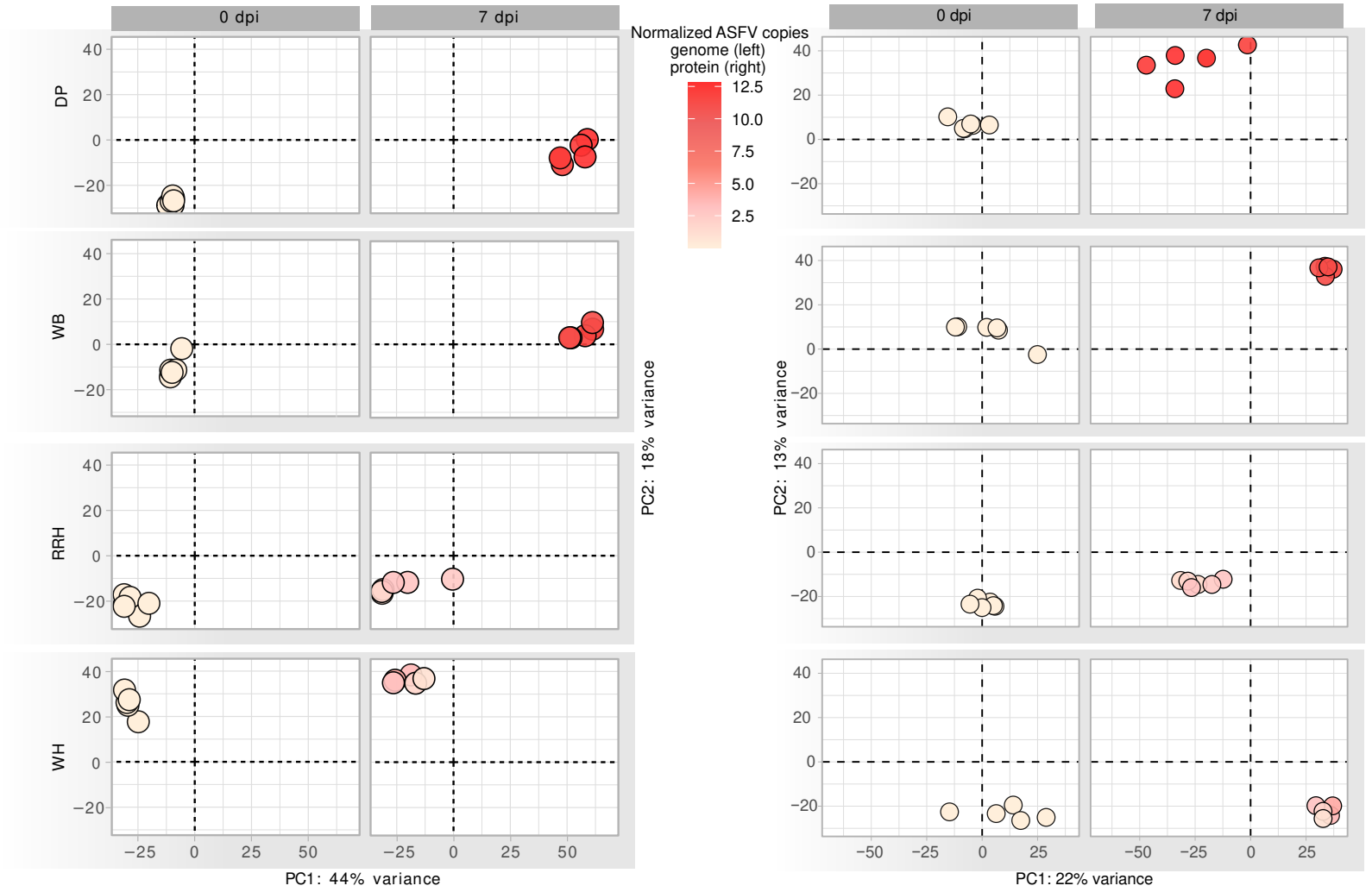
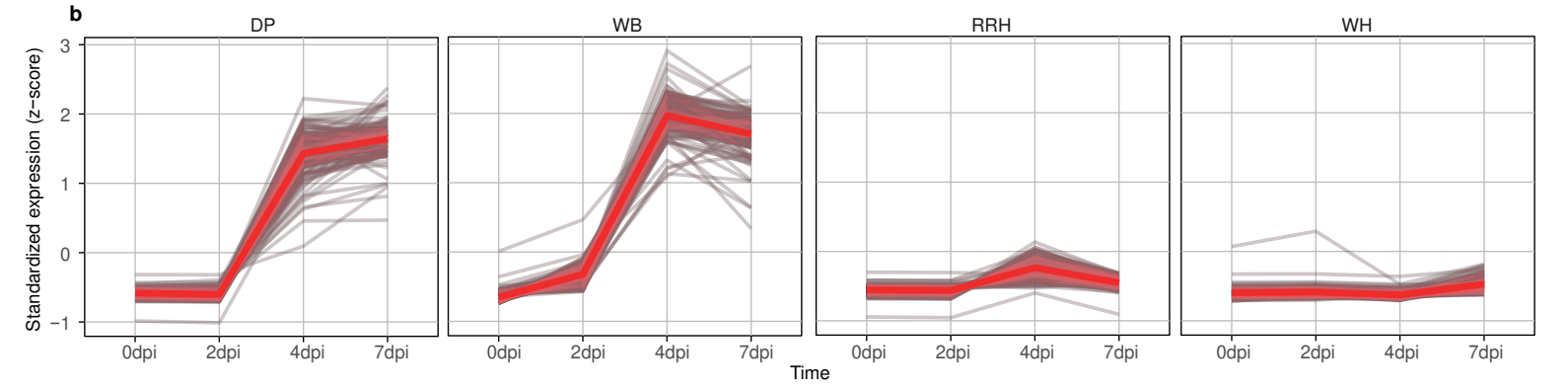
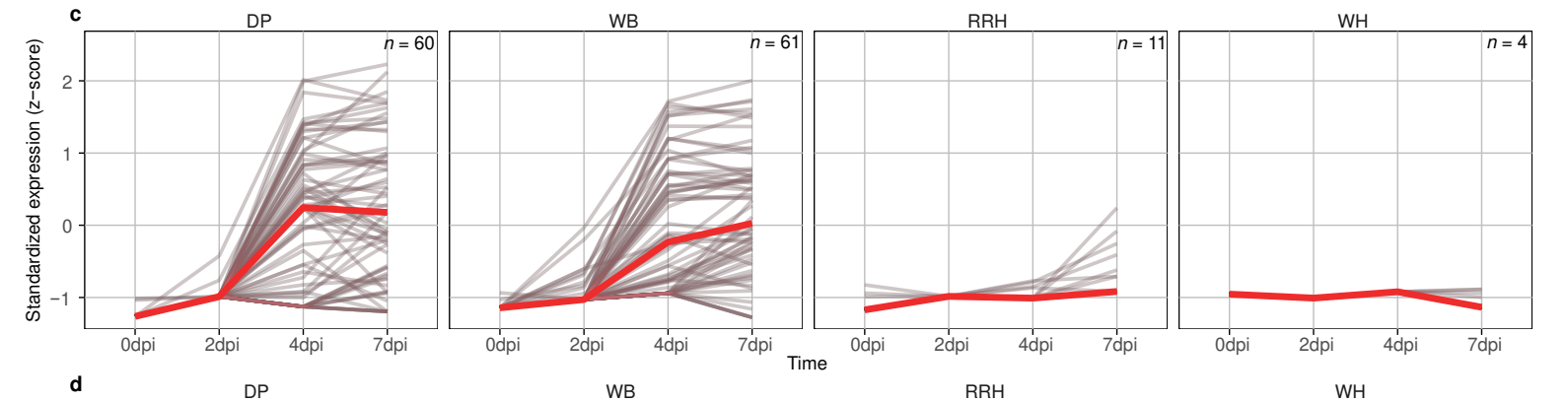

a
Species
Domestic pig (DP)
Wild Boar (WB)
Red river hog (RRH)
Warthog (WH)
Workflow
ASFV
0 dpi
2
4
7
14
bi-weekly
100
a. Whole blood
qPCR ASFV p72
WBC counting
– RBC
b. Leukocytes
bulk transcriptomics
proteomics
flow cytometry
– PMN
c. PBMCs
single-cell transcriptomics
proteomics
d. Serum/Plasma
Antibody kinetics
Cytokines and APRs
b
Probability of Survival
dpi
c
Clinical score
dpi
d
ASFV genome copies/ml
N.d.
dpi
e
CRP [ng/ml]
dpi
f
C3a [ng/ml]
dpi
g
α-ASFV-p72
Inhibition [%]
dpi
h
Monocytes [×10³/µl]
dpi
i
Monocytes [% of live, single cells]
dpi
j
p72⁺ Monocytes [%]
dpi
Domestic pig (DP)
Wild boar (WB)
Red River hog (RRH)
Warthog (WH)
k
DP
WB
RRH
WH
IHC
HE

Fig. 1 | Severe clinical outcome of ASFV infection in Eurasian compared to African pigs. a, Schematic overview of the experimental ASFV infection trial in domestic pigs (DP), wild boar (WB), red river hogs (RRH) and warthogs (WH), indicating sampling schedule for blood, swabs and necropsy, and the allocation of samples to downstream assays (qPCR, flow cytometry, bulk RNAseq, scRNAseq, and proteomics). **b**, Kaplan-Meier curve shows survival after infection. **c**, time course of clinical scores for DP, WB, RRH, and WH. **d**, ASFV genome loads in blood, N.d.; not detected. **e**, Plasma concentrations of the acute-phase protein C-reactive protein (CRP). **f**, Plasma levels of the complement activation marker C3a. **g**, ASFV-p72-specific antibodies in serum; grey areas indicate the respective intervals for questionable results in ELISA, values above this range were considered positive. **h**, Total monocyte counts obtained by automated WBC analysis. **i**, Frequencies of CD172a+CD14+ monocytes and **j**, percent of ASFV infected monocytes (CD172a+CD14+ASFV-p72+) determined by flow cytometry. **k**, Representative spleen sections from 7 dpi showing ASFV infected cells by immunohistochemistry (IHC) and tissue lesions by haematoxylin–eosin (HE) staining; arrows indicate ASFV positive cells in IHC, stars and white arrows mark lesions in HE. Each dot represents an individual animal, with group means indicated by lines. Compact letter displays denote statistically significant differences between groups; different letters indicate $P < 0.05$.


0 dpi
7 dpi
Normalized ASFV copies
genome (left)
protein (right)
12.5
10.0
7.5
5.0
2.5
DP
WB
RRH
WH
PC2: 18% variance
PC2: 13% variance
PC1: 44% variance
PC1: 22% variance


b
DP
WB
RRH
WH
Standardized expression (z-score)
0dpi
2dpi
4dpi
7dpi
Time


c
DP
WB
RRH
WH
n = 60
n = 61
n = 11
n = 4
Standardized expression (z-score)
0dpi
2dpi
4dpi
7dpi
Time

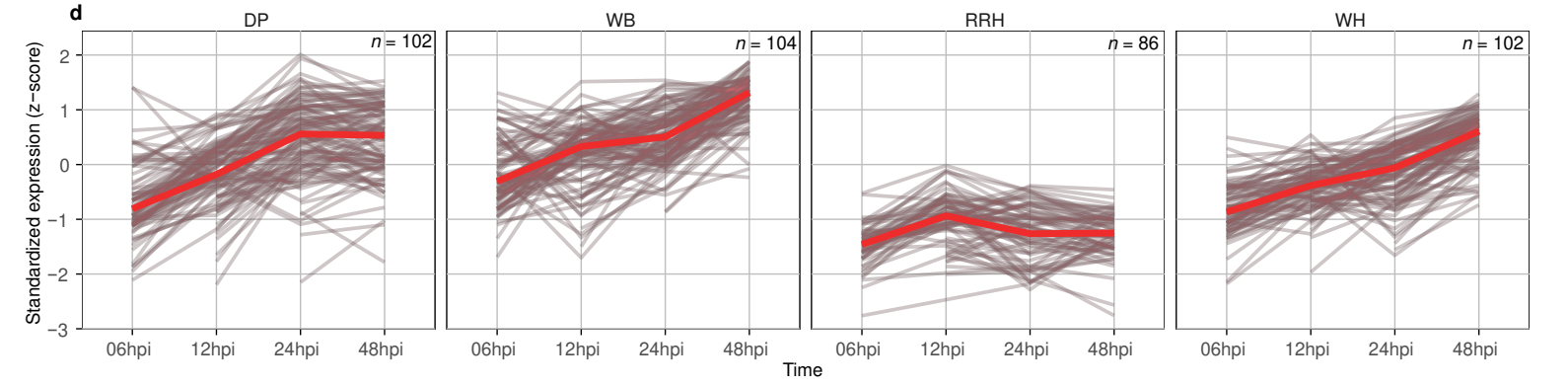

d
DP
WB
RRH
WH
n = 102
n = 104
n = 86
n = 102
Standardized expression (z-score)
06hpi
12hpi
24hpi
48hpi
Time

Fig. 2 | ASFV gene and protein expression kinetics in blood leukocytes and purified monocytes. a, Principal component analysis (PCA) of ASFV gene and protein expression in blood at 0 and 7 days post infection (dpi). Left panels show PCA of ASFV transcript abundance from bulk RNAseq of whole blood leukocytes for domestic pigs (DP), wild boar (WB), red river hogs (RRH) and warthogs (WH); right panels show PCA of ASFV protein abundance from leukocyte proteomes at the same time points. Each point represents an individual animal, with colour indicating normalized ASFV copies (genome on the left, protein on the right). **b**, Temporal kinetics of ASFV gene expression in whole blood leukocytes based on bulk RNAseq. For each species, standardized expression (z-score) of all detected ASFV genes is plotted over time (0, 2, 4, and 7 dpi); grey lines represent individual genes and the red line denotes the mean expression profile. **c**, Temporal kinetics of ASFV protein expression in whole blood leukocyte proteomes. Standardized expression (z-score) of all detected ASFV proteins is shown for each species at 0, 2, 4, and 7 dpi, with grey lines indicating individual proteins and the red line the mean profile (DP, n = 60 proteins; WB, n = 61; RRH, n = 11; WH, n = 4). **d**, ASFV protein expression in purified monocytes infected in vitro. Monocytes isolated from each species at 0 dpi were inoculated with ASFV and analysed by proteomics at 6, 12, 24, and 48 h post infection (hpi). Plots show standardized expression (z-score) of all detected ASFV proteins over time, with grey lines representing individual proteins and red lines the mean profile (DP, n = 102 proteins; WB, n = 104; RRH, n = 86; WH, n = 102).

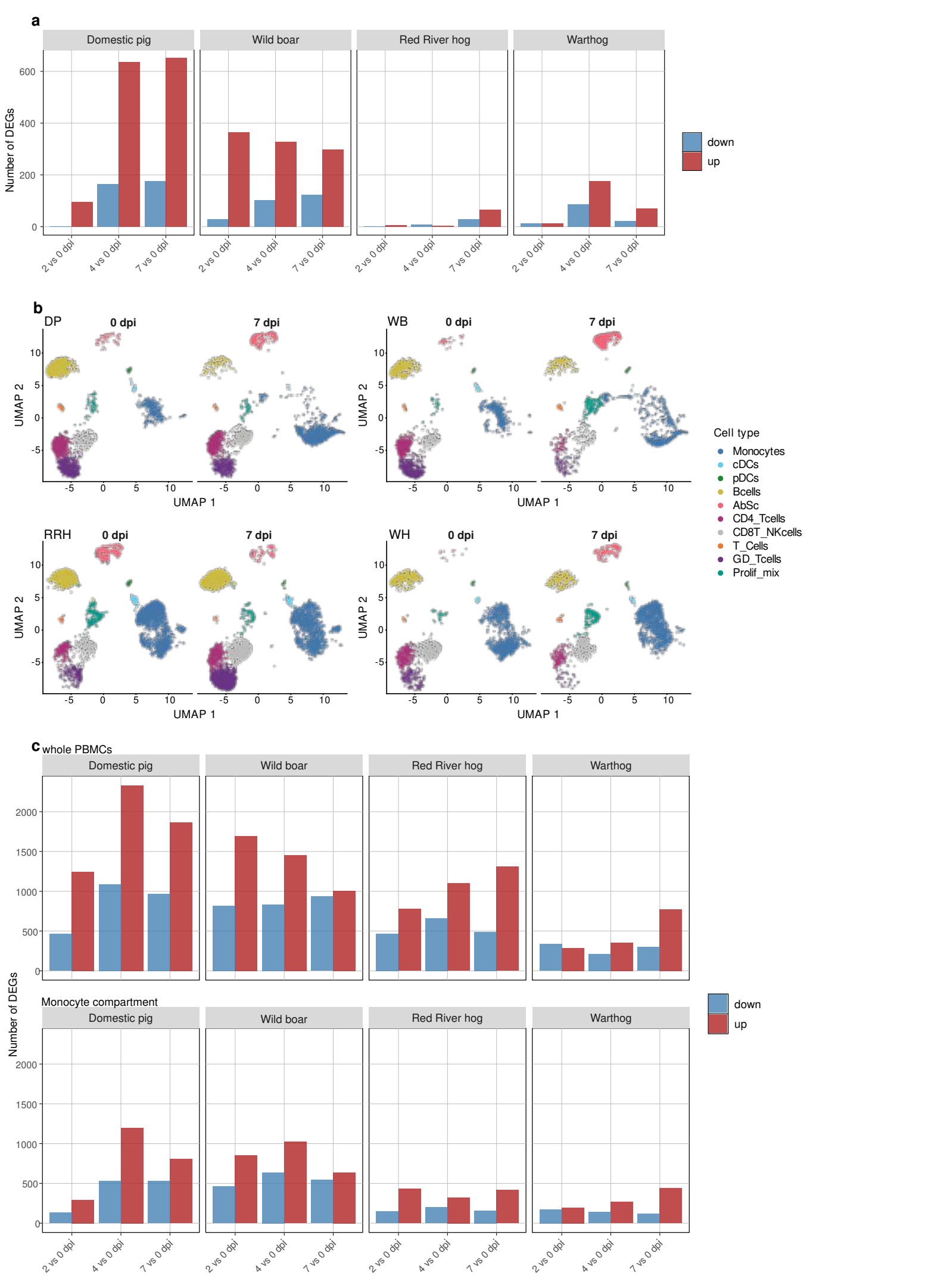

a
Domestic pig
Wild boar
Red River hog
Warthog
Number of DEGs
0
200
400
600
2 vs 0 dpi
4 vs 0 dpi
7 vs 0 dpi
down
up
b
DP
WB
RRH
WH
0 dpi
7 dpi
UMAP 1
UMAP 2
Cell type
Monocytes
cDCs
pDCs
Bcells
AbSc
CD4_Tcells
CD8T_NKcells
T_Cells
GD_Tcells
Prolif_mix
c
whole PBMCs
Monocyte compartment
Domestic pig
Wild boar
Red River hog
Warthog
Number of DEGs
0
500
1000
1500
2000
down
up

Fig. 3 | ASFV-induced host transcriptional responses in whole blood and PBMCs. a, Bar plots showing the number of differentially expressed host genes (DEGs) identified by bulk RNAseq in whole blood leukocytes of domestic pigs (DP), wild boar (WB), red river hogs (RRH) and warthogs (WH). Upregulated (red) and downregulated (blue) genes are shown separately for each species and time comparison (2 vs 0 dpi, 4 vs 0 dpi, 7 vs 0 dpi). **b**, UMAP projections of scRNAseq data from PBMCs at 0 and 7 days post infection for each species. Cells are coloured by major immune cell type (monocytes, conventional dendritic cells [cDCs], plasmacytoid dendritic cells [pDCs], B cells, antibody-secreting cells [AbSc], $CD4^+$ T cells, CD8 T/NK cells, γδ T cells and proliferating mixed cells), illustrating shifts in PBMC composition and transcriptional state over time. **c**, Bar plots summarizing the number of DEGs detected by scRNAseq. The upper row shows upregulated (red) and downregulated (blue) genes across all PBMCs for each species and time comparison, while the lower row shows the corresponding DEG counts restricted to the monocytic compartment, highlighting monocyte-specific transcriptional changes.

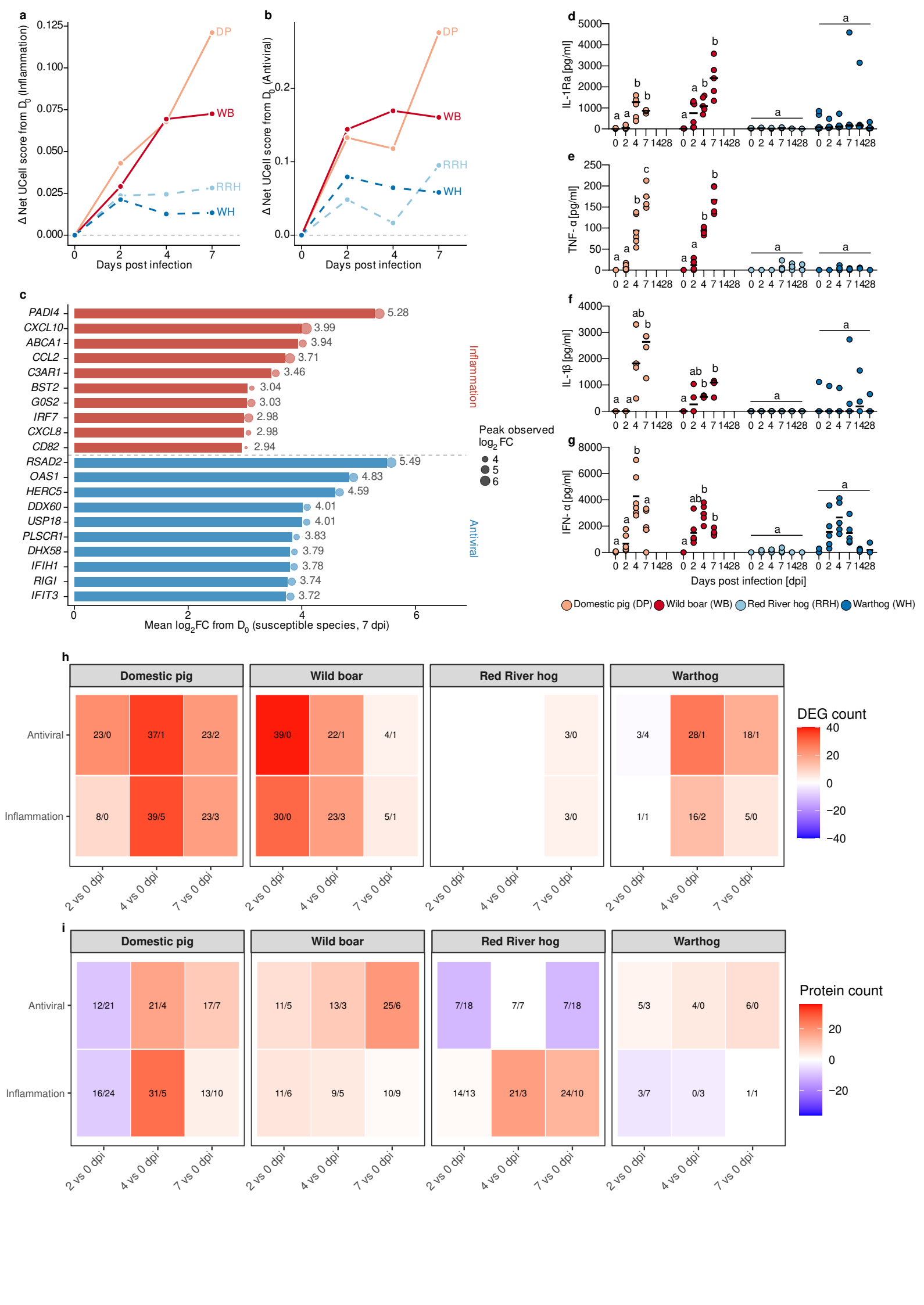

a
Δ Net UCell score from D0 (Inflammation)
Days post infection
DP
WB
RRH
WH
b
Δ Net UCell score from D0 (Antiviral)
Days post infection
c
PADI4 5.28
CXCL10 3.99
ABCA1 3.94
CCL2 3.71
C3AR1 3.46
BST2 3.04
G0S2 3.03
IRF7 2.98
CXCL8 2.98
CD82 2.94
RSAD2 5.49
OAS1 4.83
HERC5 4.59
DDX60 4.01
USP18 4.01
PLSCR1 3.83
DHX58 3.79
IFIH1 3.78
RIGI 3.74
IFIT3 3.72
Inflammation
Antiviral
Peak observed log2 FC
Mean log2FC from D0 (susceptible species, 7 dpi)
d
IL-1Ra [pg/ml]
e
TNF- α [pg/ml]
f
IL-1β [pg/ml]
g
IFN- α [pg/ml]
Days post infection [dpi]
Domestic pig (DP)
Wild boar (WB)
Red River hog (RRH)
Warthog (WH)
h
Domestic pig
Wild boar
Red River hog
Warthog
Antiviral
Inflammation
23/0 37/1 23/2
8/0 39/5 23/3
39/0 22/1 4/1
30/0 23/3 5/1
3/0
3/0
3/4 28/1 18/1
1/1 16/2 5/0
2 vs 0 dpi
4 vs 0 dpi
7 vs 0 dpi
DEG count
i
Protein count
12/21 21/4 17/7
16/24 31/5 13/10
11/5 13/3 25/6
11/6 9/5 10/9
7/18 7/7 7/18
14/13 21/3 24/10
5/3 4/0 6/0
3/7 0/3 1/1

Fig. 4 | Antiviral and inflammatory host responses across suid species. a, Changes in inflammatory transcriptional activity in PBMCs over time quantified by scRNAseq. Lines show the mean change in Net UCell score for an inflammation-related gene module relative to day 0 (Δ score from 0 dpi) in domestic pigs (DP), wild boar (WB), red river hogs (RRH) and warthogs (WH) at days 0, 2, 4, and 7 post infection. **b**, As in a, but for an antiviral gene module, depicting Δ Net UCell scores for antiviral genes over time in PBMCs from each species. **c**, Ranked mean $\log_2$ fold change (FC) of the top 10 differentially expressed genes (DEGs) associated with inflammation (red) and antiviral responses (blue) in susceptible species (DP and WB) at 7 dpi compared to 0 dpi. Bars indicate mean $\log_2$FC across DP and WB; dot size reflects the peak observed $\log_2$FC for each gene. **d–g**, Serum cytokine kinetics measured by ELISA. Concentrations of IL-1Ra (**d**), TNF-α (**e**), IL-1β (**f**) and IFN-α (**g**) are shown for DP, WB, RRH and WH at indicated time points; each dot represents an individual animal and lines denote group means. Compact letter displays above time points indicate statistically significant differences between groups; different letters denote $P < 0.05$. **h**, Heatmaps summarizing the number of DEGs in bulk RNAseq related to antiviral and inflammatory pathways. For each species and comparison (2 vs 0 dpi, 4 vs 0 dpi, 7 vs 0 dpi), the number of upregulated/downregulated antiviral (top row) and inflammatory (bottom row) genes is shown, with colour indicating DEG count. **i**, as in **h**, but for leukocyte proteomics. Heatmaps display the number of antiviral (top row) and inflammatory (bottom row) proteins with increased or decreased abundance in each species and time comparison, with colour reflecting protein count.

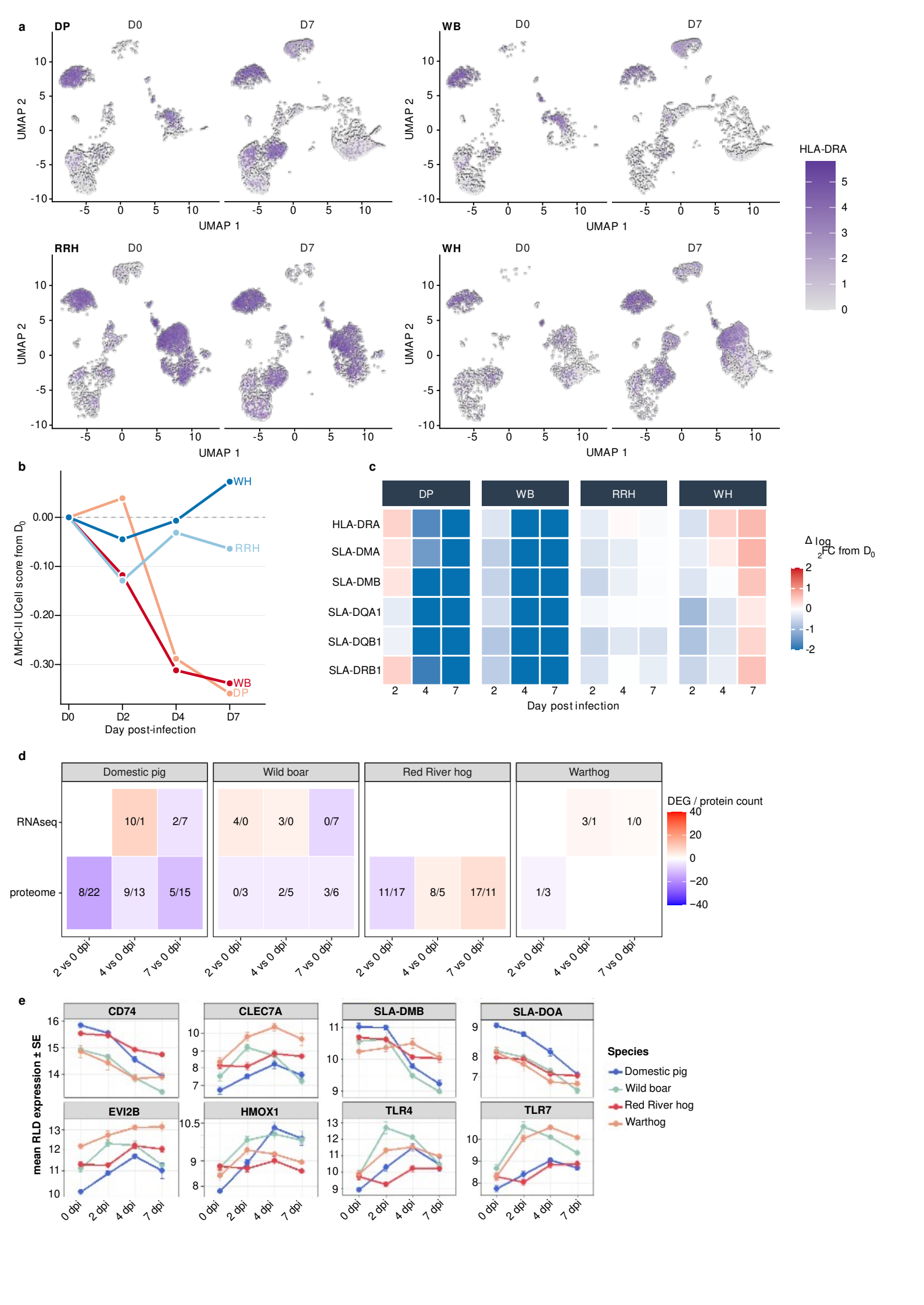

a
DP
D0
D7
WB
RRH
WH
UMAP 1
UMAP 2
HLA-DRA
b
Δ MHC-II UCell score from D0
Day post-infection
c
HLA-DRA
SLA-DMA
SLA-DMB
SLA-DQA1
SLA-DQB1
SLA-DRB1
Day post infection
Δ log2FC from D0
d
Domestic pig
Wild boar
Red River hog
Warthog
RNAseq
proteome
DEG / protein count
e
CD74
CLEC7A
SLA-DMB
SLA-DOA
EVI2B
HMOX1
TLR4
TLR7
mean RLD expression ± SE
Species
Domestic pig
Wild boar
Red River hog
Warthog

Fig. 5 | **MHCII-dependent antigen presentation collapses in Eurasian pigs compared to African pigs. a**, UMAP projections of PBMC scRNA-seq data from domestic pigs (DP), wild boar (WB), red river hogs (RRH) and warthogs (WH) at day 0 and day 7 post infection, with HLA-DRA-positive cells highlighted by colour intensity, illustrating the distribution of MHCII-expressing cells over time in each species. **b**, Change in MHCII module activity over the course of infection quantified by scRNA-seq. Lines show the mean change in Net UCell score for an MHCII-related gene set relative to day 0 (Δ score from 0 dpi) in DP, WB, RRH and WH at 0, 2, 4, and 7 days post infection (dpi). **c**, Heatmaps summarizing changes in expression of key antigen-presentation genes in bulk RNA-seq. For each species, Δ $\log_2$ fold change from 0 dpi is shown at 2, 4, and 7 dpi for *HLA-DRA* and porcine MHCII components *SLA-DMA, SLA-DMB, SLA-DQA1, SLA-DQB1,* and *SLA-DRB1*. **d**, Combined overview of differentially expressed genes (top row) and proteins (bottom row) associated with antigen processing and presentation. For each species and time comparison (2 vs 0 dpi, 4 vs 0 dpi, 7 vs 0 dpi), tiles indicate the number of upregulated/downregulated RNA-seq DEGs (top) and proteomic hits (bottom), with colour reflecting DEG/protein count (red, increase; blue, decrease). **e**, Bulk RNA-seq expression kinetics of selected antigen-presentation and pattern-recognition genes. Line plots show mean regularized log (RLD) expression ± SEM. for *CD74, EVI2B, CLEC7A, SLA-DMB, SLA-DOA, HMOX1, TLR4* and *TLR7* in DP, WB, RRH and WH at 0, 2, 4, 7 and 14 dpi, with species indicated by colour.

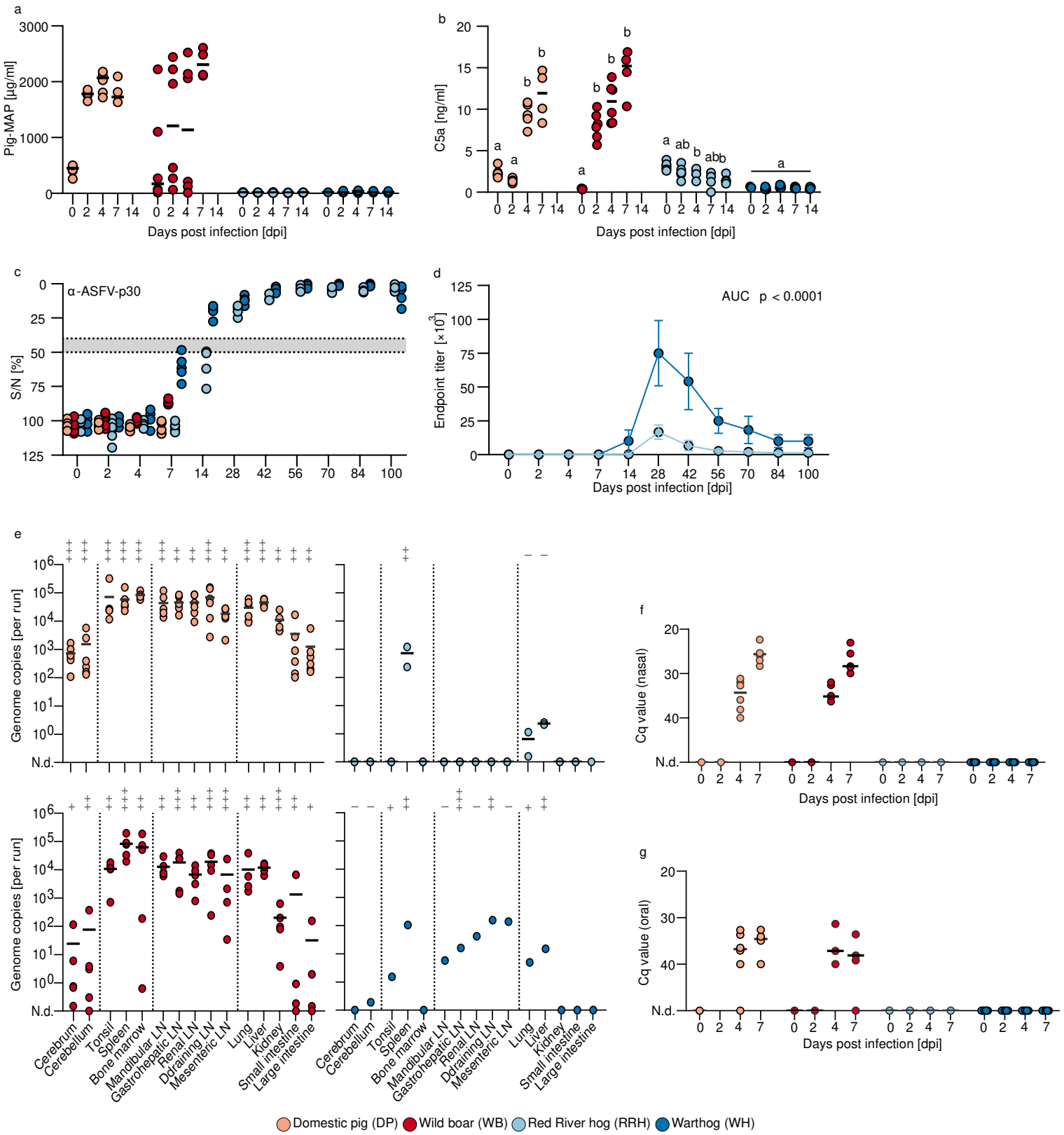


Fig. S1 | Humoral markers of inflammation, antiviral immunity and viral dissemination. a, Plasma concentrations of porcine major acute-phase protein (Pig-MAP) over time in domestic pigs (DP), wild boar (WB), red river hogs (RRH) and warthogs (WH). Each dot represents an individual animal; lines denote group means. Compact letter displays indicate statistically significant differences between groups; different letters denote $P < 0.05$. **b**, Plasma levels of complement component C5a measured by ELISA at indicated days post infection, shown as individual values with group means and compact letter displays for statistical differences. **c**, ASFV-p30-specific antibodies in serum determined by ELISA, expressed as signal-to-noise (S/N) ratio over time. Horizontal dashed lines mark the interval for questionable results; values above this range were considered positive. **d**, ASFV antibody endpoint titres in serum assessed by immunoperoxidase test (IPT) and plotted over the full sampling period; points show mean ± SEM per time point. The area under the curve (AUC) was compared between species (*P* value indicated). **e**, ASFV genome loads and virus isolation results in tissues collected at necropsy. For each species, genome copies per run (qPCR) are shown for indicated organs; N.d.; not detected. Plus (+) and minus (–) symbols above bars denote positive or negative virus isolation from the corresponding tissue. **f,g**, qPCR detection of ASFV genome in nasal (**f**) and oral (**g**) swabs, shown as Cq values at indicated time points; "N.d." indicates samples in which ASFV genome was not detected.

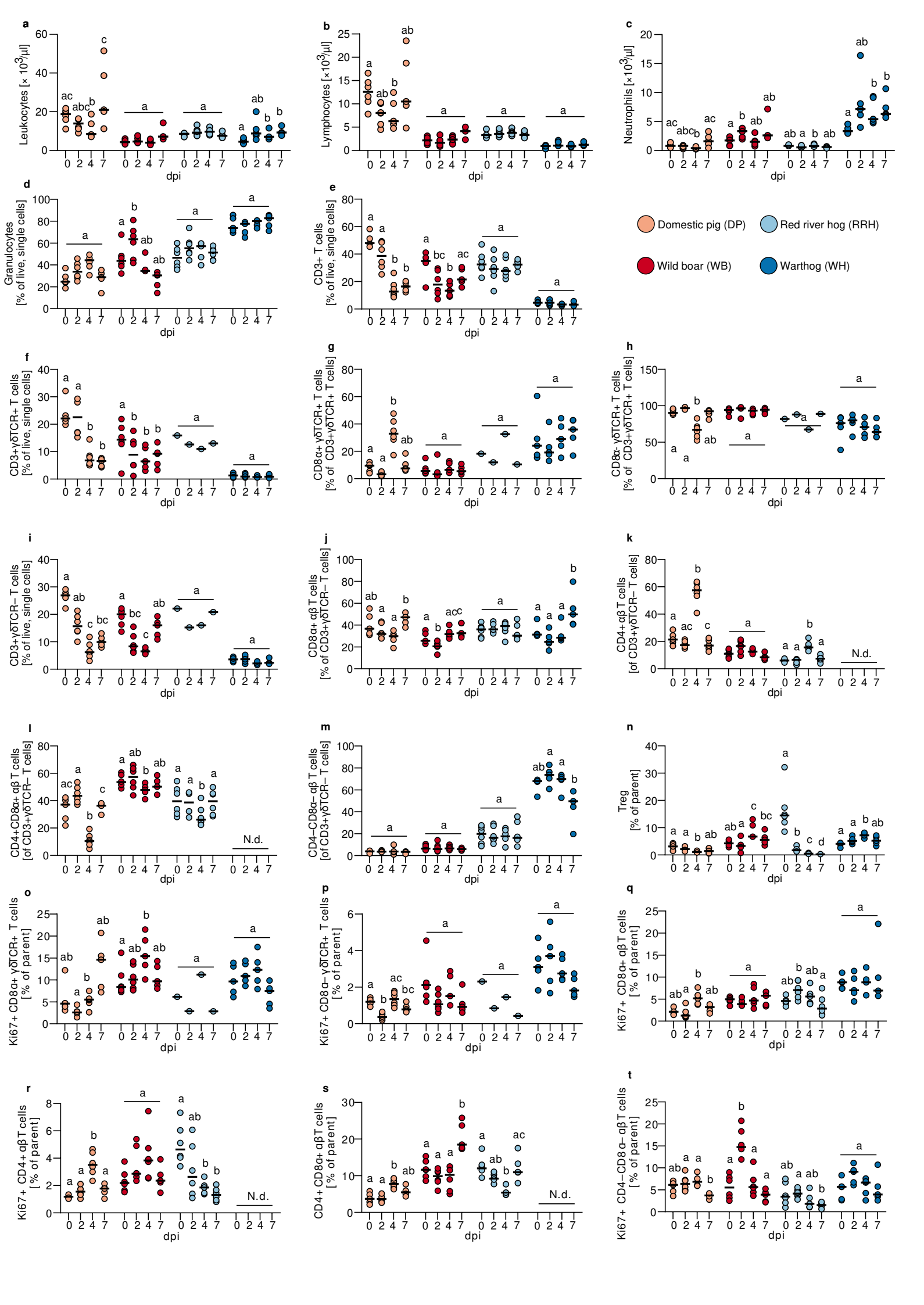

a
Leukocytes [× 10^3/µl]
b
Lymphocytes [×10^3/µl]
c
Neutrophils [×10^3/µl]
d
Granulocytes [% of live, single cells]
e
CD3+ T cells [% of live, single cells]
Domestic pig (DP)
Red river hog (RRH)
Wild boar (WB)
Warthog (WH)
f
CD3+γδTCR+ T cells [% of live, single cells]
g
CD8α+ γδTCR+ T cells [% of CD3+γδTCR+ T cells]
h
CD8α- γδTCR+ T cells [% of CD3+γδTCR+ T cells]
i
CD3+γδTCR− T cells [% of live, single cells]
j
CD8α+ αβ T cells [% of CD3+γδTCR− T cells]
k
CD4+αβ T cells [of CD3+γδTCR− T cells]
l
CD4+CD8α+ αβ T cells [of CD3+γδTCR− T cells]
m
CD4−CD8α− αβ T cells [of CD3+γδTCR− T cells]
n
Treg [% of parent]
o
Ki67+ CD8α+ γδTCR+ T cells [% of parent]
p
Ki67+ CD8α− γδTCR+ T cells [% of parent]
q
Ki67+ CD8α+ αβT cells [% of parent]
r
Ki67+ CD4+ αβT cells [% of parent]
s
CD4+ CD8α+ αβT cells [% of parent]
t
Ki67+ CD4−CD8α− αβT cells [% of parent]
dpi
0 2 4 7
N.d.

Fig. S2 | Leukocyte counts and T-cell subset dynamics during ASFV infection. a–c, Automated complete blood counts showing total leukocyte (**a**), lymphocyte (**b**) and neutrophil (**c**) numbers per µl blood over time in domestic pigs (DP), wild boar (WB), red river hogs (RRH) and warthogs (WH). **d–h**, Flow-cytometric analysis of granulocytes and major T-cell subsets. Granulocytes are shown as percentage of live, single cells (**d**). Frequencies of $CD3^+$ T cells (**e**), $CD3^+\gamma\delta TCR^+$ T cells (**f**), $CD3^+\gamma\delta TCR^-$ T cells (**g**) and $CD8\alpha^+$ αβ T cells among $CD3^+\gamma\delta TCR^-$ T cells (**h**) are plotted over time. **i m**, αβ T-cell subset composition. Panels show $CD4^+$ αβ T cells (**i**), $CD8\alpha^+$ $\gamma\delta TCR^+$ T cells among $CD3^+\gamma\delta TCR^+$ T cells (**j**), $CD4^+CD8\alpha^+$ αβ T cells (**k**), $CD4^-CD8\alpha^-$ αβ T cells (**l**) and $CD4^+CD8\alpha^+$ αβ T cells expressed as proportion of the parent αβ T-cell gate (**m**). N.d.; indicates subsets not detected at specific time points. **n**, Frequencies of regulatory T cells (Treg) expressed as percentage of the parent $CD4^+$ T-cell population. **o**, Frequencies of $CD8\alpha^-$ $\gamma\delta TCR^+$ T cells among $CD3^+\gamma\delta TCR^+$ T cells. **p–t**, Proliferation of T-cell subsets assessed by Ki-67 staining. Panels show Ki-67^+ $CD4^+$ αβ T cells (**p**), Ki-67^+ $CD8\alpha^+$ αβ T cells (**q**), Ki-67^+ $CD8\alpha^+\gamma\delta TCR^+$ T cells (**r**), Ki-67^+ $CD8\alpha^-\gamma\delta TCR^+$ T cells (**s**) and Ki-67^+ $CD4^-CD8\alpha^-$ αβ T cells (**t**) as percentage of the respective parent gate. Each dot represents an individual animal; lines indicate group means. Compact letter displays denote statistically significant differences between species at a given time point, with different letters indicating $P < 0.05$.

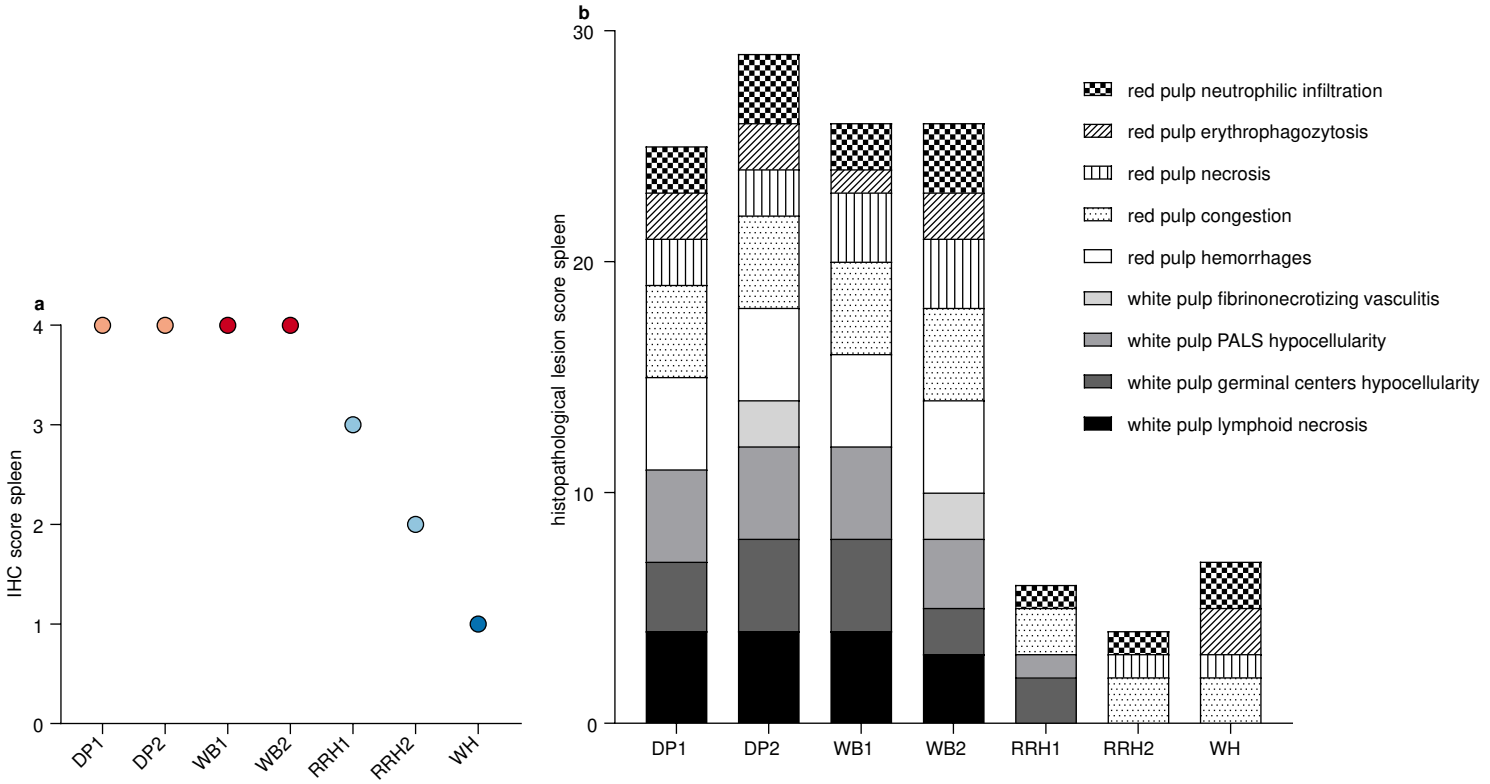
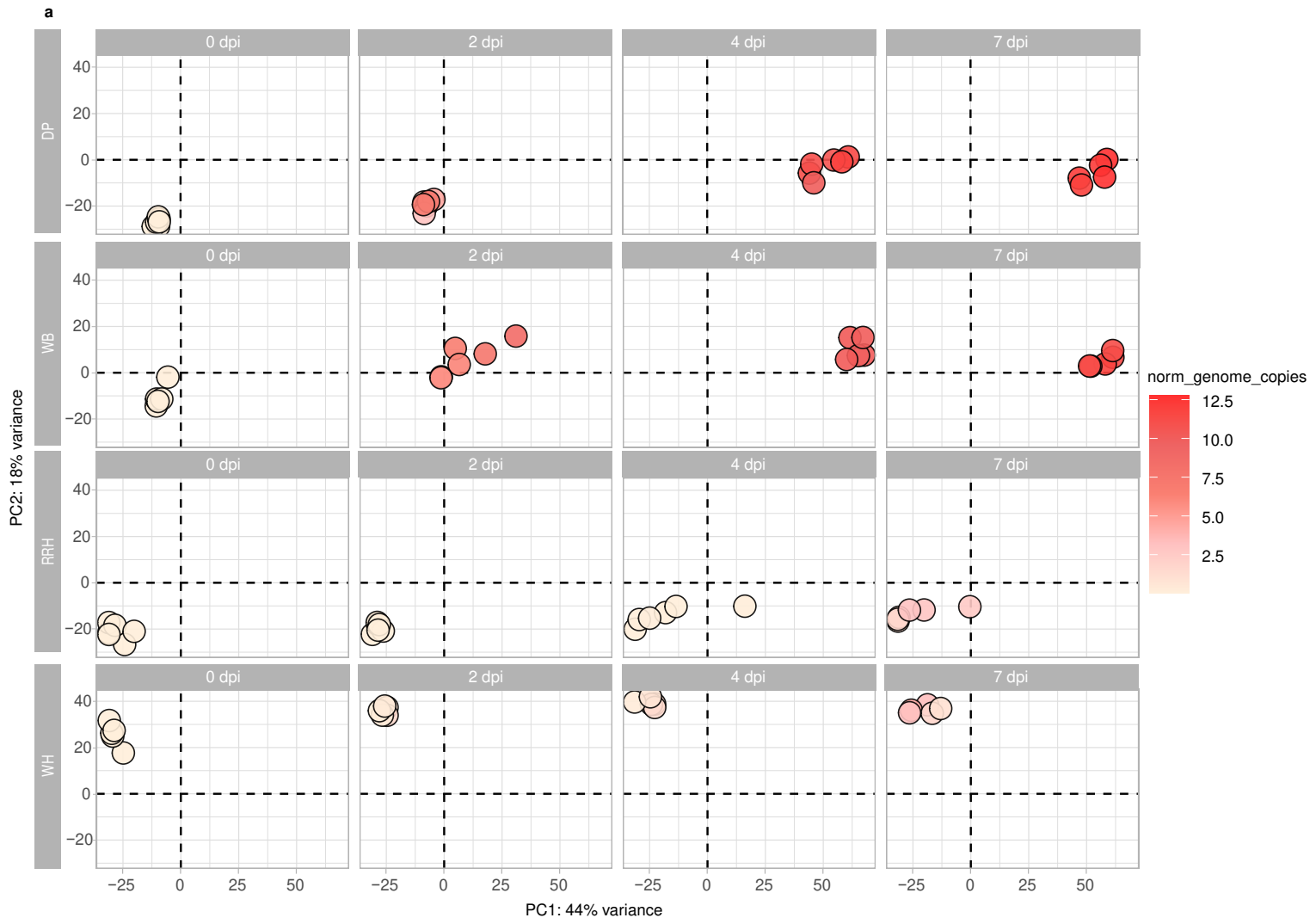


Fig. S3 | Spleen immunohistochemistry and lesion scoring. a, Immunohistochemistry (IHC) scores for ASFV antigen in spleen tissue from individual animals (DP1, DP2, WB1, WB2, RRH1, RRH2, WH) at 7 days post infection. Scores range from 0 to 4 and reflect the extent of ASFV-positive cells per section. **b**, Stacked bar plots showing histopathological lesion scores in the spleen for the same animals. Total scores (0–30) are decomposed into contributions from specific lesion categories, including white pulp lymphoid necrosis, germinal centre hypocellularity, periarteriolar lymphoid sheath (PALS) hypocellularity, fibrinonecrotizing vasculitis, red pulp haemorrhages, congestion, necrosis, erythrophagocytosis and neutrophilic infiltration.


a
0 dpi
2 dpi
4 dpi
7 dpi
DP
WB
RRH
WH
PC2: 18% variance
PC1: 44% variance
norm_genome_copies
12.5
10.0
7.5
5.0
2.5

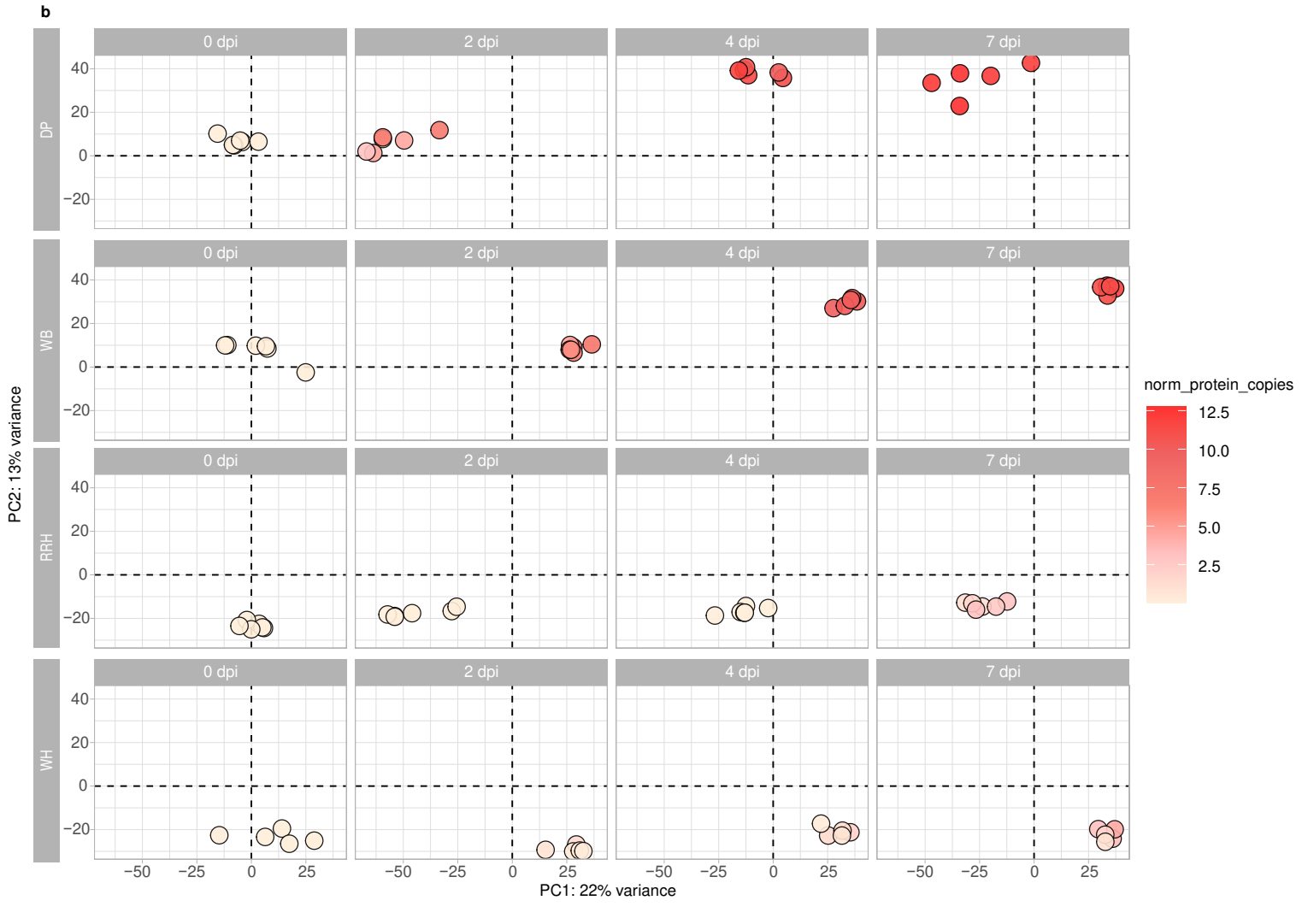

b
0 dpi
2 dpi
4 dpi
7 dpi
DP
WB
RRH
WH
PC2: 13% variance
PC1: 22% variance
norm_protein_copies
12.5
10.0
7.5
5.0
2.5

Fig. S4 | Principal component analysis of ASFV gene and protein expression in blood. a, PCA of ASFV transcriptomes from bulk RNA-seq of whole blood leukocytes in domestic pigs (DP), wild boar (WB), red river hogs (RRH) and warthogs (WH). Panels are faceted by species and time point (0, 2, 4, and 7 days post infection). Each point represents an individual animal, positioned by PC1 (44% variance) and PC2 (18% variance), and coloured according to normalized ASFV genome copies (norm_genome_copies). **b**, PCA of ASFV proteomes from whole blood leukocyte proteomics for the same species and time points. Points show individual animals plotted by PC1 (22% variance) and PC2 (13% variance), with colour indicating normalized ASFV protein copies (norm_protein_copies).

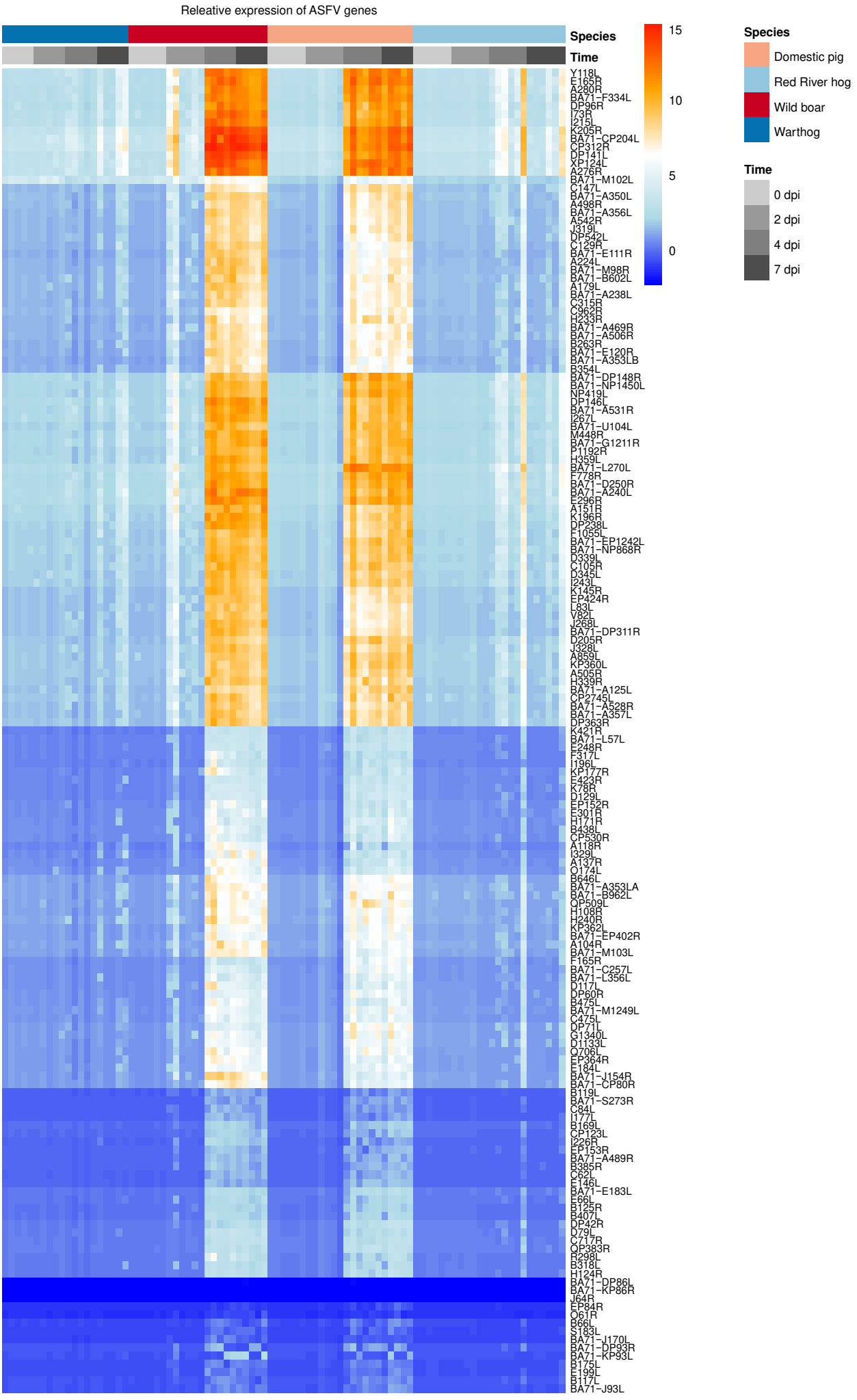


Fig. S5 | ASFV gene expression in whole blood leukocytes. Heatmap showing standardized expression of ASFV genes detected by bulk RNA-seq in whole blood leukocytes from domestic pigs, wild boar, red river hogs and warthogs at 0, 2, 4 and 7 days post infection. Each row corresponds to an individual ASFV gene, including structural, enzymatic and immune-modulatory genes, and each column represents a species–timepoint combination. Colour intensity indicates relative expression (z-score) from low (blue) to high (red), with side bars denoting species and timepoint groupings.

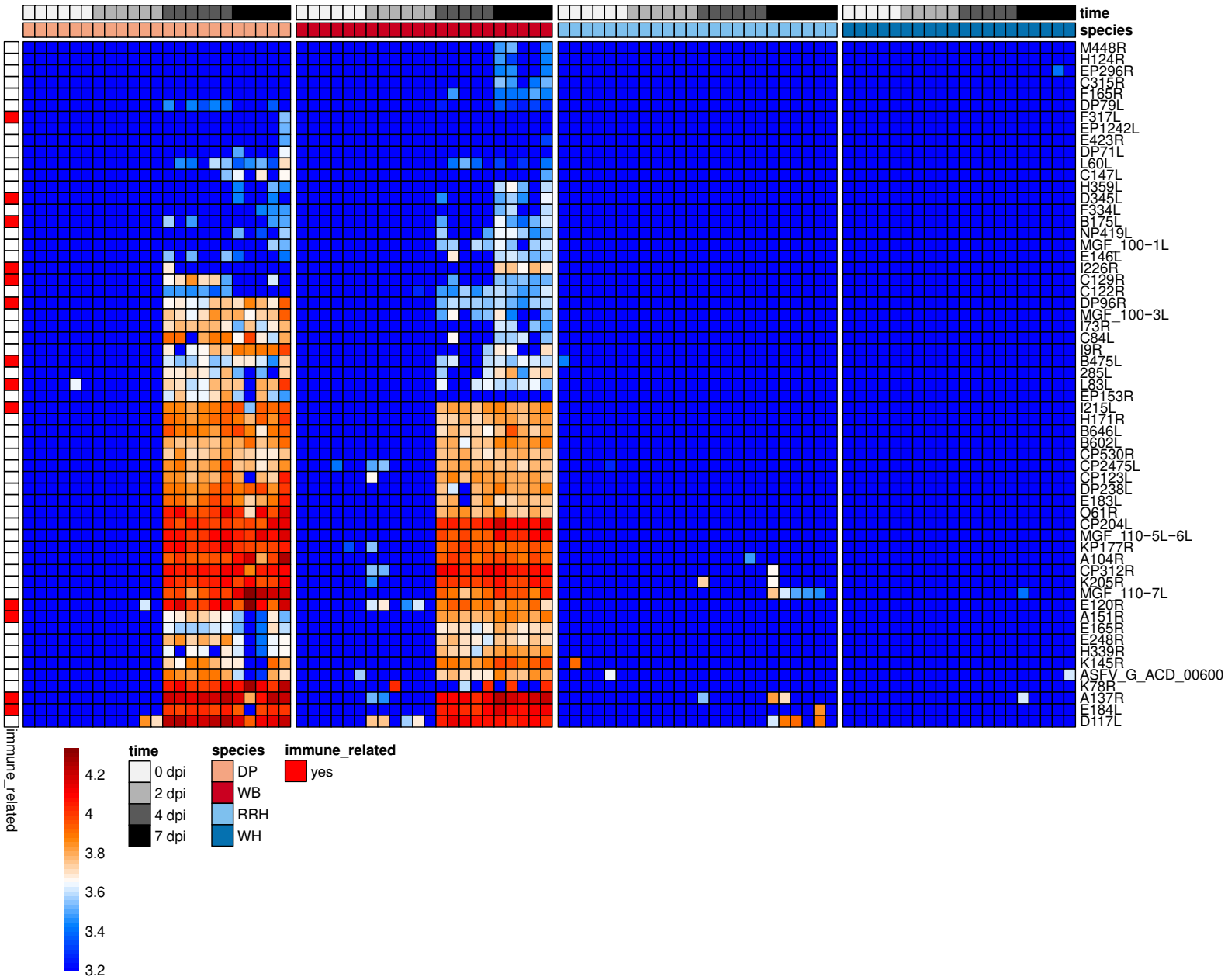


Fig. S6 | **ASFV protein expression in whole blood leukocytes.** Heatmap showing standardized expression (z-score) of ASFV proteins detected in whole blood leukocyte proteomes from domestic pigs (DP), wild boar (WB), red river hogs (RRH) and warthogs (WH) at 0, 2, 4, and 7 days post infection. Rows correspond to individual ASFV proteins, including structural components and immune-modulatory factors (for example, B646L, CP204L, EP153R, I215L, I73R, members of MGF_100, MGF_110 and other multigene families), and columns represent individual samples grouped by species and time point. Colour intensity indicates standardized protein abundance, with warmer colours reflecting higher expression. The left annotation bar marks proteins previously classified as modulators of the host immune response (immune-related).

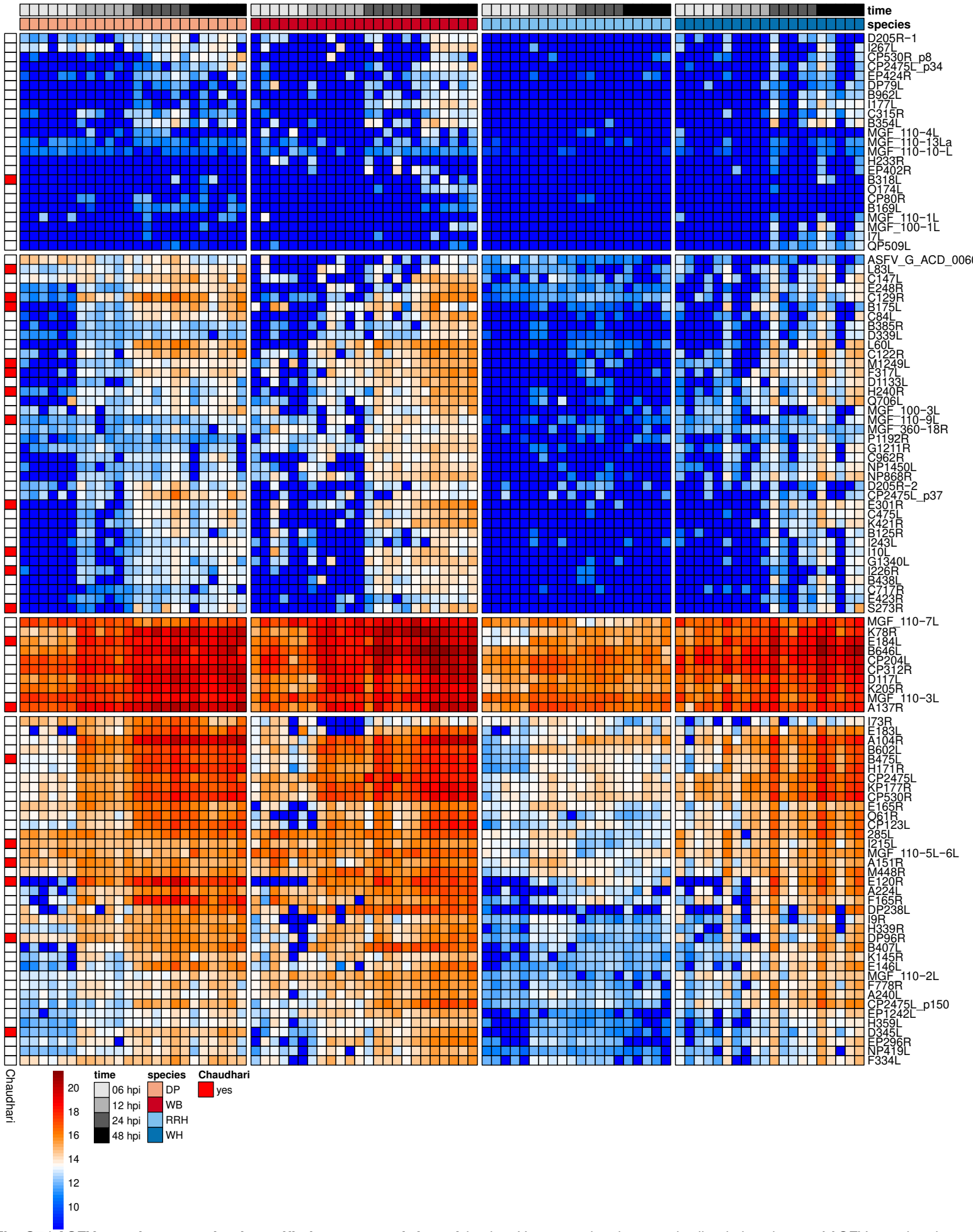


Fig. S7 | ASFV protein expression in purified monocytes infected *in vitro***.** Heatmap showing standardized abundance of ASFV proteins detected in proteomes of purified peripheral monocytes from domestic pigs (DP), wild boar (WB), red river hogs (RRH) and warthogs (WH) after in vitro infection with ASFV *Armenia08*. Monocytes were isolated at 0 dpi and analysed at 6, 12, 24 and 48 hours post infection (hpi). Rows correspond to individual ASFV proteins, including structural components and immune-modulatory factors (for example, B646L, CP204L, EP402R, KP177R, I215L, I73R, members of MGF_100, MGF_110 and MGF_360), and columns represent individual samples grouped by species and time point. Colour intensity indicates standardized protein abundance (z-score), with warmer colours reflecting higher expression. The lower annotation bar indicates species, the upper bar indicates sampling time, and an additional annotation marks proteins previously described in Chaudhari et al. as modulators of the host immune response (immune-relevant).

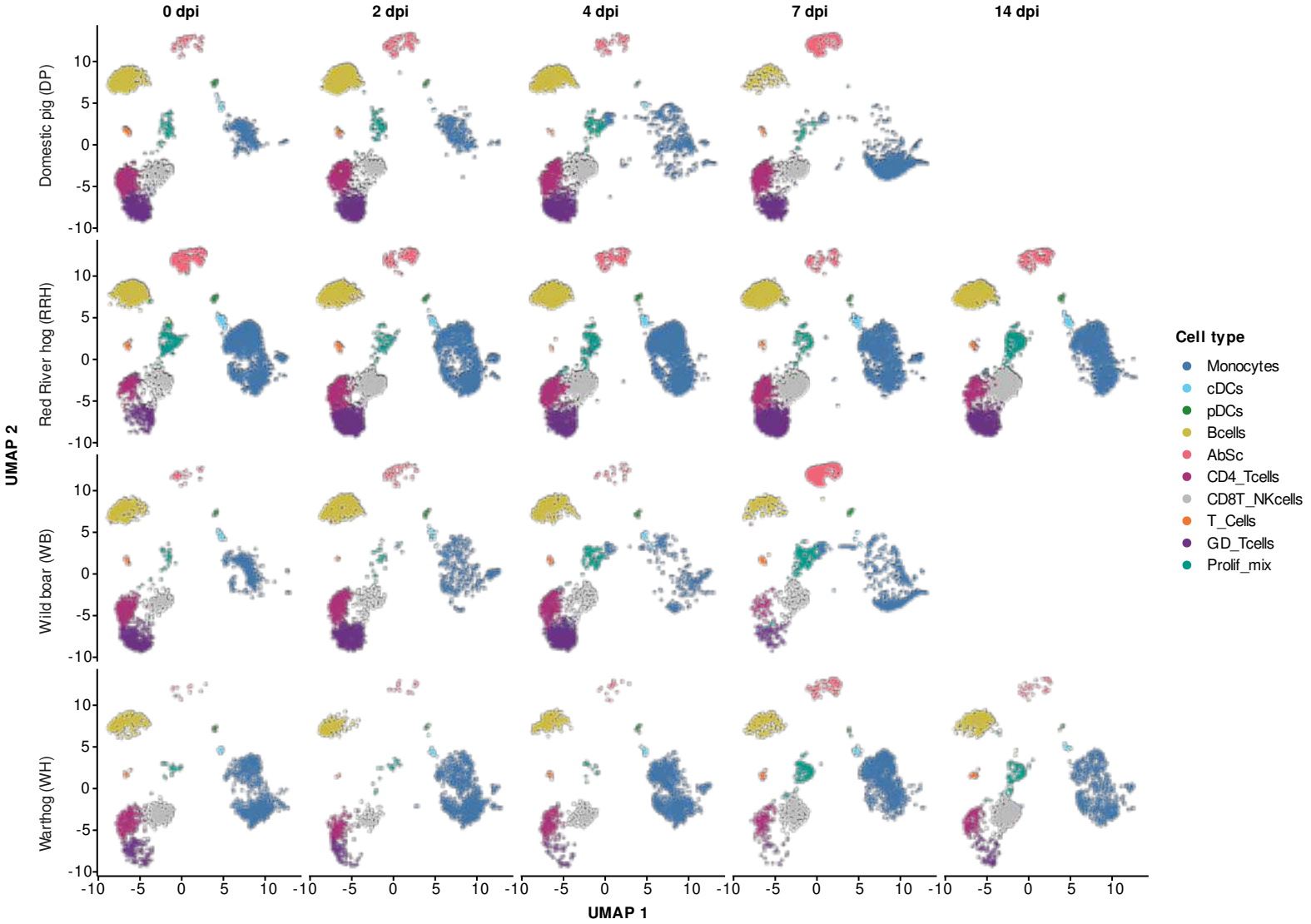


Fig. S8 | Full UMAP overview of PBMC single-cell transcriptomes. UMAP projections of scRNAseq data from peripheral blood mononuclear cells (PBMCs) of domestic pigs (DP), wild boar (WB), red river hogs (RRH) and warthogs (WH) across all sampled time points (0, 2, 4, 7 and, 14 days post infection). For each species, panels are arranged by time point, and cells are coloured according to major immune cell type: monocytes, conventional dendritic cells (cDCs), plasmacytoid dendritic cells (pDCs), B cells, antibody-secreting cells (AbSc), $CD4^+$ T cells, CD8 T/NK cells, γδ T cells, other T cells and proliferating mixed cells (Prolif_mix). Axes show UMAP1 and UMAP2 coordinates, providing a global view of PBMC composition and transcriptional states over the course of infection in each species.

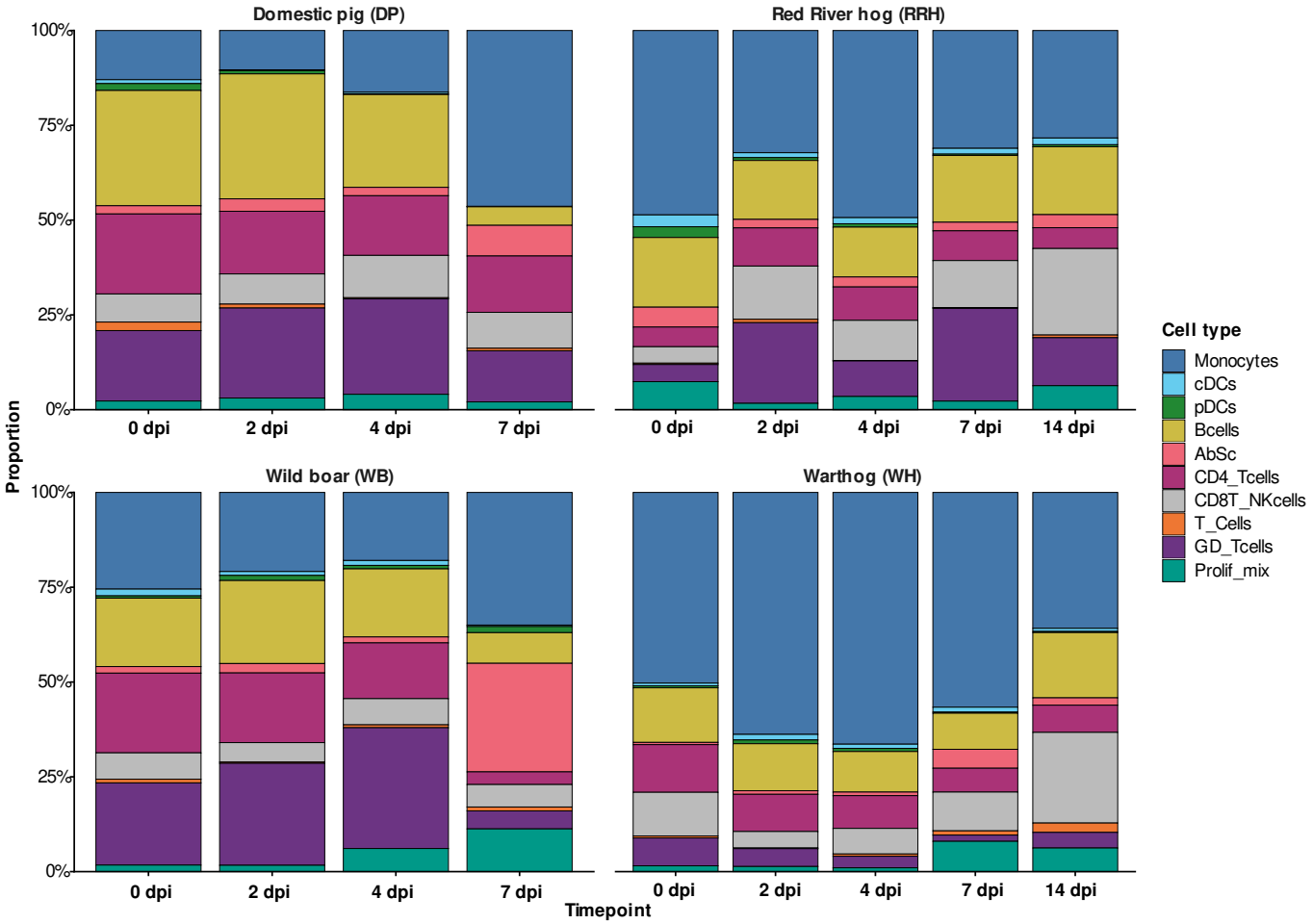


Fig. S9 | **Composition of PBMC immune cell subsets over time by scRNAseq.** Stacked bar plots showing the relative proportions of major leukocyte subsets in peripheral blood mononuclear cells (PBMCs) from domestic pigs (DP), wild boar (WB), red river hogs (RRH) and warthogs (WH) at indicated time points (0, 2, 4, 7, and 14 days post infection, where available). For each species, bars represent the fraction of total PBMCs assigned to monocytes, conventional dendritic cells (cDCs), plasmacytoid dendritic cells (pDCs), B cells, antibody-secreting cells (AbSc), $CD4^+$ T cells, CD8 T/NK cells, other T cells, γδ T cells (GD_Tcells) and proliferating mixed cells (Prolif_mix), as defined by scRNA-seq clustering and marker gene expression.

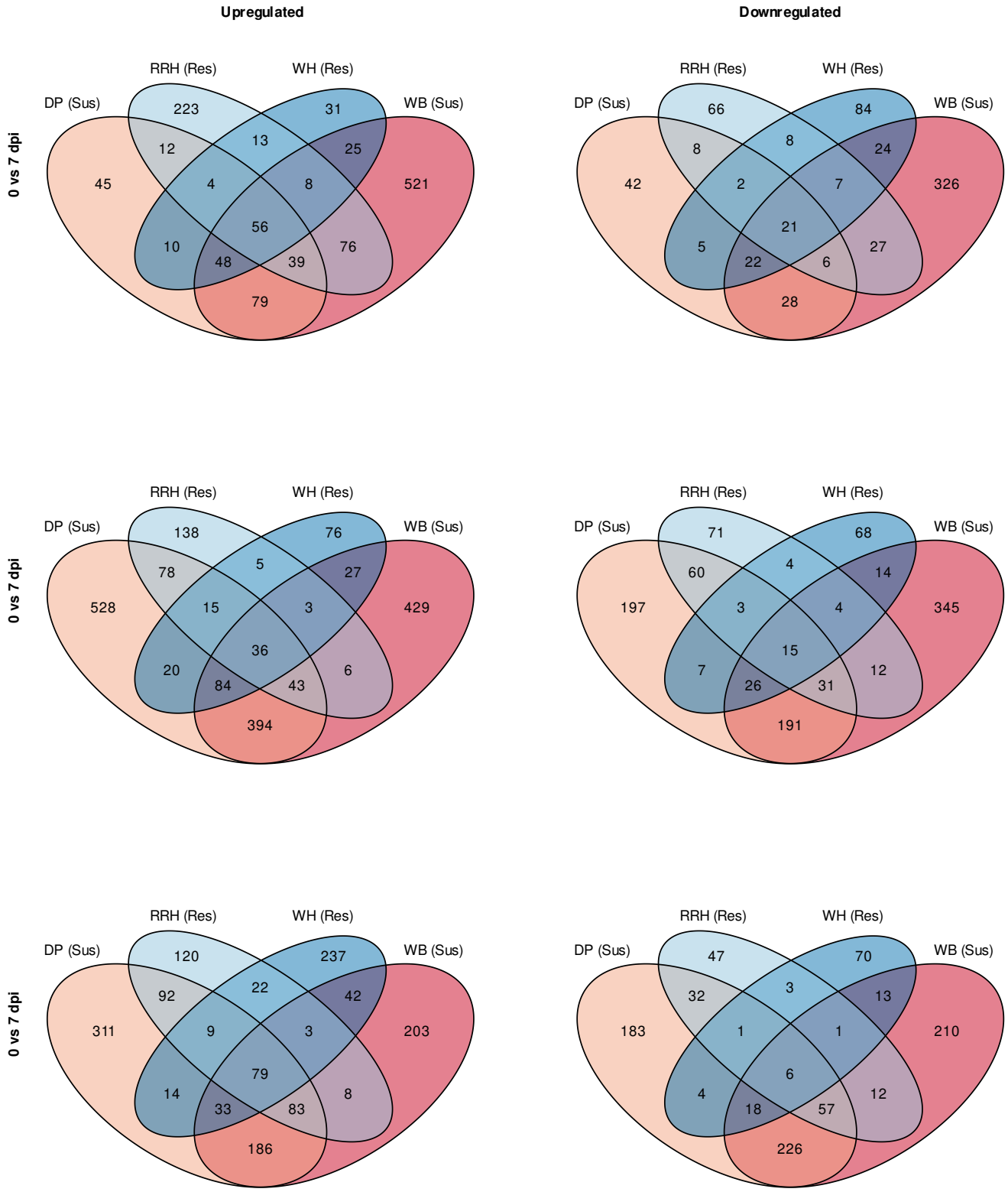


Fig. S10 | Overlap of monocyte transcriptional responses across suid species. Venn diagrams summarizing differentially expressed genes (DEGs) in the monocyte compartment between day 0 and day 7 post infection (dpi) for susceptible species (domestic pig, DP; wild boar, WB) and resistant species (red river hog, RRH; warthog, WH). Separate diagrams are shown for upregulated and downregulated genes in each comparison, with numbers indicating the total DEGs unique to or shared between DP, WB, RRH and WH. Each row of diagrams corresponds to a specific DEG subset (for example, all upregulated genes, all downregulated genes, or selected functional gene groups) in the 0 vs 7 dpi contrast.

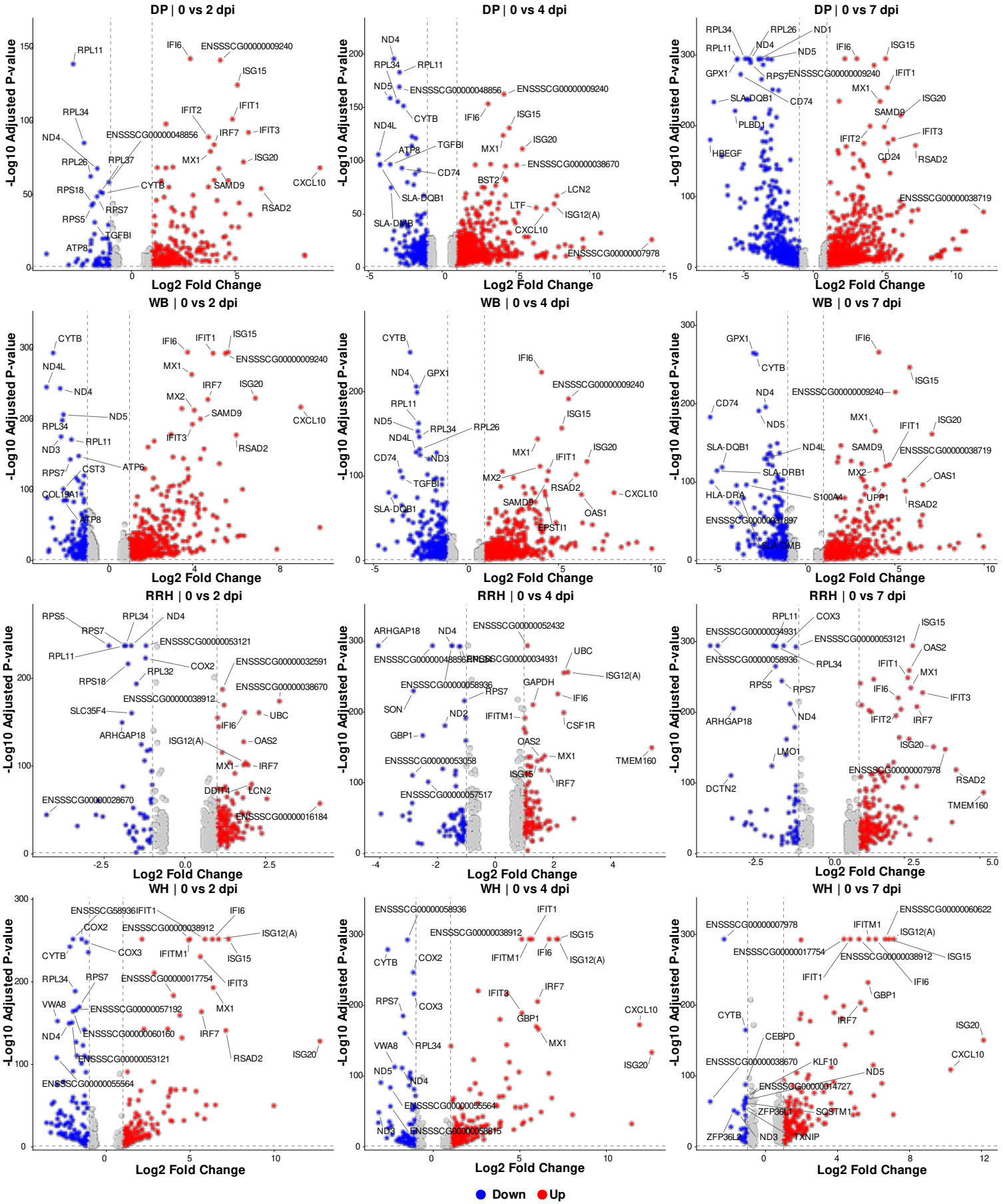


Fig. S11 | **Monocyte transcriptome differential expression analysis across suid species.** Volcano plots summarizing differentially expressed genes (DEGs) in blood monocytes between baseline (0 dpi) and later time points in domestic pigs (DP), wild boar (WB), red river hogs (RRH) and warthogs (WH) based on scRNA-seq. Each panel shows $\log_2$ fold change (x-axis) versus $-\log_{10}$ adjusted *P* value (y-axis) for the 0 vs 2 dpi, 0 vs 4 dpi and 0 vs 7 dpi comparisons within one species. Genes passing the significance threshold (false discovery rate–adjusted P < predetermined cut-off and absolute $\log_2$ fold change above the vertical dashed lines) are coloured red (upregulated) or blue (downregulated), while non-significant genes appear in grey. Selected genes of interest, including interferon-stimulated genes (for example *ISG15, IFIT1–3, MX1/2, OAS1/2, RSAD2*), chemokines (for example *CXCL10*), mitochondrial and ribosomal genes, and antigen-presentation genes (for example *HLA-DRA/SLA-DQB1, CD74*), are labelled to illustrate their position within the fold-change and significance landscape for each species and time comparison.

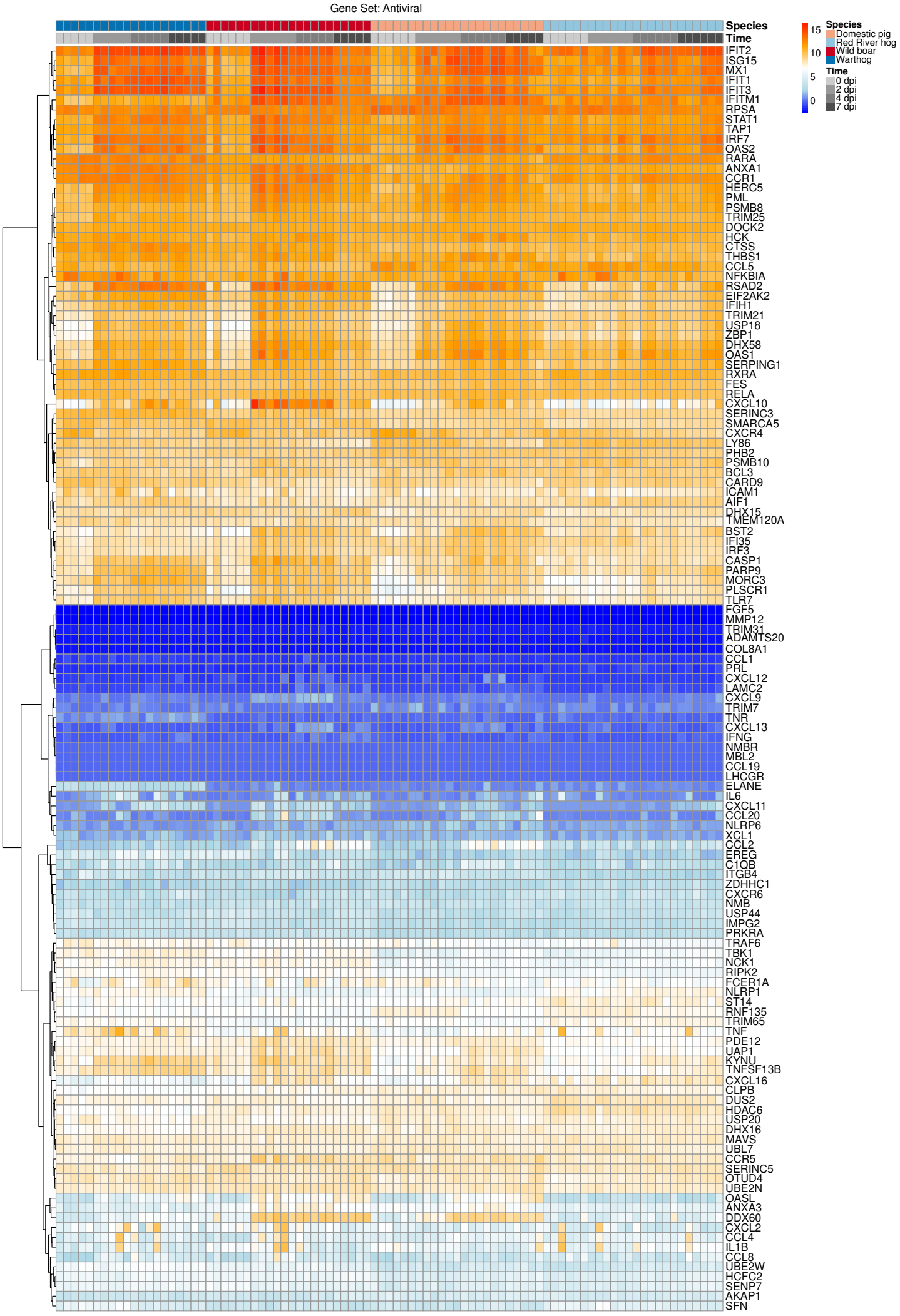


Fig. S12 | Bulk transcriptomic kinetics of antiviral gene set. Heatmap showing standardized expression of genes belonging to an antiviral response gene set in whole blood leukocytes from domestic pigs, wild boar, red river hogs und warthogs at 0, 2, 4, 7 und 14 dpi. Rows correspond to individual genes, columns to species and time points; colour intensity indicates relative expression (scale 0–15)

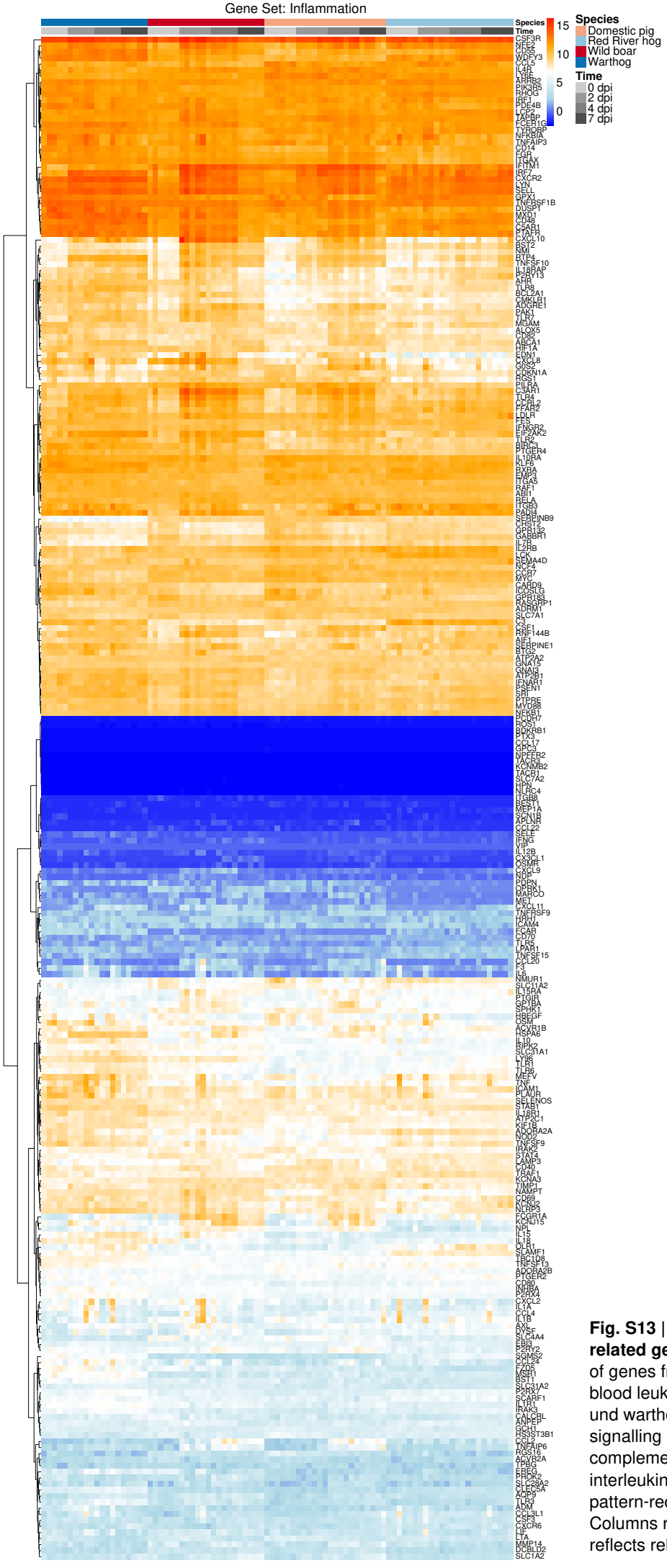


Fig. S13 | Bulk transcriptomic kinetics of inflammation-related gene set. Heatmap depicting standardized expression of genes from an inflammation-associated gene set in whole blood leukocytes of domestic pigs, wild boar, red river hogs und warthogs at 0, 2, 4, 7 und 14 dpi. Rows include receptors, signalling molecules and effector genes involved in complement, chemokine and cytokine signaling, interferon and interleukin pathways, TNF-receptor superfamily members, pattern-recognition receptors, as well as effector molecules. Columns represent species and time points; colour intensity reflects relative expression on a 0–15 scale.

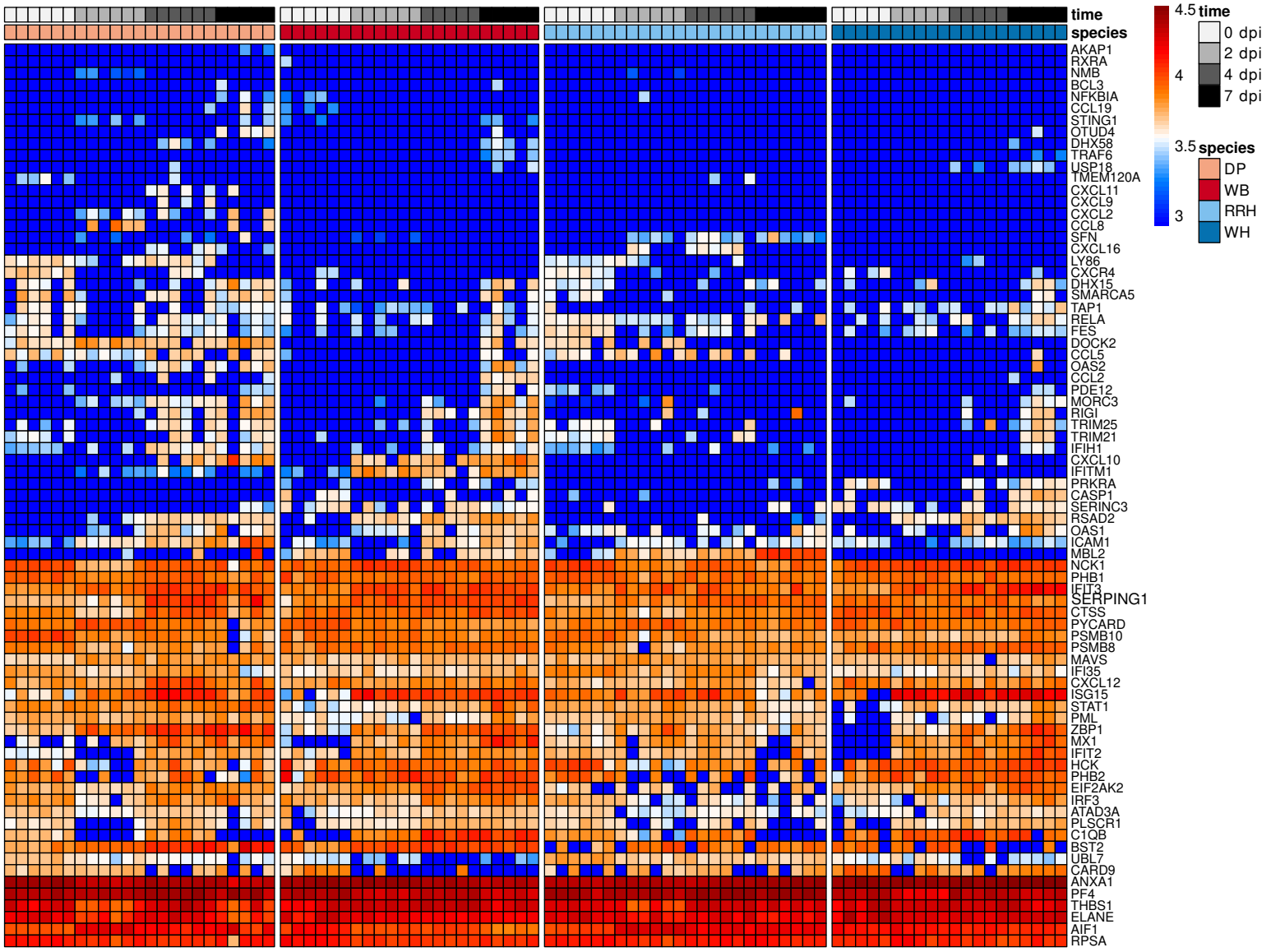


Fig. S14 | Antiviral host protein signatures in whole blood leukocytes. Heatmap showing standardized abundance (z-score) of host proteins associated with antiviral responses in whole blood leukocyte proteomes from domestic pigs (DP), wild boar (WB), red river hogs (RRH) and warthogs (WH) at 0, 2, 4, and 7 days post infection. Rows correspond to the top regulated proteins selected from a curated gene-set enrichment analysis (GSEA) database of antiviral pathways, including sensors (for example RIGI, IFIH1, STING1, DHX58), signalling adaptors and transcription factors (for example MAVS, TRAF6, RELA, STAT1, IRF3), effector interferon-stimulated genes (for example ISG15, MX1, OAS1/2, RSAD2, IFIT1–3, IFITM1, BST2), chemokines and cytokine-related molecules (for example CXCL9/10/11, CCL2/5, CXCL2, CXCL12, PF4, THBS1), and components of complement and antigen processing (for example C1QB, CTSS, PSMB8/10, SERPING1). Columns represent individual samples grouped by species and time point; colour intensity indicates relative protein abundance, with warmer colours reflecting higher expression and cooler colours lower expression.

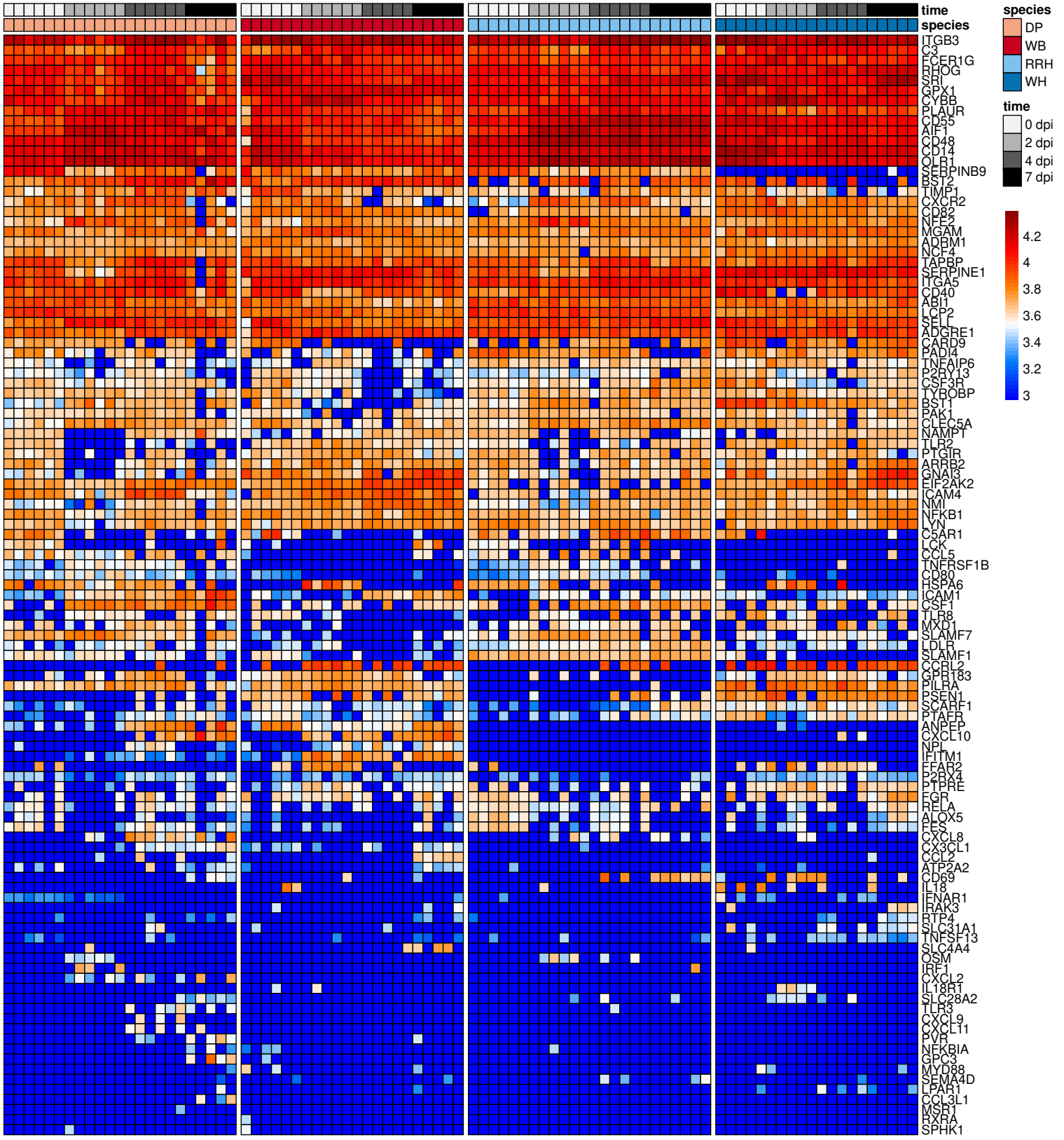


Fig. S15 | **Inflammatory host protein signatures in whole blood leukocytes.** Heatmap showing standardized abundance (z-score) of host proteins associated with inflammatory responses in whole blood leukocyte proteomes from domestic pigs (DP), wild boar (WB), red river hogs (RRH) and warthogs (WH) at 0, 2, 4, and 7 days post infection. Rows correspond to the top regulated proteins selected from a curated GSEA-based inflammation gene set, including complement and Fc-receptor components (for example C3, C5AR1, FCER1G), adhesion and migration molecules (for example ICAM1/4, ITGA5, ITGB3, SELL, SCARF1), pattern-recognition and signalling molecules (for example TLR2/3/8, MYD88, NFKB1/NFKBIA, RELA, IRAK3, CARD9), chemokines and cytokine-related mediators (for example CXCL2/8/9/10/11, CCL2/3L1/5, CX3CL1, IL18, IL18R1, OSM, TNFSF13), and additional inflammatory regulators such as CSF1/3R, SERPINE1, PADI4, NAMPT, SPHK1 and LPAR1. Columns represent individual samples grouped by species and time point; colour intensity indicates relative protein abundance, with warmer colours reflecting higher expression and cooler colours lower expression.

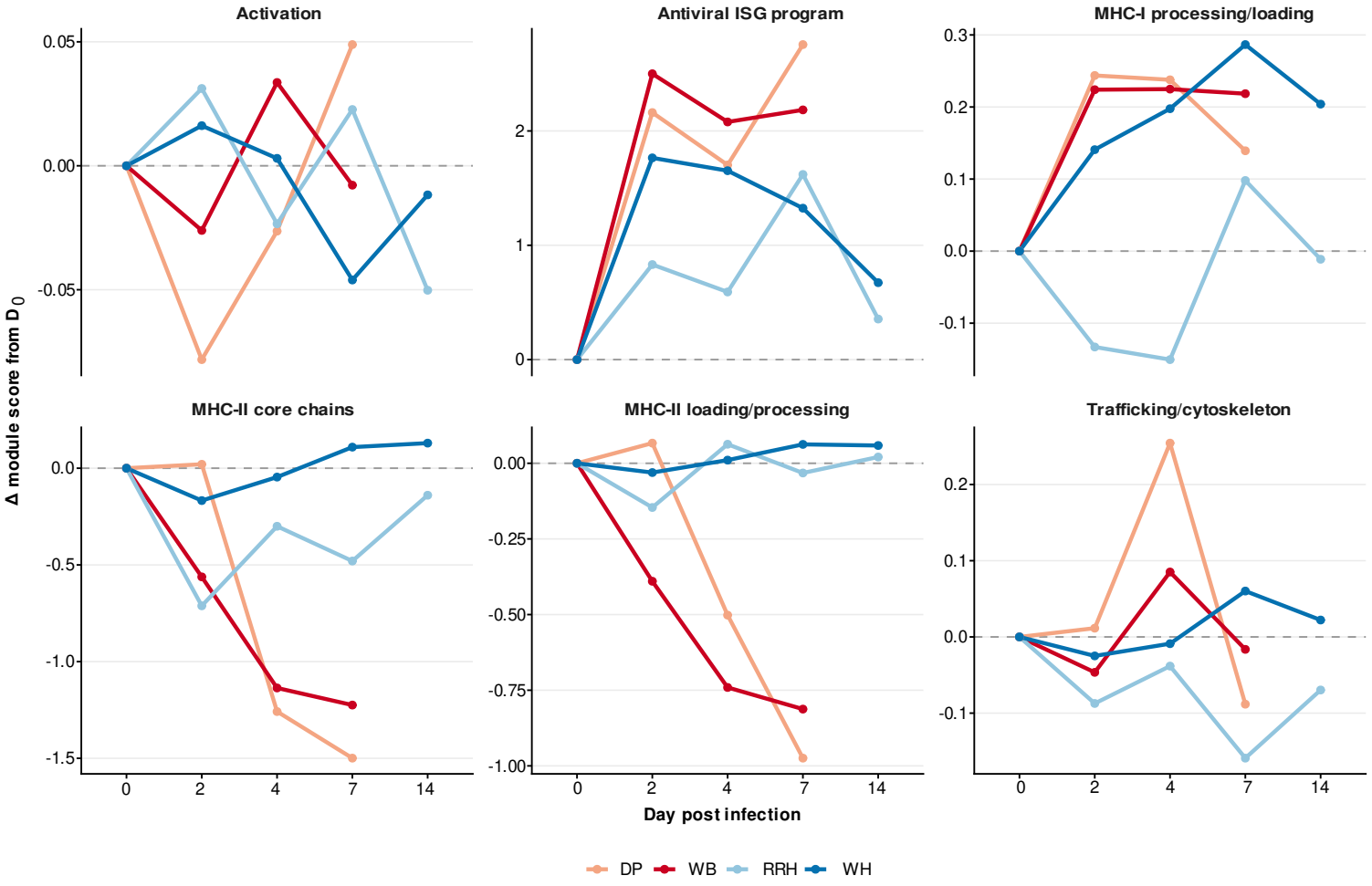


Fig. S16 | PBMC module scores for antigen presentation and antiviral pathways. Line plots depicting changes in UCell module scores for six gene sets in PBMCs across infection in DP, WB, RRH and WH. Each panel shows the mean change in module score relative to 0 dpi (Δ score from D0) at 0, 2, 4, 7, and 14 days post infection, with separate lines for each species. The analysed modules correspond to activation (general immune activation genes), an antiviral interferon-stimulated gene (ISG) programme, MHC-I processing/loading, MHC-II core chains, MHC-II loading/processing and trafficking/cytoskeleton genes involved in vesicular transport and structural dynamics of antigen-presenting cells.

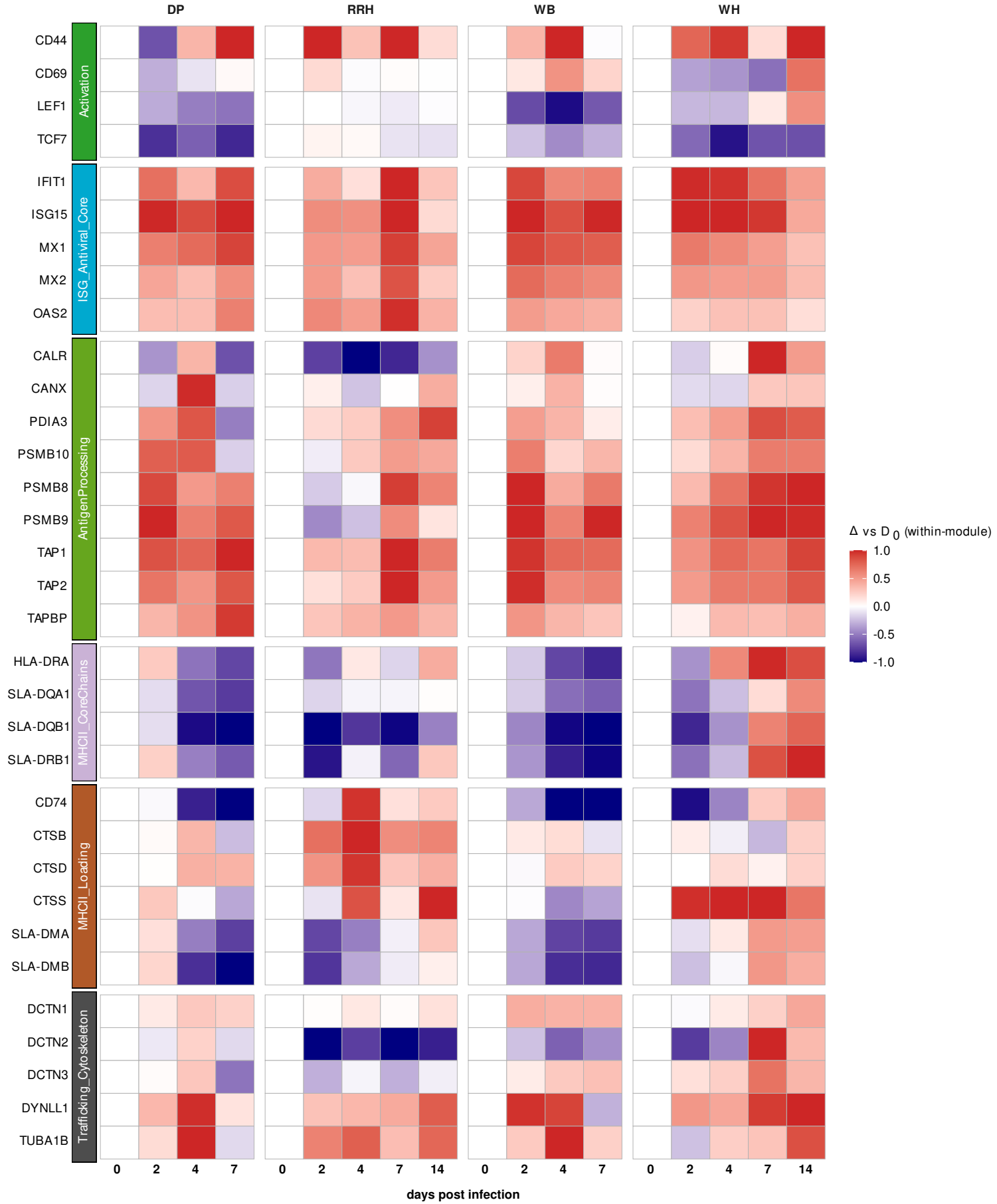


Fig. S17 | Gene-level scRNA-seq kinetics for activation and antigen-presentation pathways. Heatmap showing changes in expression of selected genes within six scRNA-seq modules, including Activation, ISG_Antiviral_Core, AntigenProcessing, MHCII_CoreChains, MHCII_Loading, and Trafficking_Cytoskeleton, in PBMCs from domestic pigs (DP), wild boar (WB), red river hogs (RRH) and warthogs (WH) over time. Rows correspond to individual genes assigned to each module, including activation markers (*TCF7, LEF1, CD69, CD44*), antiviral ISGs (*OAS2, MX1/2, ISG15, IFIT1*), antigen-processing genes (*TAPBP, TAP1/2, PSMB8/9/10, PDIA3, CANX, CALR*), MHCII core chain genes (*SLA-DRB1, SLA-DQB1, SLA-DQA1, HLA-DRA*), MHCII loading/processing genes (*SLA-DMA/B, CTSS, CTSD, CTSB, CD74*) and trafficking/cytoskeleton genes (*TUBA1B, DYNLL1, DCTN1/2/3*). Columns represent species and days post infection (0, 2, 4, 7, and, where available, 14 dpi); colour intensity indicates the change in within-module expression relative to 0 dpi (Δ vs D0), with warmer colours reflecting increased expression and cooler colours decreased expression.

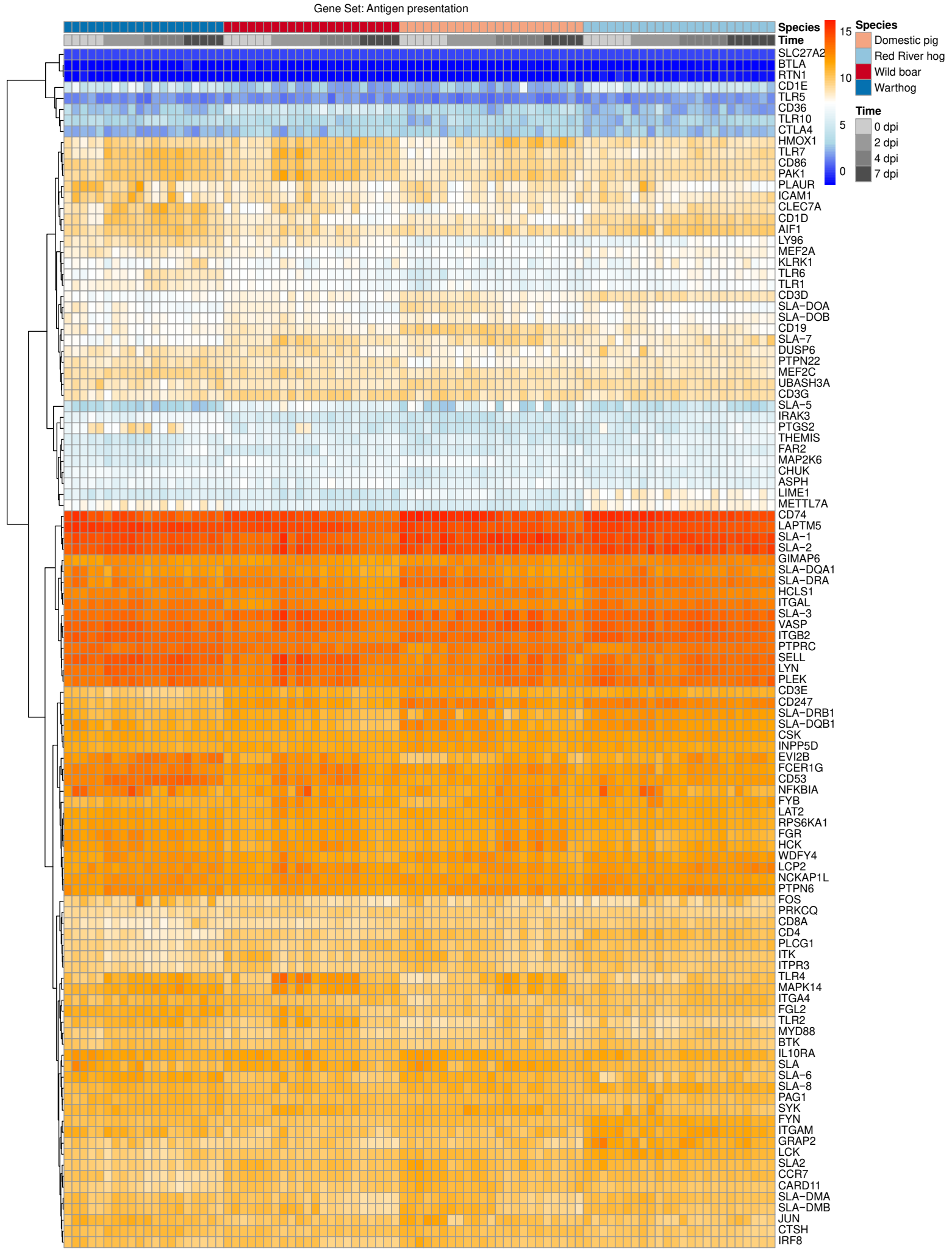


Fig. S18 | Bulk transcriptomic kinetics of antigen-presentation gene set. Heatmap summarizing standardized expression of genes within an antigen-presentation gene set in whole blood leukocytes of domestic pigs, wild boar, red river hogs und warthogs at 0, 2, 4, 7 und 14 dpi. Rows correspond to genes involved in antigen presentation and T-cell activation, including MHC and co-stimulatory molecules, proximal TCR-signalling components, adaptor and signalling proteins, as well as antigen-processing and myeloid lineage-associated genes. Columns show species and time points; colour encodes relative expression intensity (scale 0–15).

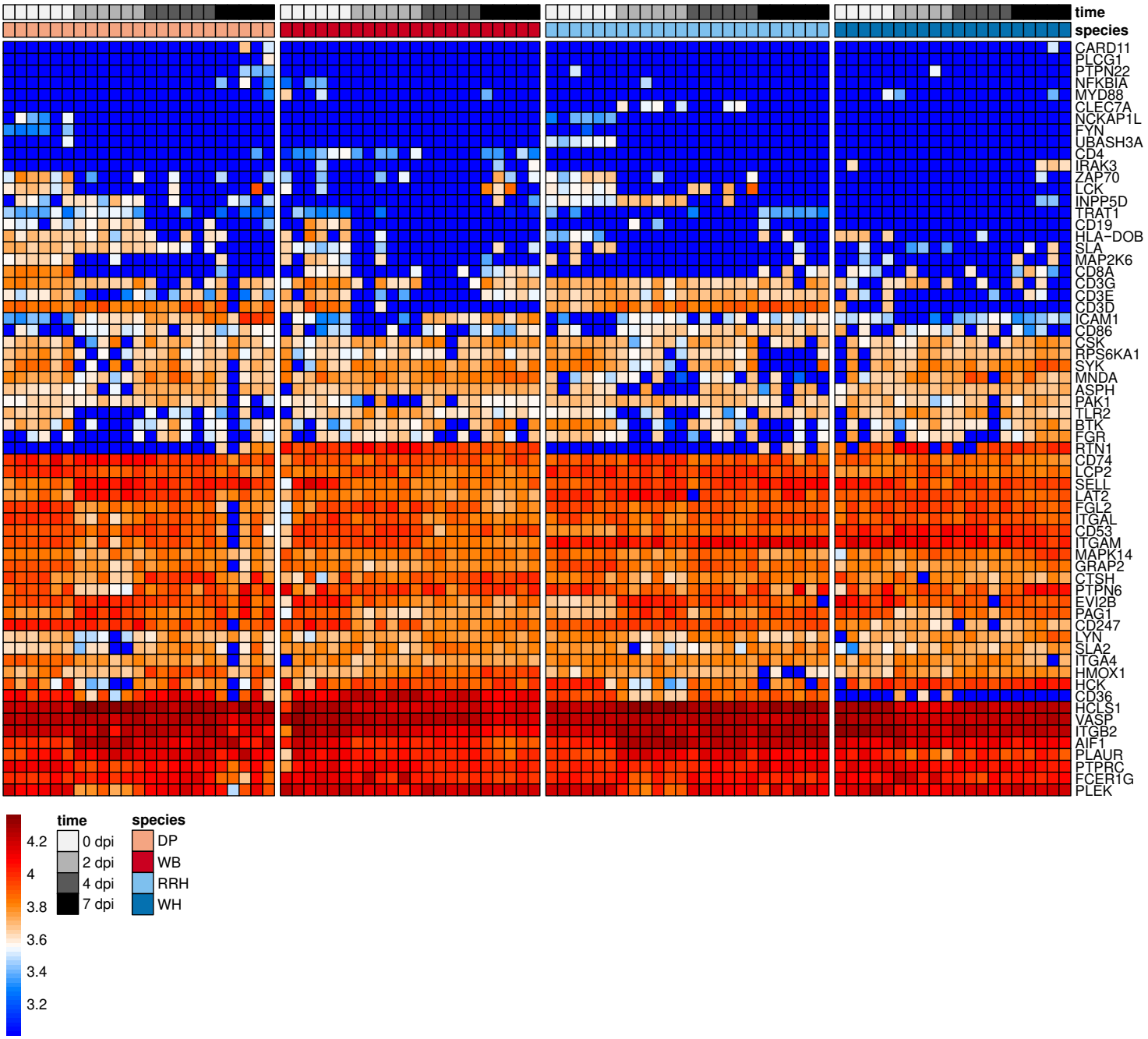


Fig. S19 | Antigen processing and presentation protein signatures in whole blood leukocytes. Heatmap showing standardized abundance (z-score) of host proteins involved in antigen processing, presentation and T-cell activation in whole blood leukocyte proteomes from domestic pigs (DP), wild boar (WB), red river hogs (RRH) and warthogs (WH) at 0, 2, 4 and 7 days post infection. Rows correspond to the selected proteins, including proximal T-cell receptor signalling molecules (for example CD3D/E/G, CD4, CD8A, ZAP70, LCK, FYN, TRAT1, GRAP2, CARD11, PLCG1, SYK, BTK, PTPN6/22, CSK), co-stimulatory and adhesion molecules (for example CD19, CD53, CD86, SLAM family proteins, ICAM1, ITGAL, ITGAM, ITGA4, ITGB2, SELL, CD36, PLAUR, PTPRC), innate receptors and upstream signalling components (for example TLR2, CLEC7A, MYD88, NFKBIA, FCER1G), and MHCII-associated and antigen-processing proteins (for example HLA-DOB, CD74, CTSH). Columns represent individual samples grouped by species and time point; colour intensity indicates relative protein abundance, with warmer colours reflecting higher expression and cooler colours lower expression.

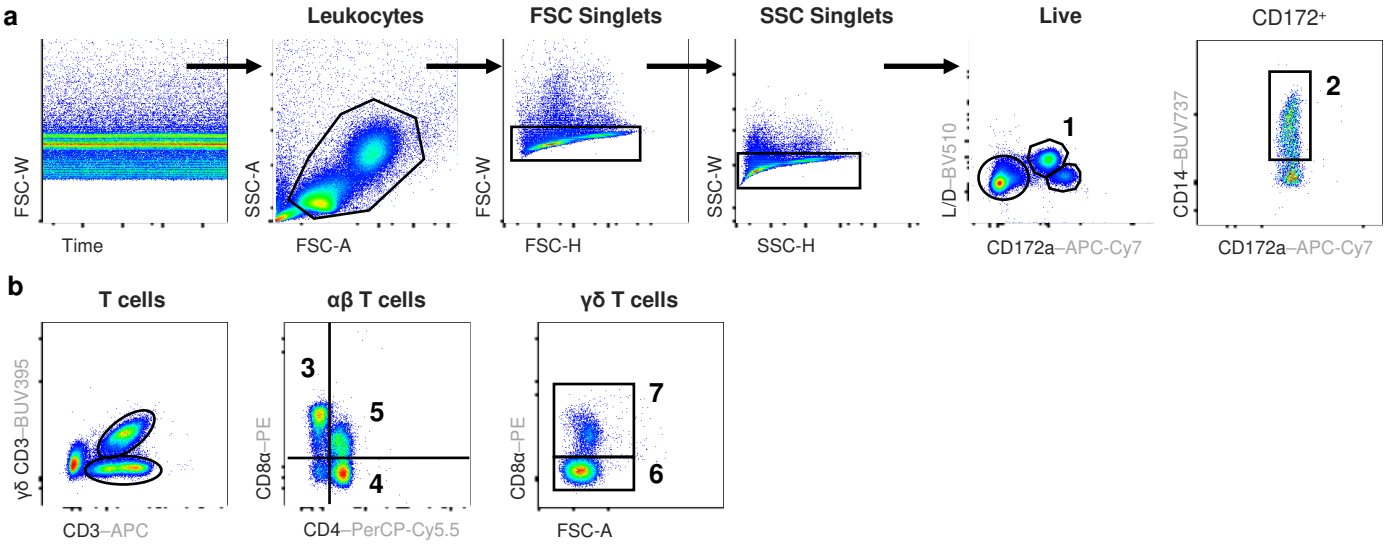


Fig. S20 | **General gating strategy for whole blood. a**, Stable flow was verified in a time plot. Leukocytes were gated according to their FSC/SSC properties, while small debris was excluded. Doublets were excluded by consecutive FSC-W vs. FSC-H and SSC-W vs. SSC-H gating. Dead cells were excluded with Zombie Fixable Viability Dye (L/D). Myeloid cells were identified as CD172a+ and further divided into autofluorescent (L/D low) polymorphonuclear granulocytes (1) and L/D−/CD14+ monocytes (2). **b**, Live CD172a− lymphocytes were divided into αβ and γδ T cells. αβ T cells were further identified as CD4−CD8α+ cytotoxic T cells (3), CD4+CD8α− helper T cells (4), and CD4+CD8α+ memory T cells (5). γδ T cells were further identified as either CD8α− (6) or CD8α+ (7) gd T cells.

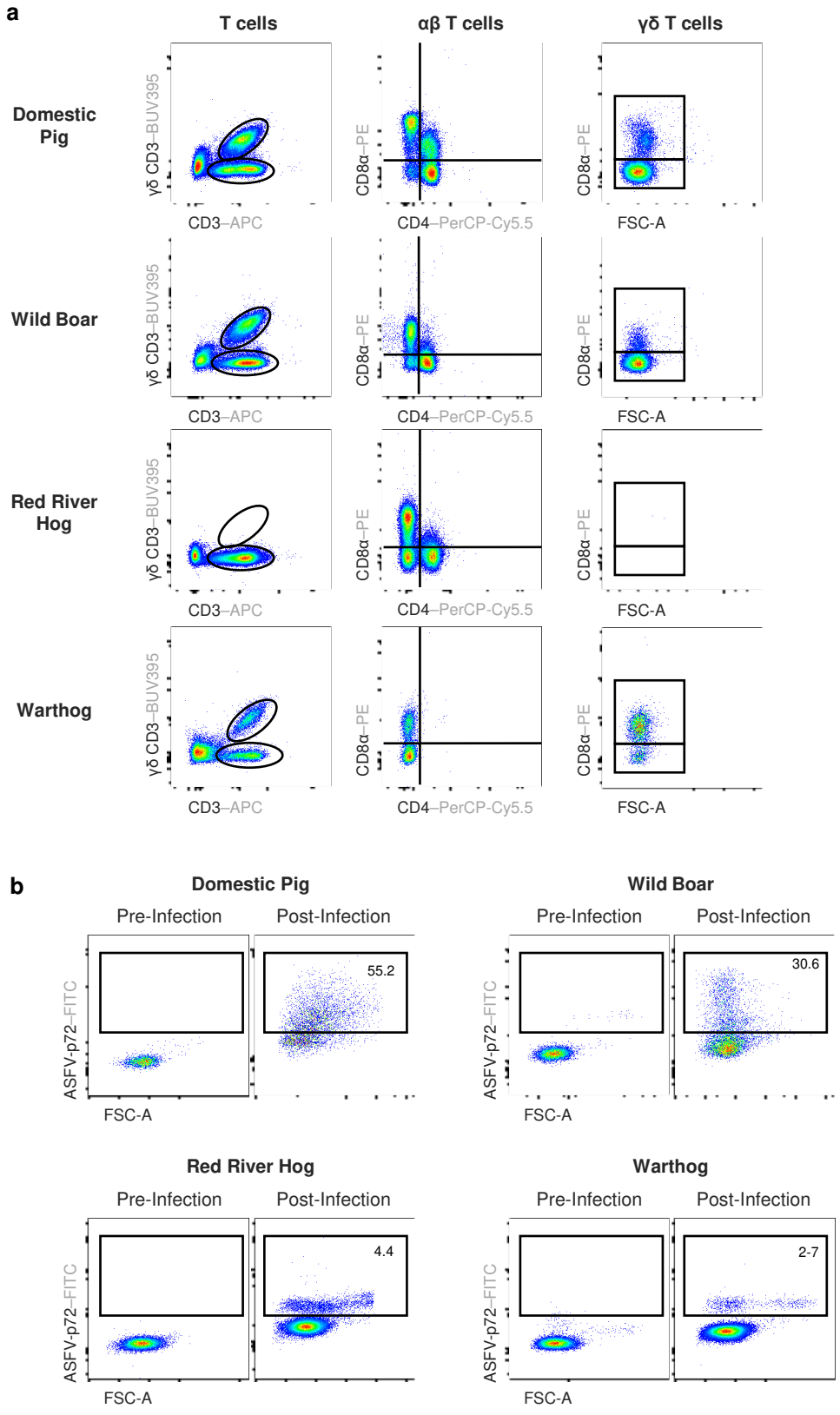


Fig. S21 | **Representative flow plots for all species.** Cells were identified according to the gating strategy described in Fig. S20. **a**, Representative plots show identification of CD3+ T cells among live, single CD172− cells, subdivision into αβ and γδ T cells, and identification of αβ and γδ T cell subsets according to CD4 and CD8α expression. b , Representative plots of ASFV-p72 expression in CD172+CD14+ monocytes either pre- or post-infection. Numbers in gates indicate frequencies.

SUPPLEMENTARY TABLES

Table S1: Signature ASFV genes expressed in all pig species. Table is provided as separate Excel-file.

Table S2: Overview of criteria used to define the moderate humane endpoint for each individual. Individual parameters were scored from 0–3 according to severity. A score of 4 represented a predefined humane endpoint requiring immediate euthanasia (not entering the cumulative score).

Parameter	**Score**	**Clinical Description**
Activity	0	Alert, curious, rises immediately
	1	Slightly lethargic, rises hesitantly but independently
	2	Lethargic, rises only when forced, lies down again
	3	Somnolent, unable to rise
	4	**Conditions associated with uncontrollable pain**
Posture	0	Relaxed posture, straight back
	1	Stiff when rising, slightly arched back
	2	Persistently arched back, stiff gait
	3	Severely arched back or unable to stand
	4	**Recumbency**
Respiration	0	Normal respiratory rate, no abnormalities (10–15/min)
	1	Slightly increased respiratory rate, occasional sneezing or coughing (>20/min)
	2	Clearly increased respiratory effort and respiratory sounds (>20/min)
	3	Marked tachypnoea (>30/min), open-mouth breathing, pronounced dyspnoea
	4	**Coughing with foamy discharge and cyanosis with respiratory distress**
Locomotion	0	Coordinated movements without abnormalities
	1	Mild lameness and/or unsteady gait
	2	Moderate lameness and/or clear ataxia or hindlimb weakness, still ambulatory
	3	Severe lameness and/or paralysis, unable to walk
	4	**Neurological seizures**
Skin	0	Uniform pale pink skin, bristles flat
	1	Localized reddening of the skin
	2	Bluish-red discoloured cold skin areas, petechial haemorrhages
	3	Black-blue discoloration, loss of sensitivity, extensive skin haemorrhages
	4	**Uncontrollable mucosal bleeding or bleeding from body openings**
Eyes/Conjunctiva	0	Pale pink
	1	Reddened, clear discharge
	2	Strongly reddened, cloudy discharge
	3	Strongly reddened, purulent discharge, vascular injection
	4	**Ocular haemorrhages with increased intraocular pressure**
Faeces/Vomiting	0	Normal faeces, normal quantity
	1	Mild diarrhoea or very firm faeces
	2	Semi-liquid diarrhoea or signs of constipation, vomiting
	3	Watery (bloody) diarrhoea or constipation, bloody vomiting
	4	**Rectal prolapse**
Appetite	0	Eagerly consumes offered feed
	1	Consumes offered feed hesitantly
	2	Does not eat but still shows interest in feed
	3	No feed intake, no interest in feed
	4	**No feed intake for >48 h**

Body condition	0	Full abdomen, rounded appearance
	1	Empty abdomen
	2	Empty abdomen, reduced musculature
	3	Sunken flanks, vertebrae and ribs visible

Termination Criteria: Animals reaching a cumulative clinical score above 15 during infection were removed from the study. Animals displaying severe signs indicative of unacceptable suffering were also euthanized irrespective of the cumulative score. Such conditions, represented by an individual score of 4 in the respective category, included seizures or conditions that could not be treated adequately under experimental conditions, such as irreducible rectal prolapse. Any individual score of 4 resulted in immediate euthanasia, even when the total clinical score remained below the predefined threshold. The respective finding was documented in detail by the attending veterinarian.

Table S3: Protein sequence identity of humoral markers between domestic pig and wild boar (*Sus scrofa domesticus*, *Sus scrofa scrofa*), warthog (*Phacochoerus africanus*), and red river hog (*Potamochoerus porcus*). For multiple aligned sequences, the isoform with highest length is shown.

	UniProt accession (*S. scrofa*)	**Identity to *P. africanus***	**Identity to *P. porcus***
CRP C-reactive protein	O19062.1	218/222 (98%) (XP_047638945.1)	N.d.
MAP Major acute phase protein (Inter-alpha-trypsin inhibitor heavy chain H4, ITIH4)	P79263.1	901/929 (97%) (XP_047632604.1)	N.d.
C3 Complement C3	P01025.2	1631/1661 (98%) (XP_047633289.1)	N.d.
C5a Complement 5a	P01032.1	71/74 (96%) (XP_047624251.1)	N.d.
IFN-γ Interferon-γ	P17803	164/166 (99%) (XP_047643106.1)	N.d.
TNF-α Tumor necrosis factor-α	P23563.1	229/233 (98%) (XP_047653006.1)	N.d.
IL1-ra Interleukin-1 receptor antagonist	Q29056.1	152/156 (97%) (XP_047622110.1)	N.d.
IL-1β Interleukin-1β	P26889	230/268 (86%) (XP_047637129.1)	N.d.
IL-6 Interleukin-6	P26893.2	207/212 (98%) (XP_047609872.1)	N.d.
IL-10 Interleukin-10	Q29055.1	174/175 (99%) (XP_047609331.1)	N.d.
IFN α-1 Interferon α-1	P49879.1	183/189 (97%) (XP_047625488.1)	N.d.

N.d., None detected.

Table S4: Overview of individuals pooled in each library in scRNAseq (18 libraries in total).

	Domestic pig	Red river hog	Wild boar	Warthog
Day 0	3 male, 3 female	3 male, 3 female	5 male, 1 female	4 male, 1 female
Day 2	3 male, 3 female	3 male, 3 female	5 male, 1 female	4 male, 1 female
Day 4	3 male, 3 female	3 male, 3 female	5 male	4 male, 1 female
Day 7	2 female (#7 and #10)	3 male, 3 female	5 male	4 male, 1 female
Day 14	—	2 male (#16 and #17), 2 female (#12 and #14)	—	3 male (#21, #22, #24), 1 female (#23)

Note: Due to euthanasia at 0 dpi in critical condition, warthog #20 was excluded from all analyses.

Table S4: List of antibodies used for surface and intracellular marker staining in flow cytometry.

Antigen	Clone	Conjugate	Isotype	Source	Catalog#	RRID
CD3ε	PPT3	APC	M IgG1	Southern Biotech	4510-11	AB_2796016
CD4	74-12-4	PerCP	M IgG2b	BD Biosciences	561474	AB_10683310
CD8α	76-2-11	PE	M IgG2a	Southern Biotech	4520-09	AB_2796033
CD14	TÜK4	Biotin	M IgG2a	Bio-Rad	MCA1568B	AB_2259976
γδ-CD3	PPT16	—	M IgG2b	in-house	—	—
FoxP3	FJK-16s	PE-Cy7	R IgG2a	ThermoFisher	25-5773-82	AB_891552
Ki-67	B56	BV786	M IgG1	BD Biosciences	563756	AB_2732007
α-IgG1	A85-1	APC-Cy7	R IgG	Biolegend	406620	AB_2571947
α-IgG2b	R12-3	BUV395	R IgG2a	BD Biosciences	743180	AB_2741331
Biotin	Streptavidin	BUV737	—	BD Biosciences	612775	AB_2870104

M, mouse; R, rat.

Supplementary Files

This is a list of supplementary files associated with this preprint. Click to download.

- StudyGroupMembers.docx
- SupplementaryTableS1.xlsx